Design and Analysis of a Single Mode Bend Insensitive Equiangular Spiral Photonic Crystal Fiber with Large Effective Area

by

Md. Asiful Islam

MASTER OF SCIENCE IN ELECTRICAL AND ELECTRONIC ENGINEERING

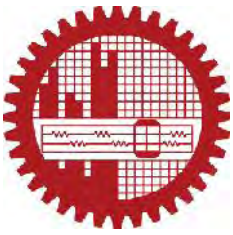

Department of Electrical and Electronic Engineering
BANGLADESH UNIVERSITY OF ENGINEERING AND TECHNOLOGY
March 2013

The thesis titled **"Design and Analysis of a Single Mode Bend Insensitive Equiangular Spiral Photonic Crystal Fiber with Large Effective Area"** submitted by Md. Asiful Islam, Student No.: 0411062205, Session: April, 2011, has been accepted as satisfactory in partial fulfillment of the requirement for the degree of MASTER OF SCIENCE IN ELECTRICAL AND ELECTRONIC ENGINEERING on March 30, 2013.

BOARD OF EXAMINERS

1. _____

Dr. Md. Shah Alam — Chairman (Supervisor)
Professor
Department of Electrical and Electronic Engineering,
BangladeshUniversity of Engineering and Technology,
Dhaka-1000, Bangladesh.

2. _____

Dr. Pran Kanai Saha — Member (Ex-officio)
Professor and Head
Department of Electrical and Electronic Engineering,
BangladeshUniversity of Engineering and Technology,
Dhaka-1000, Bangladesh.

3. _____

Dr. Satya Prasad Majumder — Member
Professor
Department of Electrical and Electronic Engineering,
BangladeshUniversity of Engineering and Technology,
Dhaka-1000, Bangladesh.

4. _____

Gp Capt Dr. Md Hossam-E-Haider — Member (External)
Senior Instructor
Department of Electrical, Electronic and Communication Engineering,
Military Institute of Science and Technology (MIST),
Mirpur Cantonment, Dhaka-1216, Bangladesh.

CANDIDATE'S DECLARATION

It is hereby declared that this thesis or any part of it has not been submitted elsewhere for the award of any degree or diploma and that all sources are acknowledged.

Signature of the Candidate

_____

Md. Asiful Islam

Dedication

To my parents

Acknowledgement

First of all, I would like to thank Allah, the almighty, for giving me the ability to complete this thesis work.

I would like to express my sincere gratitude to my supervisor, Dr. Md. Shah Alam. This thesis would not have been completed without his support and guidance. His constant encouragement gave me the confidence to carry out my work.

I would like to thank all my teachers. They gave the knowledge and directions that have helped me throughout my life. I express my gratitude to my teachers from Bangladesh University of Engineering and Technology. The knowledge I learned from the classes in my B.Sc. and M.Sc. levels were essential for this thesis.

I want to thank my friends for providing me support and encouragement. Their suggestions helped me in countless ways.

Last but not the least, I would like to thank my parents and family members. Their optimism and encouragement have allowed me to overcome any obstacle that I faced. Their unconditional support made it possible for me to complete this thesis.

ABSTRACT

The theories and properties of the conventional hexagonal lattice Photonic Crystal Fiber (PCF) are well established and their worth in different applications in fiber optics is also well accepted. On the other hand, the newly introduced equiangular spiral PCF is yet to be investigated thoroughly. In this thesis, the optical mode of the PCF structure is determined by using full vectorial finite element method (FEM) based software 'COMSOL Multiphysics' and different properties of ES-PCF are calculated therefrom. Different useful designs like dispersion compensating ES-PCF, highly birefringent ES-PCF, bend insensitive single mode ES-PCF with large effective area have been obtained. To be specific, an ES-PCF is designed having flat negative dispersion profile with average dispersion around −396 ps/nm-km and dispersion variation of only 10.4 ps/nm-km for residual dispersion compensation of the fiber optic communication link over the wavelength range 1350 nm to 1675 nm. Also, a similar design has been developed that exhibits a very high birefringence of 0.0278 as well as flat negative dispersion profile. Next, liquid crystal infiltration in some air holes in the core is exploited to achieve a completely single polarization dispersion compensating fiber having average dispersion −259 ps/nm-km with dispersion variation of only 4.58 ps/nm-km over the same wavelength range. Moreover, a new circular lattice air hole PCF (C-PCF) has been proposed for both WDM transmission and fiber to the home application. The C-PCF exhibits single modedness along with very low bending loss for the fundamental mode and effective area as high as 260 μm^2 for WDM application which is higher than the previously reported values in the literatures. Apart from the above works, a modified bend loss formula for step index fibers has been developed and verified in this thesis. Also, this modified formula applies well, though in a limited range for PCFs, in predicting bending loss. The works in this thesis is believed to be a gateway for the future research on ES-PCF and PCFs with irregular lattice structures.

CONTENTS

LIST OF TABLES

LIST OF FIGURES

LIST OF ABBRAVIATIONS

ES-PCF	**:**	Equiangular Spiral Photonic Crystal Fiber
H-PCF	**:**	Hexagonal-Lattice Photonic Crystal Fiber
LC	**:**	Liquid Crystal
LMA	**:**	Large Mode Area
MFD	**:**	Mode Field Diameter
MMF	**:**	Multi Mode Fiber
PBG	**:**	Photonic Band Gap
PCF	**:**	Photonic Crystal Fiber
RDCF	**:**	Residual Dispersion Compensating Fiber
SIF	**:**	Step Index Fiber
SMF	**:**	Single Mode Fiber
TIR	**:**	Total Internal Reflection

LIST OF SYMBOLS

n	**:**	Refractive Index
β	**:**	Propagation Constant
α	**:**	Attenuation Constant
R	**:**	Bending Radius
n_{core}	**:**	Refractive Index of the core
n_{clad}	**:**	Refractive Index of the cladding
V	**:**	Normalized Frequency
n_{FSM}	**:**	Fundamental Space Filling Mode
D	**:**	Dispersion
B	**:**	Birefringence
Λ	**:**	Pitch of a PCF
d	**:**	Air hole diameter in a PCF

CHAPTER 1
INTRODUCTION

Optical fibers have undergone an evolution in its structure since they were first introduced in the beginning of 1970s as step index fibers. Photonic crystal fibers (PCFs) are a special type of optical fiber. Pioneered by the research group of Philip St. J. Russell in the 1990s, the development of photonic crystal fibers and the exploration of the great variety of possible applications have attracted huge interest. PCFs guide light by two mechanisms. One is the modified total internal reflection that utilizes its microstructured cladding arrangement and solid core [1] and the other is the photonic band gap mechanism in PCFs having hollow cores [2]. Optical fibers have a very broad range of applications, where they serve many purposes, such as simply transporting light from a source to some other device, transmitting optically encoded data, sensing temperature or strain in some environment, generating and amplifying laser light. These properties can be more easily achieved in PCFs as these fibers offer many degrees of freedom in their design than those of conventional optical fibers. The numerous structural parameters can be tailored to obtain desirable values of dispersion, birefringence, confinement loss bending loss etc for particular applications. This phenomenon has made this one of the most active fields of current optics research.

1.1 Basic Principles of PCF

In order to form a guided mode in an optical fiber, it is necessary to introduce light into the core with a value of β, that is the component of the propagation constant along the fiber axis, which cannot propagate in the cladding. The highest β value that can exist in an infinite homogeneous medium with refractive index n is, $\beta = nk$, k being the free-space propagation constant. A two-dimensional photonic crystal, like any other material, is characterized by a maximum value of β which can propagate. At a particular wavelength, this corresponds to the fundamental mode of an infinite slab of the material, and this value, β_{eff} defines the effective refractive index n_{eff} of the material in the way, $\beta_{eff} = n_{eff} k$.

1.1.1 Modified total internal reflection

It is possible to use a two-dimensional photonic crystal as a fiber cladding, by choosing a core material with a higher refractive index than the cladding effective index. An example of this kind of structures is the PCF with a silica solid core surrounded by a photonic crystal cladding with a triangular lattice of air-holes, shown in Fig. 1.1. These fibers, also known as index-guiding PCFs, guide light through a form of total internal reflection (TIR), called modified TIR. However, they have a number of properties which vary from those of conventional optical fibers.

Fig. 1.1 A frequently used triangular lattice solid-core photonic crystal fiber design.

holes, where the central hole is missing. The gray area indicates silica, and the white circles indicate air holes with typical dimensions of a few micrometers.

1.1.2 Endlessly single-mode property

As already stated, the first solid-core PCF, shown in Fig. 1.1, which consisted of a triangular lattice of air-holes with a diameter d of about 300 nm and a hole-to-hole spacing Λ of 2.3 µm, did not ever seem to become multi-mode in the experiments, even for short wavelengths. In fact, the guided mode always had a single strong central lobe filling the core [2].

Russell has explained that this particular endlessly single-mode behavior can be understood by viewing the air-hole lattice as a modal filter or “sieve” [2]. Since light is evanescent in air, the air-holes act like strong barriers, so they are the “wire mesh” of the sieve. The field of the fundamental mode, which fits into the silica core with a single lobe of diameter between zeros slightly equal to 2Λ, is the “grain of rice” which cannot escape through the wire mesh, being the silica gaps between the air-holes belonging to the first ring around the core too narrow. On the contrary, the lobe dimensions for the higher-order modes are smaller, so they can slip between the gaps. When the ratio d/Λ, that is the air-filling fraction of the photonic crystal cladding, increases, successive higher-order modes become trapped [2]. A proper geometry design of the fiber cross-section thus guarantees that only the

fundamental mode is guided. More detailed studies of the properties of triangular PCFs have shown that this occurs for $d/\Lambda < 0.4$ [3]-[4].

By exploiting this property, it it possible to design very large-mode area fibers, which can be successfully employed for high-power delivery, amplifiers, and lasers. Moreover, by doping the core in order to slightly reduce its refractive index, light guiding can be turned off completely at wavelengths shorter than a certain threshold value.

1.1.3 Photonic bandgap guidance

Optical fiber designs completely different form the traditional ones result from the fact that the photonic crystal cladding have gaps in the ranges of the supported modal index β/k where there are no propagating modes. These are the PBGs of the crystal, which are similar to the two-dimensional bandgaps which characterize planar lightwave circuits, but in this case they have propagation with a non-zero value of β. It is important to underline that gaps can appear for values of modal index both greater and smaller than unity, enabling the formation of hollow-core fibers with bandgap material as a cladding, as reported in Fig. 1.2. These fibers, which cannot be made using conventional optics, are related to Bragg fibers, since they do not rely on TIR to guide light. In fact, in order to guide light by TIR, it is necessary a lower-index cladding material surrounding the core, but there are no suitable low-loss materials with a refractive index lower than air at optical frequencies [1]. The first PCF which exploited the PBG effect to guide light was reported in 1998 [2]-[5], and it is shown in Fig. 1.3. Notice that its core is formed by an additional air-hole in a honeycomb lattice. This PCF could only guide light in silica, that is in the higher-index material.

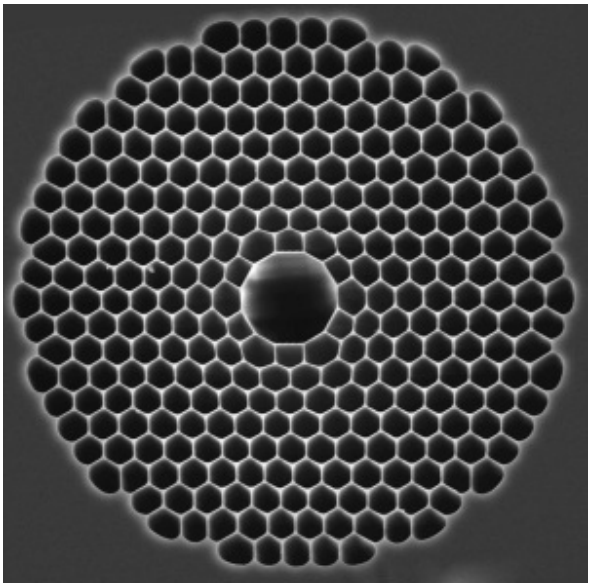

Fig. 1.2 Microscope picture of a fabricated hollow-core triangular PCF.

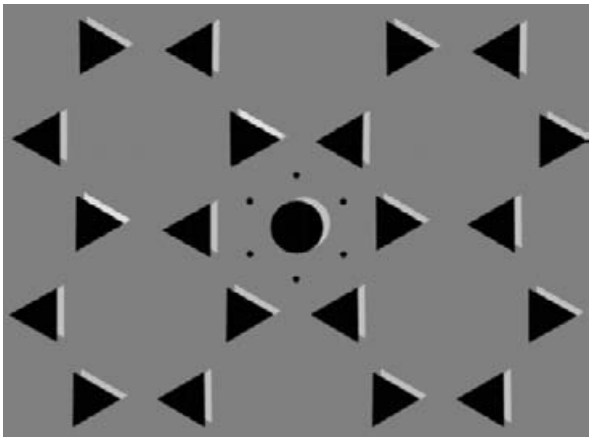

Fig. 1.3 Schematic of the cross-section of the first photonic bandgap PCF with a honeycomb air-hole lattice.

Hollow-core guidance had to wait until 1999, when the PCF fabrication technology had advanced to the point where larger air-filling fractions, required to achieve a PBG for air-guiding, became possible [2]. Notice that an air-guided mode must have $\beta/k < 1$, since thiscondition guarantees that light is free to propagate and form a mode within the hollow core, while being unable to escape into the cladding. The first hollow-core PCF, reported in Fig. 1.2, had a simple triangular lattice of air-holes, and the core was formed by removing seven capillaries in the center of the fiber cross-section. By producing a relatively large core, the chances of finding a guided mode were improved. When white light is launched into the fiber core, colored modes are transmitted, thus indicating that light guiding exists only in restricted wavelength ranges, which coincide with the photonic bandgaps [2].

1.1.4 Properties and applications of PCFs

Due to the huge variety of air-holes arrangements, PCFs offer a wide possibility to control the refractive index contrast between the core and the photonic crystal cladding and, as a consequence, novel and unique optical properties. Since PCFs provide new or improved features, beyond what conventional optical fibers offer, they are finding an increasing number of applications in ever-widening areas of science and technology.

1.1.5 Solid core fibers

Index-guiding PCFs, with a solid glass region within a lattice of air-holes, offer a lot of new opportunities, not only for applications related to fundamental fiber optics. These opportunities are related to some special properties of the photonic crystal cladding, which are due to the large refractive index contrast and the two-dimensional nature of the

microstructure, thus affecting the birefringence, the dispersion, the smallest attainable core size, the number of guided modes and the numerical aperture and the birefringence.

1.1.6 Highly birefringent fibers

Birefringent fibers, where the two orthogonally polarized modes carried in a single-mode fiber propagate at different rates, are used to maintain polarization states in optical devices and subsystems. The guided modes become birefringent if the core microstructure is deliberately made twofold symmetric, for example, by introducing capillaries with different wall thicknesses above and below the core. By slightly changing the air-hole geometry, it is possible to produce levels of birefringence that exceed the performance of conventional exceed the performance of conventional birefringent fiber by an order of magnitude. It is important to underline that, unlike traditional polarization maintaining fibers, such as bow

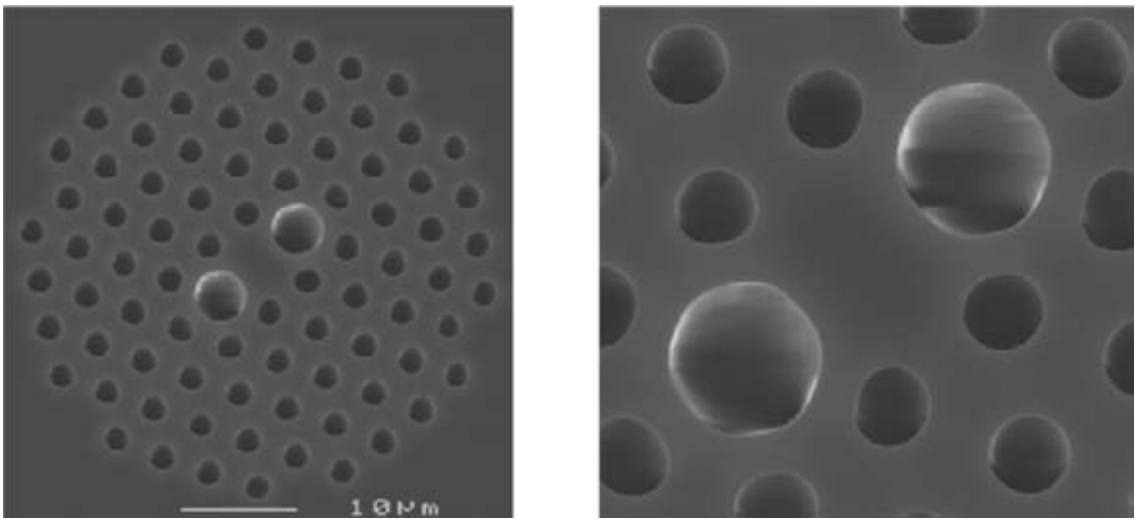

Fig. 1.4 Microscope picture of (a) the cross-section and (b) the core region of a highly birefringent triangular PCF.

tie, elliptical-core or Panda, which contain at least two different glasses, each one with a different thermal expansion coefficient, the birefringence obtainable with PCFs is highly insensitive to temperature, which is an important feature in many applications. An example of the cross-section of a highly birefringent PCF is reported in Fig. 1.4.

1.1.7 Dispersion tailoring

The tendency for different light wavelengths to travel at different speeds is a crucial factor in the telecommunication system design. A sequence of short light pulses carries the

digitized information. Each of these is formed from a spread of wavelengths and, as a result of chromatic dispersion, it broadens as it travels, thus obscuring the signal. The magnitude of the dispersion changes with the wavelength, passing through zero at 1.3 μm in conventional optical fibers. In PCFs, the dispersion can be controlled and tailored with unprecedented freedom. In fact, due to the high refractive index difference between silica and air, and to the flexibility of changing air-hole sizes and patterns, a much broader range of dispersion behaviors can be obtained with PCFs than with standard fibers. For example, as the air-holes get larger, the PCF core becomes more and more isolated, until it resembles an isolated strand of silica glass suspended by six thin webs of glass, as it is shown in Fig. 1.5. If the whole structure is made very small, the zero-dispersion wavelength can be shifted to the visible, since the group velocity dispersion is radically affected by pure

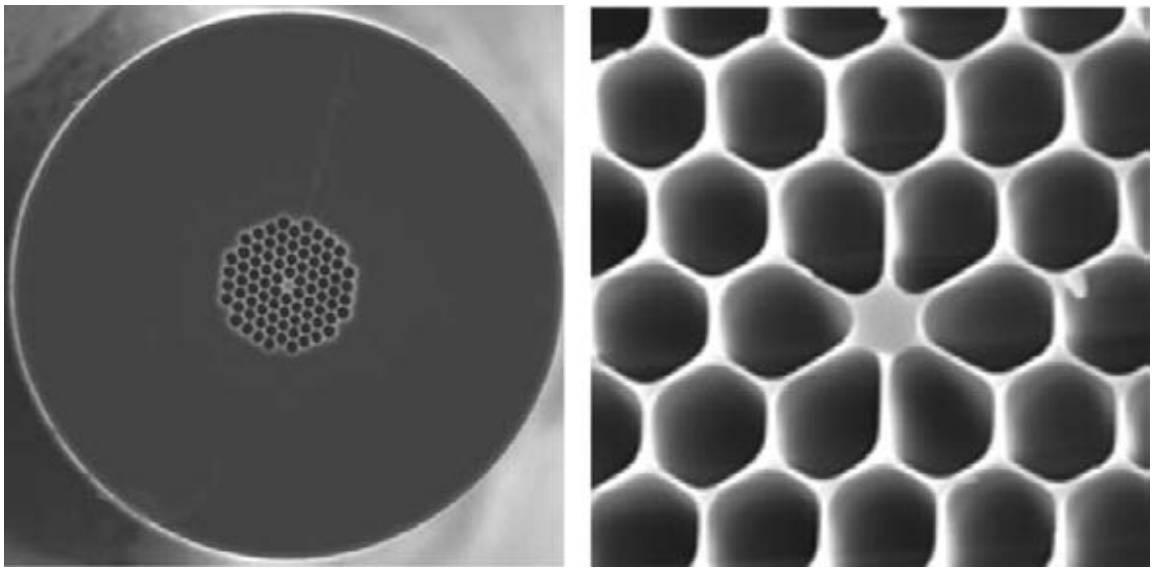

Fig. 1.5 Microscope picture of (a) the cross-section and (b) the core region of a highly nonlinear PCF.

waveguide dispersion. On the contrary, very flat dispersion curves can be obtained in certain wavelength ranges in PCFs with small air-holes, that is with low air-filling fraction. As an example, a dispersion-flattened triangular PCF with seven air hole rings, characterized by $\Lambda = 2.5$ μm and $d = 0.5$ μm, has been presented in [6].

1.1.8 Ultrahigh nonlinearities

An attractive property of solid-core PCFs is that effective index contrasts much higher than in conventional optical fibers can be obtained by making large air-holes, or by reducing the core dimension, so that the light is forced into the silica core. In this way a strong

confinement of the guided-mode can be reached, thus leading to enhanced nonlinear effects, due to the high field intensity in the core. Moreover, a lot of nonlinear experiments require specific dispersion properties of the fibers. As a consequence, PCFs can be successfully exploited to realize nonlinear fiber devices, with a proper dispersion, and this is presently one of their most important applications. An important example is the so-called supercontinuum generation, that is the formation of broad continuous spectra by the propagation of high power pulses through nonlinear media. The term supercontinuum does not indicate a specific phenomenon, but rather a plethora of nonlinear effects, which, in combination, lead to extreme spectral broadening. The determining factors for supercontinuum generation are the dispersion of the nonlinear medium relative to the pumping wavelength, the pulse length and the peak power. Since the nonlinear effects involved in the spectral broadening are highly dependent on the medium dispersion, a proper design of the dispersion properties can significantly reduce the power requirements. The widest spectra, in fact, can be obtained when the pump pulses are launched close to the zero dispersion wavelength of the nonlinear media.

1.1.9 Large mode area fibers

By changing the geometric characteristics of the fiber cross-section, it is possible to design PCFs with completely different properties, that is with large effective area. The typical cross-section of this kind of fibers, called large mode area (LMA) PCFs, consists of a triangular lattice of air-holes where the core is defined by a missing air-hole. An example of a triangular PCF is reported in Fig. 1.1. The PCF core diameter can be defined as $d = 2\Lambda - d$, which corresponds to the distance between opposite air-hole edges in the core region. When $d/\Lambda < 0.42$, the triangular PCF is endlessly single mode, that is, single mode at any wavelength [3]-[4]. In this condition it is the core size or the pitch that determines the zero-dispersion wavelength λ, the mode field diameter (MFD) and the numerical aperture (NA) of the fiber. LMA PCFs are usually exploited for high-power applications, since fiber damage and nonlinear limitations are drastically reduced. In particular, LMA fibers are currently used for applications at short wavelengths, that is in ultraviolet (UV) and visible bands, like the generation and delivery of high-power optical beams for laser welding and machining, optical lasers, and amplifiers, providing significant advantages with respect to traditional optical fibers [3].

1.1.10 Hollow core fibers

Hollow core PCFs have great potential, since they exhibit low nonlinearity [2] and high damage threshold [7]-[9], thanks to the air-guiding in the hollow core and the resulting small overlap between silica and the propagating mode. As a consequence, they are good candidates for future telecommunication transmission systems.

Another application, perhaps closer to fruition, which can successfully exploit these advantages offered by air-guiding PCFs, is the delivery of high-power continuous wave (CW), nanosecond and sub-picosecond laser beams, which are useful for marking, machining and welding, laser-Doppler velocimetry, laser surgery, and THz generation [10]. In fact, optical fibers would be the most suitable delivery means for many applications, but at present they are unusable, due to the fiber damage and the negative nonlinear effects caused by the high optical powers and energies, as well as to the fiber group-velocity dispersion, which disperses the short pulses [10]. These limitations can be substantially relieved by considering hollow-core fibers [10]. Moreover, air-guiding PCFs are suitable for nonlinear optical processes in gases, which require high intensities at low power, long interaction lengths and good-quality transverse beam profiles. Finally, the delivery of solid particles down a fiber by using optical radiation pressure has been demonstrated [2].

1.1.11 Loss mechanism

The most important factor for any optical fiber technology is loss. Losses in conventional optical fibers have been reduced over the last 30 years, and further improvement is unlikely to be reached. The minimum loss in fused silica, which is around 1550 nm, is slightly less than 0.2 dB/km. This limit is important, since it sets the amplifier spacing in long-haul communications systems, and thus is a major cost of a long-haul transmission system [1].

The optical loss α_{dB}, measured in dB/km, of PCFs with a sufficiently reduced confinement loss, can be expressed as

$$\alpha_{dB} = \frac{A}{\lambda^4} + B + \alpha_{OH} + \alpha_{IR}, \tag{1.1}$$

being A, B, α_{OH} and α_{IR} the Rayleigh scattering coefficient, the imperfection loss, and OH and infrared absorption losses, respectively. At the present time the losses in PCFs are dominated by OH absorption loss and imperfection loss [11].
Losses in hollow-core fibers are limited by the same mechanisms as in conventional fibers and in index-guiding PCFs, that is absorption, Rayleigh scattering, confinement loss, bend loss, and variations in the fiber structure along the length. However, there is the possibility to reduce them below the levels found in conventional optical fibers, since the majority of the light travels in the hollow core, in which scattering and absorption could be very low.

1.1.12 Confinement Loss

In both solid-core and hollow-core PCFs it is necessary to consider another contribution to the losses, that is the leakage or confinement losses. These are due to the finite number of

air-holes which can be made in the fiber cross section. As a consequence, all the PCF guided modes are leaky For example, in solid-core PCFs light is confined within a core region by the air-holes. Light will move away from the core if the confinement provided by the air-holes is inadequate. This means that it is important to design such aspects of the PCF structure as air-hole diameter and hole-to-hole spacing, or pitch, in order to realize low-loss PCFs. In particular, the ratio between the air-hole diameter and the pitch must be designed to be large enough to confine light into the core. On the other hand, a large value of the ratio makes the PCF multi-mode. However, by properly designing the structure, the confinement loss of single-mode PCFs can be reduced to a negligible level. Recently, several analyses have been performed in order to find the guidelines to design both index-guiding PCFs and PBG-based fibers with negligible leakage losses [12]-[14]. It has been demonstrated a strong dependence of the confinement losses on the number of air-hole rings, especially for fibers with high air-filling fraction. In particular, leakage losses can be significantly reduced by increasing the ring number [12]. Finally, simulation results have shown that in PBG fibers the leakage loss dependence on the number of air-hole rings is much weaker than in index-guiding PCFs, whereas the confinement losses exhibit a strong dependence on the position of the localized state inside the PBG [14].

The leakage loss of solid core PCFs, calculated according to the following formula, quickly decreases when the air-hole ring number or the air-hole diameter increases.

$$\text{Confinement Loss} = \frac{40\pi}{\ln(10)\lambda}\alpha \quad [\text{dB/m}], \tag{1.2}$$

where α is the imaginary part of the complex effective index. The reduction rate of the confinement loss increases in the same way with these geometric parameters. As expected, the loss decreases with larger Λ values for a fixed d/Λ. In this case, Λ and d are scaled in the same way, so a larger pitch corresponds to a larger silica core size and, as a consequence, to a higher field confinement. Since the field becomes less confined, the leakage loss increases with the wavelength. Moreover, the ring number affects the wavelength dependence, which is weaker for few air-hole rings [12].

1.1.13 Bending loss

As already stated, an alternative route to fabricate LMA fibers is offered by PCFs, which can be designed to be endlessly single-mode, unlike conventional fibers that exhibit a cut-off wavelength below which higher-order modes are supported. As for standard optical fibers, the practical achievable mode area in PCFs is limited by the macrobending loss [15]-[17]. Conventional fibers suffer additional loss if bent more tightly than a certain critical radius. For wavelengths longer than a certain value, that is the “long-wavelength bend loss edge,” all guidance is effectively lost. The same behavior is observed also in PCFs, which show even a “short-wavelength bend loss edge” [18], caused by bend-induced coupling

from the fundamental to the higher-order modes, which leak out of the core. In fact, at short wavelengths the guided mode is mainly confined into the silica [18] and when $\lambda << \Lambda$ the field can escape through the interstitial space between the neighboring air-holes. As a consequence, the fiber becomes more sensitive to bending. By considering triangular PCFs, shown in Fig. 1.1, a large air-filling fraction, that is a high d/Λ value, results in a better resistance to the bending loss, whereas the hole-to-hole spacing Λ roughly determines the position of the minimum of the bending loss curve, which roughly occurs at $\Lambda/2$ [16]. Since LMA PCFs are generally designed with Λ > 7-8 µm, the standard telecommunication window falls in the short-wavelength edge. In spite of that, it has been demonstrated that LMA PCFs exhibit bending losses comparable with those of similarly sized conventional fibers at 1550 nm [15]. Moreover, it has been experimentally shown that PCFs optimized for visible applications are more robust towards bending at any of the wavelengths from 400 to 1000 nm compared to a conventional fiber which is single-mode at the visible wavelengths [19]. PCFs with larger relative air-hole diameters, that is with higher d/Λ, are less sensitive to bending loss. However, the demand for single-mode operation and the need for large-mode size limits the increase of d/Λ, and other solutions must be adopted.

1.2 Fabrication Technology of PCFs

1.2.1 Stack and draw (SaD) technique

Fabrication of PCF, like the standard stack and draw (SaD) technique for conventional fiber fabrication, starts with a fiber preform. PCF preforms are formed by stacking a number of capillary silica tubes and rods to form the desired air/silica structure. This way of creating the preform allows a high level of design flexibility as both the core size and shape as well as the index profile throughout the cladding region can be controlled. When the desired preform has been constructed, it is drawn to a fiber in a conventional high-temperature drawing tower and hair-thin photonic crystal fibers are readily produced in kilometer lengths. Through careful process control, the air holes retain their arrangement all through the drawing process and even fibers with very complex designs and high air filling can be produced. Finally, the fibers are coated to provide a protective standard jacket that allows robust handling of the fibers. The final fibers are comparable to standard fiber in both robustness and physical dimensions and can be both striped and cleaved using standard tools. Though it seems that SaD is not suitable for the fabrication of more complex PCFs (like equiangular spiral PCFs) [20] other than hexagonal lattice PCFs, a technique has been proposed in [21] to adapt the standard SaD for complex structures.

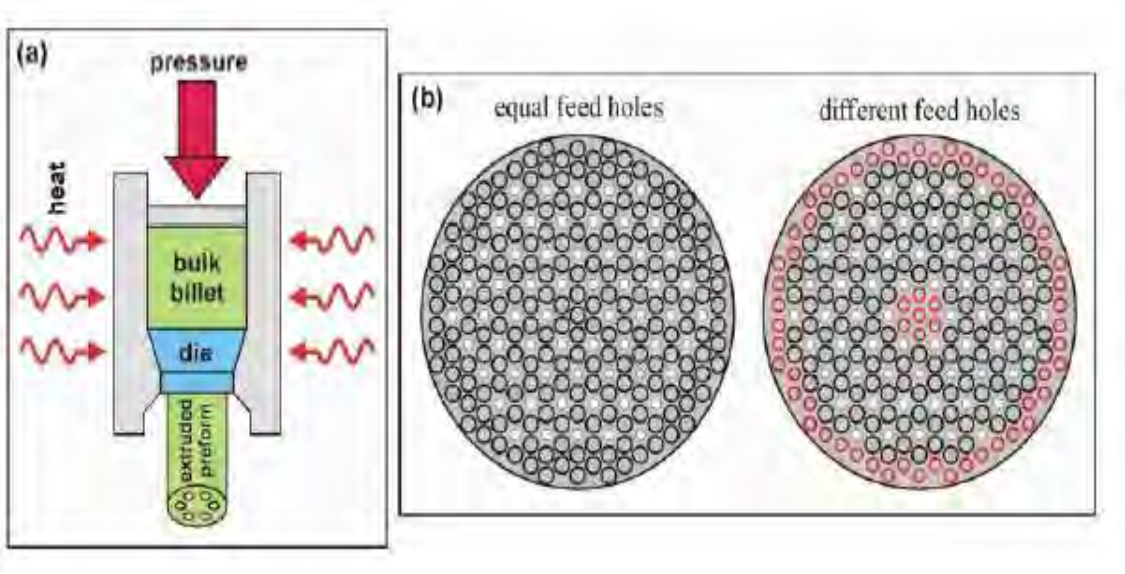

Fig. 1.6 (a) Sketch of extrusion process and (b) extrusion die concepts with equal and different size feed holes for a target preform structure having 60 holes (4 rings), white filled circles are blocking elements, black and red circles are feed holes.

1.2.2 Extrusion and filling technology

In this sub-section, a method of realizing complex PCF structures is presented.

Extrusion of complex performs:

The successful realization of a range of Micro structured optical fiber (MOF) depends on the use of complex air/glass structures within the fiber cross-section. Stacking, drilling and casting techniques have been used to fabricate structured preforms. These techniques all have limitations in the number of transverse features, hole shapes and configurations that can be achieved. A promising alternative technique is billet extrusion, which has been shown to be a versatile, reproducible single-step approach to fabrication of soft glass and polymer preforms with up to 12 holes. In [22], a new die design concept has been presented along with advances in the extrusion process control, which together overcome these issues to allow the first demonstration of truly complex extruded glass preforms. The flow of material within the die is explored for a range of structures and materials, and the efficacy of the extruded preforms for low-loss fiber fabrication is demonstrated. In Fig. 1.6, the overall process has been shown. This new die design allows great flexibility in the selection of the size, shape and distribution of the feed holes, which provides control of the material flow through the die in a manner that is truly scalable, reconfigurable, easily understood

and thus optimized. The die design also offers independent control of the hole shape and configuration within a preform for the first time.

Filling technology for multi-material PCF devices:

The optical properties of silica-air photonic crystal fiber (PCF) can be radically altered by filling its hollow channels with materials such as metals, polymers or semiconductors. Various different techniques have been used previously, including high-pressure chemical vapor deposition and pumping in of molten metal at high pressure. Chemical routes have the drawback that the end products of the reaction remain in the channels, often adversely affecting the optical properties. Filling with pure molten material does not suffer from this disadvantage, so that structures of high optical quality can readily be produced. In [23], the optical properties of PCFs in which one, two or more holes, adjacent to the core, are filled with semiconductors, glasses or metals by using a pressure cell technique have been reported. In Fig. 1.7, SEM image of fabricated a filled channel of PCF has been shown. This filling procedure allows the core mode to interact strongly with the material of the wire, leading to a strong modification of the light transmission.

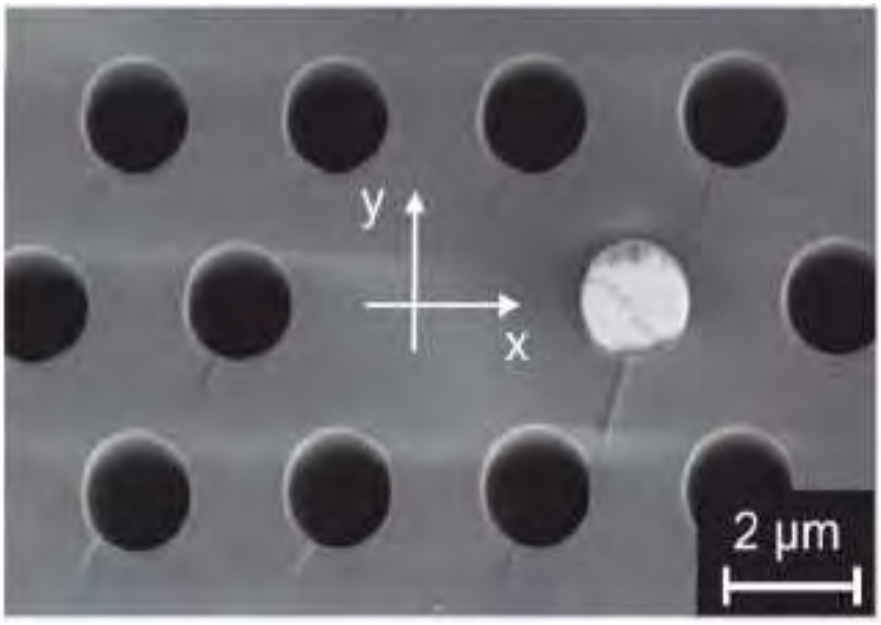

Fig. 1.7 Scanning-electron-micrograph image of a cleaved end-face of a germanium-filled endlessly single mode PCF. Germanium wire is on the right side (d_{wire} = 1.6 µm).

1.2.3 Sol-gel technique for fabricating irregular shaped PCF

Microstructured fibers possess an array of air columns embedded within a silica matrix, which extend along the z axis of the fiber. Several methods have been developed for the fabrication of microstructured fibers including the stack and draw of glass capillaries, sol-gel casting, prefrom drilling, extrusion, and even out gassing of a porous preform during draw. All of the aforementioned methods have various advantages and tradeoffs in terms of ease of fabrication, cost, design flexibility, material contamination, and precision. Here, we like to introduce the sol-gel casting technology towards the fabrication of irregular shaped microstructured optical fibers. The sol-gel casting technique was originally developed for the production of large jacket tubes for optical fiber preforms and has been modified for the fabrication of microstructured fiber [24]. A number of microstructured fibers fabricated using the sol-gel casting method, are shown in Fig. 1.8.

A mold containing an array of mandrel elements is assembled and then filled with colloidal silica dispersed at high pH with an average particle size of 40 nanometers. The pH is lowered causing the sol to gel. At the wet gel stage, the mandrel elements are removed, leaving air columns within the gel body. The gel body is then treated thermo chemically to remove water, organic and transition metal contaminants. The dried porous gel body is then sintered near 1600° C into viscous glass and subsequently drawn into fiber. The air holes are pressurized during draw to obtain the desired size and air-fill fraction. To maintain uniformity along the length of the preform, the mandrels are individually tensioned and the positioning and spacing is inspected and recorded with a digital camera. The aforementioned process is graphically represented in Fig. 1.9.

As a casting method, the sol-gel technique can fabricate any structure, which can be assembled into a mold. The hole size, shape and spacing may all be adjusted independently. By comparison, stack and draw methods are limited to closest-packed geometries such as triangular or honeycomb lattices and cannot easily generate circular patterns such as the one shown in Fig. 1.8 (d). Drilling methods allow adjustment of both the hole size and spacing, but are generally limited to a small number of holes and restricted to circular shapes. Furthermore, drilling of preforms leads to roughened surfaces along the air hole so that extra steps of etching and polishing of the inner surfaces are desired. Extrusion techniques provide design freedom, but are typically limited to soft glasses for which the material loss values are exceedingly high. Several designs such as fibers for higher nonlinearity, dispersion flattened designs require independent spacing, hole size or even noncircular holes. The sol-gel casting method provides additional design flexibility that will be necessary for such fibers. Sol-gel casting is not without its own set of challenges. The mandrel elements are removed during the wet gel stage, while the gel body is still fragile. Removal of the mandrels at this stage places strain on the gel and for gel bodies with air-fill

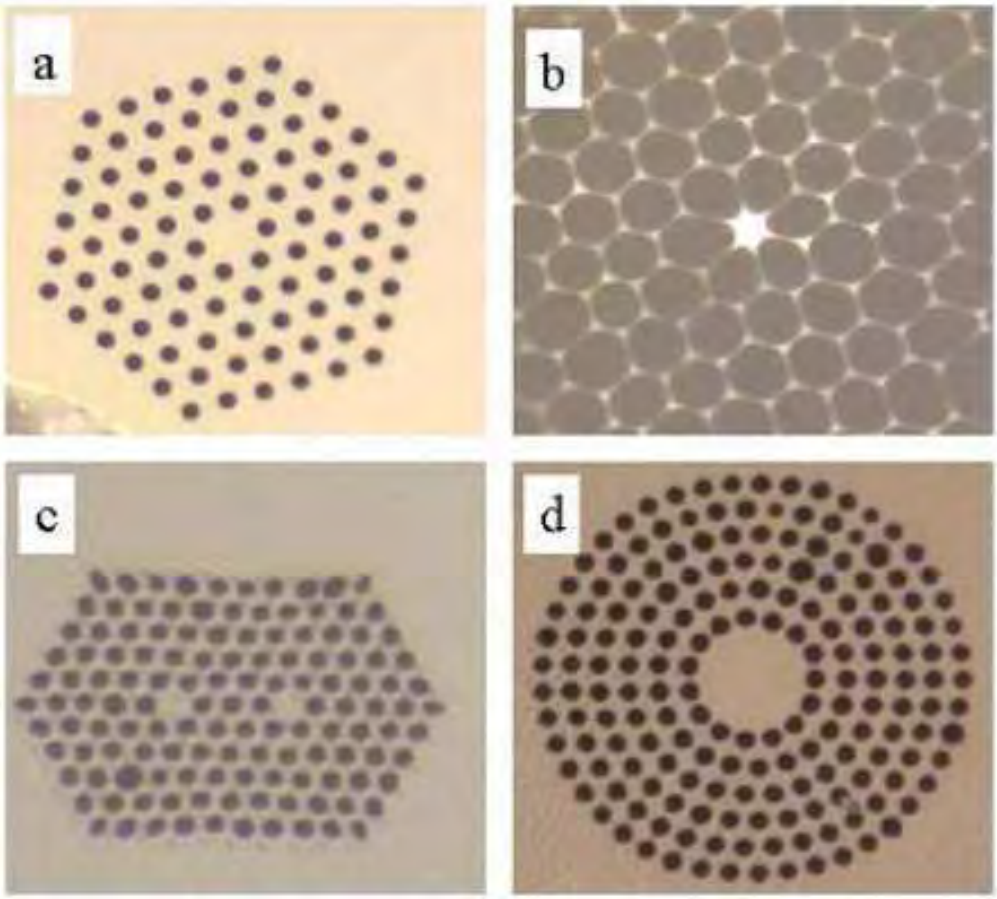

Fig. 1.8 Cross-sectional images of sol-gel derived microstructured fibers. The dark regions correspond to air columns while the bright regions are silica. a) endlessly single-moded design, b) high delta, highly nonlinear fiber, c) dual core structure and d) circular core microstructured fiber.

fractions >25%, cracking of the gel body is common and lowers the overall yield. Numerous microstructured fiber designs such as hollow core photonic band gap fibers or highly nonlinear fibers require air-fill fractions near 90%. To fabricate fibers with high air-fill fractions, the low air-fill fraction glass preforms are etched with HF uniformly along the length of the preform. An example of using HF etching to increase the air fill-fraction of a preform is shown in Fig. 1.10. Additionally, the air-fill fraction may be increased by pressurizing the air holes during draw. The larger design freedom, low-cost starting

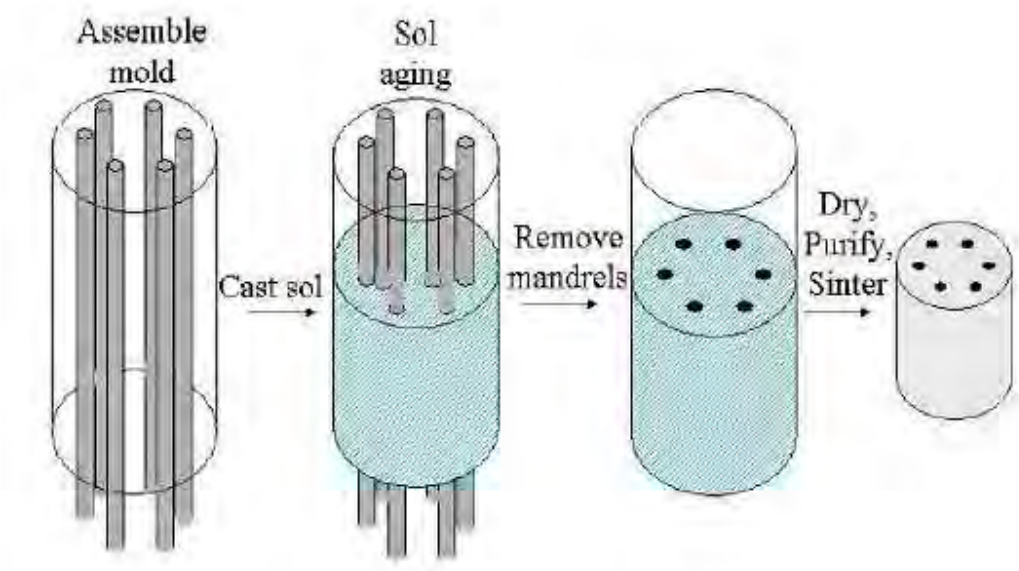

Fig. 1.9 Schematic representation of sol gel fabrication technique.

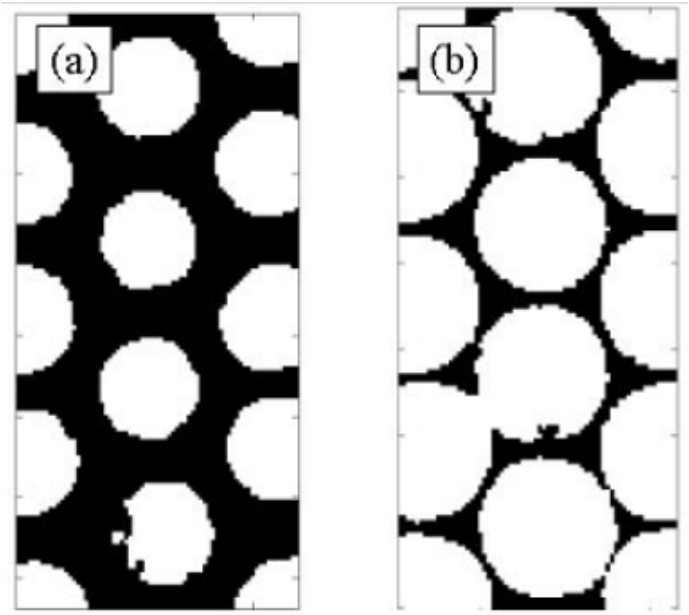

Fig. 1.10 Cross sectional images of a sol-gel derived microstructured prefrom before (a) and after (b) HF etching. The air-fill fraction in the cladding was increased from 46% up to 78%.

materials, dimensional precision, low material contamination and the ability to scale up to large preforms (> 10 km of fiber) makes this fabrication method an attractive approach towards high performance, low-cost microstructured fiber.

Before entering the main discussion containing the works done in this thesis, it is worth presenting a review on the literature of the related works reported in the past. As PCFs have a number of parameters which can be tuned over a large range, it is possible to control the contrast between core and cladding refractive indices. As a consequence, novel and unique optical properties may result. In order to increase the number of parameters that can be tuned to achieve desirable properties, arrangement of the cladding air holes other than the hexagonal one have been reported [20]. Here, an equiangular spiral (ES) design has been proposed to achieve ultrahigh nonlinearity. It is to be noted that we can alter only three parameters in hexagonal lattice PCF: pitch, Λ, cladding air hole diameter, d and number of air hole rings, N in the cladding. On the other hand, in ES-PCF, we have more than three parameters to alter.

1.3 Literature Review

1.3.1 Literature on Bend Loss Formula

After [20], not much work has been done on ES-PCF. In order to assess its applicability in optical fiber communication systems, a further investigation on its characteristic properties needs to be carried out. With this view, the primary goal of this thesis is to obtain useful properties using ES-PCF through numerical analysis. Before entering the numerical analysis, a modification of the renowned bend loss formula, originally developed for step index fibers proposed by Marcuse [25], is suggested. This modified formula improves the bend loss estimation in step index fibers and it is applicable equally well for PCFs. Finally, a novel quasi-PCF is proposed which is different from both hexagonal lattice PCF and ES-PCF and its worth is shown through a number of applications.

Various theoretical methods exist to predict curvature loss in optical waveguides. The usual approach is to use a simplified formula introduced by Marcuse [25], applicable to weakly guided waveguides, including most optical fibers, for sufficiently large radii of curvature. This formula agrees well with experiment for single-mode fiber, after adjustments are made for bend-induced stress [26]. However, for multimode fiber it can be quite inaccurate [27] as it overestimates bend loss at a large amount. Other analytical bend loss formulae are similarly limited, in that none are known to reliably predict bend loss in multimode fibers. This has become a significant problem with the development of the coiled multimode fiber amplifier [28], which uses bend loss to strip out the higher order fiber modes, and thereby achieve single-mode, large mode area operation. Optimizing these devices, and understanding their ultimate limitations, requires that mode-dependent bend loss be

predicted accurately. A modification of Marcuse's simplified bend loss formula is suggested by Schermer [27] but it underestimates the bend loss at a similar large amount for multimode fibers. Though the authors identified the reason behind this, the remedy against requires a simulated data which weakens the justification of using an analytical formula. Thus, a formula for predicting bend loss for multimode fibers having greater accuracy is worth developing.

1.3.2 Evolution of Equiangular Spiral (ES) PCF

As numerous air holes are arranged in the cladding of PCFs, it is possible to obtain a tightly confined optical mode with small effective area and large nonlinearity which coupled with flat, anomalous dispersion has led to successful broadband supercontinuum generation (SCG) in hexagonal lattice PCFs (H-PCFs) [29]. In order to achieve even larger nonlinearity, ES-PCF was coined by Agrawal et. al. in 2009 [20]. Fig. 1.11 shows the air hole pattern in H-PCF and ES-PCF. In ES-PCF, the cladding air hole pattern mimics the "spira mirabilis" [equiangular spiral (ES)] and appears in nature in nautilus shells and sunflower heads. It leads to efficient feature growth/packing of seeds and the growth of this type of curve does not alter the shape of the curve. In the ES-PCF, each arm of air holes forms a single ES of radius r_o, angular increment θ, and the radius of

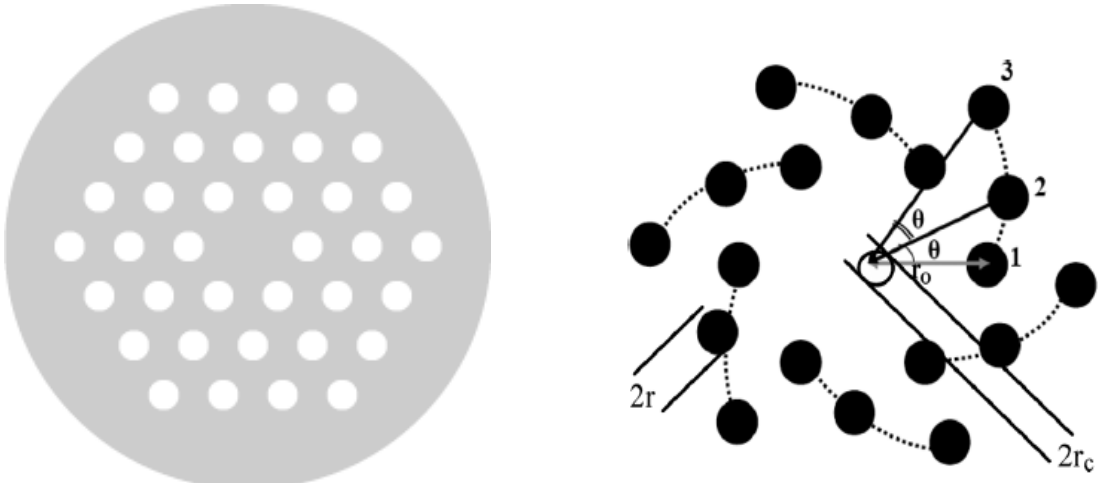

(a) (b)

Fig. 1.11 Air hole arrangements in the cladding of (a) a hexagonal lattice PCF, (b) an equiangular spiral PCF.

each air hole is fixed at r. In the ES, the radii drawn at any equal intervals of θ are in a geometric progression; therefore, the pitch (distance between air holes) in a ring increases with the ring number.

One can have an intuitive idea from Fig. 1.11(b) that it is possible to obtain a more tightly confined optical mode in the core region with the help of the compact air hole arrangement of ES-PCF than that of H-PCF. This unique feature is exploited in [20] to achieve a very high nonlinearity higher than those of [29].

After this work, nothing much is reported on ES-PCF in the literature. A detailed analysis of other characteristics of ES-PCF such as: dispersion profile, singlemodedness, birefringence, confinement loss, bending properties etc may worth some value. With this motivation behind, most of the works of this thesis are related to ES-PCF.

1.3.3 Some Recent Works on Photonic Crystal Fibers

In this section, some recent developments and applications of H-PCFs are discussed. Based on the discussion, the objectives of the thesis will be stated.

Residual dispersion compensation

The PCFs have several characteristics that permit their use as an excellent transmission medium for short and large distances. A long-haul optical fiber transmission system requires small but nonzero flattened dispersion characteristics [30]. So, a dispersion management scheme should be there to nullify the accumulated positive dispersion in the system. For this purpose, a fiber having a large negative dispersion called dispersion compensating fiber (DCF) has to be introduced as a part of the communication system [31]-[33]. A flat negative dispersion of about −98.3 ps/nm-km with absolute dispersion variation of about 1.1 ps/nm-km was reported over *S*+*C*+*L* wavelength bands in [33]. The design in [31] exhibits ultraflattened negative dispersion over *S*+*C*+*L*+*U* wavelength bands and average dispersion of about −179 ps/nm-km with an absolute dispersion variation of 2.1 ps/nm-km over 1480 nm to 1675 nm (195 nm bandwidth). More recently, a genetic algorithm based optimization technique has been reported in [28] to achieve a flattened negative dispersion over E+*S*+*C*+*L*+*U* wavelength bands with an average dispersion of −212 ps/nm-km with a dispersion variation of 11 ps/nm-km by employing a small Ge-doped core at the center. All these analyses are done on the microstructured fiber with hexagonal-lattice of air holes. But, the polarization issue was not considered anywhere.

Liquid crystal infiltrated PCFs

Nematic liquid crystals are anisotropic materials consisting of rod-like molecules whose axis coincides with the anisotropy's optical axis. When confined in closed cylindrical cavities in the absence of external stimuli, the liquid crystal's director distribution is determined by the physics of elastic theory and the anchoring conditions at the cavity's surface [34]. Under the application of a static electric field the director's orientation can be controlled, since the liquid crystal molecules tend to align their axis according to the applied field. In an alternative approach, the properties of nematic liquid crystals can be tuned thermally owing to the dependence of the refractive index values on temperature. In [35], the authors proposed and theoretically analyze a novel photonic crystal-liquid crystal (PC-LC) core fiber design. The fiber consists of a triangular lattice of air holes opened in an optical glass enhanced by a hollow cylindrical core filled by common nematic liquid crystal, thus embodying both the design tailoring advantages of common holey fibers and the intrinsic controllable anisotropy of the liquid crystal material. The fiber's characteristics, namely modal dispersion curves, birefringence and modal intensity profiles are studied for a uniform distribution of the nematic director. Though this particular director orientation is in a sense ideal, it can be thought as the limiting orientation of more realistic patterns, and, in addition, it demonstrates the salient points for this special class of fibers. It is verified that the fiber can function in a single-mode/single-polarization operation (selectively HE_x or HE_y), it can exhibit high- or low-birefringence, or switch between on-off states, depending on the structural design.

Mode degeneration in bent PCFs

In many practical applications, PCFs encounter bends, twists, and stress. It is well known that when a fiber is bent, the modal field shifts in the outward direction and suffers from radiation loss. One of the main disadvantages suffered by standard silica fiber has been that significant bending loss arises due to the low index contrast between the core and the cladding when compared to that of a PCF. However, sometimes the need for a small bending radius may be unavoidable in a specific optical waveguide: on the other hand, bending effects have also been exploited to design functional devices such as ring resonators, arrayed waveguide filters, optical delay lines, S-bend attenuators, to suppress higher order modes etc. [36]-[38]. Similarly, efforts have also been expended to better understand the behavior of bent PCFs [39]. The authors in [40] report on the variation of the key modal parameters in PCFs that arises from the change in the coupling between the fundamental core mode and the localized cladding mode across the air holes.

Bend insensitive single mode PCFs with large effective area

The high leakage loss of a bent PCF can be minimized to an acceptable level by appropriately choosing the air hole diameters. But, apart from low bending loss, other two conditions are to be met simultaneously for practical applications [41]. These are, the higher order modes which are usually unavoidable in a low bending loss PCF, should be suppressed and the effective mode area of the fundamental mode of the PCF should be very close to that of a typical single mode fiber (SMF) to minimize the splice loss. This is a challenge to meet these three conditions simultaneously as they are usually conflicting. However, several such designs have been reported in the literatures [42]-[45] for hexagonal lattice PCFs.

1.4 Objectives of the Thesis

The simplified bend loss formula developed by Marcuse overestimates the bend loss slightly in single mode fibers and largely in multimode fibers. An improvement of the formula has been proposed in [27], but it underestimates the bend loss especially for large mode area fibers. Not much work has been done after this to improve the accuracy of the formula especially for PCFs.

1. The objective of this thesis is to improve the accuracy of bend loss calculations for conventional step index (SI) fibers. The estimated bend losses will be compared to the simulated and experimental results to validate its accuracy. Finally, the technique will be applied to the newly designed ES-PCF.

2. As indicated in [46], a central air hole in the PCF structure is useful to shift the dispersion curve up and down. Also, the large number of variables that can be altered in an ES-PCF may help in achieving a flat large negative dispersion profile over a wide wavelength range. With this motivation behind, an ES-PCF with central air holes will be proposed to achieve a very large negative flat dispersion profile even more negative than those of cited over the telecommunication wavelength bands.

3. Infiltrating liquid crystal in the air holes of a PCF results interesting phenomena such as single polarization or high birefringence [35]. Exploiting this technique in ES-PCF, a single polarization fiber will be designed to achieve large negative dispersion profile with a flatness more than the reported ones.

4. When a fiber is bent, the index distribution of the core and cladding is altered that can be determine by the technique of conformal mapping [27]. It can be shown that there exists some cladding modes confined between the air hole rings in the cladding in a bent PCF. Though the analysis of mode degeneration between the fundamental core mode and a cladding mode is carried out in [40] for H-PCFs, a detailed analysis of the bending

properties especially the cladding modes on ES-PCFs are yet to be done. In this paper, the ES-PCF will be investigated to observe the coupling between fundamental core mode and cladding mode.

5. Bend insensitive single mode fibers with large effective modal area are necessary for fiber to the home applications [44], for high speed WDM communications [42] and in fiber lasers where even larger effective area is needed to handle high power with reduced nonlinearity [45]. As most of the fibers reported for these applications are based on triangular lattice PCFs (H-PCFs), this thesis concentrates on finding a bend insensitive single mode ES-PCF with large effective area. Also, there is a subsidiary target of developing a new design of circularly arranged air hole PCF for the same applications.

1.5 Scope of the Thesis

This thesis dissertation is arranged in the following manner: chapter one (this chapter) is composed of the basic principles of light propagation in PCFs. Also, Review of literature of the recently reported works on PCF especially on spiral PCF and objective of this thesis have been presented in this chapter. Chapter two is composed of the full vectorial Finite Element Method (FEM) adopted to obtain the optical mode of the PCF numerically. Development of a modified bend loss formula will be depicted in chapter three. Chapter four consists of the step by step design and analysis procedure to obtain some useful characteristics using primarily spiral PCF and also a novel circular lattice PCF. Finally, chapter five contains the concluding remarks.

CHAPTER 2
FULL VECTORIAL FINITE ELEMENT METHOD

Photonic crystal fibers (PCFs) which are characterized by a cladding of air capillaries most commonly arranged in a triangular lattice, have been a key topic of research in the field of optical fiber communication. The form of the central defect core is responsible for the PCF's light guiding mechanism: index guiding in the case of a solid core, or band gap-guiding when low-index or hollow cores are used. Numerical software plays an important role in the design of waveguides and fibers. For a fiber cross section, even the simplest shape is difficult and cumbersome to deal with analytically. As this thesis is concentrated on index guiding PCF, the methodology of simulating the different characteristics of PCF will be discussed here.

Though the silica glass (SiO_2) fiber is forming the backbone of modern communication systems now a days, other materials have been used too as the background of PCF in this thesis, to obtain useful properties like flat and large negative dispersion profile, high birefringence, low bending loss, large effective modal area etc. The refractive index of the core, n_1 is taken as the index of pure material or it may be higher when doped with some other material at a certain molar fraction. The cladding consists of a number of air holes with a background of core material. The effective index of the cladding, n_2 determined as the fundamental space filling mode [47] is lower than n_1 ensuring that there is at least one confined mode for a single mode PCF and more than one mode for a multimode PCF. For a confined mode, there is no energy flow in the radial direction, thus the wave must be evanescent in the radial direction in the cladding. This is true only if the effective index of the confined mode, n_{eff} is greater than n_2. On the other hand, the wave cannot be radially evanescent in the core region. Thus, $n_1 > n_{\text{eff}} > n_2$. The waves are more confined when n_{eff} is close to the upper limit in this interval. The refractive indices change with the change in wavelength. These different values of indices at different wavelengths are obtained from the corresponding Sellmeier equation. The radius of the cladding is chosen to be large enough so that the field of confined modes is zero at the exterior boundaries.

The optical mode analysis is made on a cross-section in the *x-y* plane of the fiber. The wave propagates in the *z*- direction and has the form

$$\overline{H}(x, y, z, t) = \overline{H}(x, y)e^{j(\omega t - \beta z)} \tag{2.1}$$

where ω is the angular frequency and β the propagation constant. An eigenvalue equation for the magnetic field, $\overline{H}$ is derived from Helmholtz equation

$$\nabla \times (n^{-2}\nabla \times \overline{H}) - k_o^2 \overline{H} = 0 \tag{2.2}$$

which is solved for the eigenvalue $\lambda = -j\beta$.

As boundary condition along the outside of the cladding, the magnetic field is set to zero. As the amplitude of the field decays rapidly as a function of the radius of the cladding this is a valid boundary condition.

2.1 Formulation in Detail

The Electric field intensity, $\overline{E}$ and the Magnetic field intensity, $\overline{H}$ associated with the fiber to be simulated can be written as,

$$\overline{E}(x, y, z, t) = \overline{E}(x, y)e^{j(\omega t - \beta z)} \tag{2.3}$$

$$\overline{H}(x, y, z, t) = \overline{H}(x, y)e^{j(\omega t - \beta z)} \tag{2.4}$$

The constant β in the exponential is the propagation constant. In those cases where β is a complex number, we can define the attenuation constant $\alpha = -\mathrm{Im}(\beta)$, which expresses how the wave decreases, $e^{-\alpha z}$.

The following formulations are derived from Maxwell-Ampère's and Faraday's laws:

$$\nabla \times \overline{H} = j\omega\varepsilon\overline{E} \tag{2.5}$$

$$\nabla \times \overline{E} = -j\omega\mu\overline{H} \tag{2.6}$$

These equations are used in the perpendicular electromagnetic waves application mode in the software COMSOL Multiphysics [48]. Here, $\lambda = -\delta_z - j\beta$ is calculated as the eigenvalue.

The derivation in the following section assumes that the eigenvalue is a complex number with the real part equal to zero, $\lambda = -j\beta$. All occurrences of $j\beta$ or $-\beta^2$ can be replaced with $\delta_z + j\beta$ or $(\delta_z + j\beta)^2$. This is only a simplification to make the expressions easier to read. Perpendicular hybrid-mode waves treats the case of transversal fields and inhomogeneous materials. The formulation for perpendicular hybrid-mode waves is shown below:

Here, we let $\varepsilon_{\mathrm{rct}}$ and μ_{rt} denote the 2-by-2 tensors in the transversal *xy*-plane,

$$\varepsilon_{rc} = \begin{bmatrix} \varepsilon_{\mathrm{rcxx}} & \varepsilon_{\mathrm{rcxy}} \\ \varepsilon_{\mathrm{rcyx}} & \varepsilon_{\mathrm{rcyy}} \end{bmatrix} \qquad \mu_r = \begin{bmatrix} \mu_{rxx} & \mu_{rxy} \\ \mu_{ryx} & \mu_{ryy} \end{bmatrix} \tag{2.7}$$

Here, $\varepsilon_{\mathrm{rct}}$ and μ_{rt} are the complex relative permittivity and permeability in the transversal *xy*-plane. Now, the magnetic field intensity, $\overline{H}$ can be expressed as,

$$\overline{H}(x, y, z) = \overline{x}H_x + \overline{y}H_y + \overline{z}H_z = \overline{H}_t + \overline{z}H_z \tag{2.8}$$

Here, $\overline{H}_t$ is the transverse component of the magnetic field intensity, $\overline{H}$.

From Maxwell's equations,

$$\nabla.\overline{B} = 0 \tag{2.9}$$

Here, $\overline{B}$ is the magnetic flux density. Expressing equation (2.9) in terms of magnetic field intensity, $\overline{H}$, we get,

$$\nabla_t.\mu_{rt}\overline{H}_t - j\beta\mu_{rzz}H_z = 0 \tag{2.10}$$

Now, equation (2.2) can be expressed as,

$$\nabla\times(\varepsilon_{rc}{}^{-1}\nabla\times\overline{H}) - k_o^2\mu_r\overline{H} = 0 \tag{2.11}$$

Here, ε_{rc} is the complex permittivity and μ_r is the real part of the complex permeability. We get the following equation from (2.11) using (2.8),

$$\nabla_t\times(\varepsilon_{rczz}{}^{-1}\nabla_t\times\overline{H_t}) - j\beta\varepsilon_{rct}\nabla_t H_z - \left(k_0^2\mu_{rt} - \beta^2\varepsilon_{rct}\right)\overline{H}_t = 0 \tag{2.12}$$

Now, substituting equation (2.10) into equation (2.12) we get,

$$\nabla_t\times(\varepsilon_{rczz}{}^{-1}\nabla_t\times\overline{H_t}) - \varepsilon_{rct}\nabla_t\left(\mu_{rzz}^{-1}\nabla_t.\mu_{rt}H_t\right) - \left(k_0^2\mu_{rt} - \beta^2\varepsilon_{rct}\right)\overline{H}_t = 0 \tag{2.13}$$

We can solve this equation as an eigenvalue problem both for $\lambda = -j\beta$ and $\lambda = -j\omega$. In the first case it becomes an eigenmode problem and in the second case it becomes an eigenfrequency problem. For this thesis, eigenmode problem is of interest.

2.1.1 Use of hybrid edge-nodal triangular elements

Various elements are being developed to solve different microwave and optical problems through FEM. The hybrid type edge/nodal triangular as well as rectangular elements are such special elements, and have found a great deal of practical applications for hybrid mode analysis. In this work, we used triangular type hybrid element which is composed of edge and nodal elements, where edge elements model the transverse field ensuring tangential continuity along the element interfaces and nodal elements model the axial fields. As the edge elements assign the degrees of freedom to the edges, they allow the field to change its direction abruptly and thus are capable of modeling the field properly at sharp edges at

which singularity occurs. With hybrid elements, the FEM overcomes all the shortcomings, that clouded many of the analyses before.

A hybrid edge-nodal triangular element which is used in our calculation is shown in Fig. 2.1. Here the edge element has three tangential unknowns, ϕ_{t1} to ϕ_{t3}, and a nodal (conventional Lagrange) element has three axial unknowns, ϕ_{z1} to ϕ_{z3}. They are combined to form an element as shown in Fig. 2.1(c) and is used in our analysis.

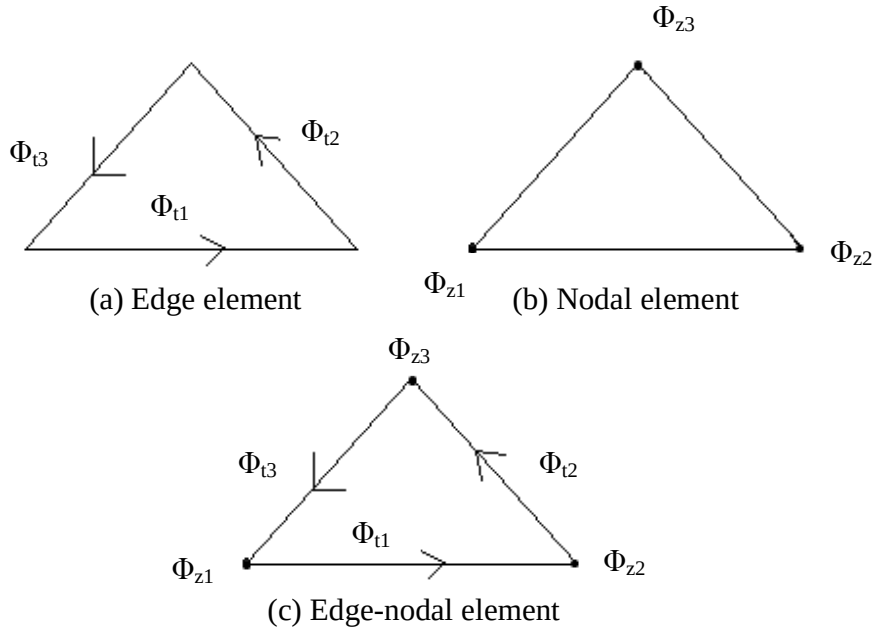

Fig. 2.1 Hybrid edge-nodal triangular element.

2.2 Boundary and Interface Conditions

The interior boundaries of the cross-sectional geometry of the PCF are set at continuity boundary conditions. The outermost boundary of the cross-section is set at perfect electric conductor boundary condition when solving for magnetic field intensity, $\overline{H}$. Perfect magnetic conductor boundary condition is used when solving for electric field, $\overline{E}$. This is a valid boundary condition as the radius of the geometry is chosen large enough for the electric or magnetic field to decay to zero.

2.2.1 Perfect magnetic conductor

The perfect magnetic conductor boundary condition,

$$\bar{n} \times \overline{H} = 0$$

sets the tangential component of the magnetic field to zero at the boundary. Also, it implies that, $\bar{n}.\bar{D} = 0$ for a perfect magnetic conductor.

2.2.2 Perfect electric conductor

The perfect magnetic conductor boundary condition,

$$\bar{n} \times \bar{E} = 0$$

sets the tangential component of the electric field to zero at the boundary. Also, it implies that, $\bar{n}.\bar{B} = 0$ for a perfect electric conductor.

2.2.3 Continuity

The continuity boundary condition,

$$\bar{n} \times \left(\bar{H}_1 - \bar{H}_2\right) = 0$$

$$\bar{n} \times \left(\bar{E}_1 - \bar{E}_2\right) = 0$$

is the natural boundary condition ensuring continuity of the tangential components of the electric and magnetic fields.

2.2.4 Perfectly Matched Layer (PML)

A perfectly matched layer is an artificial boundary condition implying perfect absorption of incident field. This boundary condition is required for approximating infinite zone beyond the waveguide outer edge to a finite domain of numerical analysis. Effect of PML on numerical solutions obtained will be more prominent when confinement of field in the PCF is weak. This layer can also be utilized to find out the complex part of effective index.

There are several different PML formulations. However, all PML's essentially act as a lossy material. The lossy material, or lossy layer, is used to absorb the fields traveling away from the interior of the grid. The PML is anisotropic and constructed in such a way that there is no loss in the direction tangential to the interface between the lossless region and the PML. However, in the PML there is always loss in the direction normal to the interface.

The PML was originally proposed by J. P. Berenger in 1994 [49]. In that original work he split each field component into two separate parts. The actual field components were the sum of these two parts but by splitting the field Berenger could create an (non-physical) anisotropic medium with the necessary phase velocity and conductivity to eliminate reflections at an interface between a PML and non-PML region.

Arguably the best PML formulation today is the Convolutional-PML (CPML). CPML constructs the PML from an anisotropic, dispersive material. CPML does not require the fields to be split and can be implemented in a relatively straightforward manner.

The PML region can be viewed as a perfect absorber with a certain magnitude of conductivity. However, the optimized conductivity is calculated from certain sets of equations. In our work, we have considered cylindrical PML available in the commercial software.

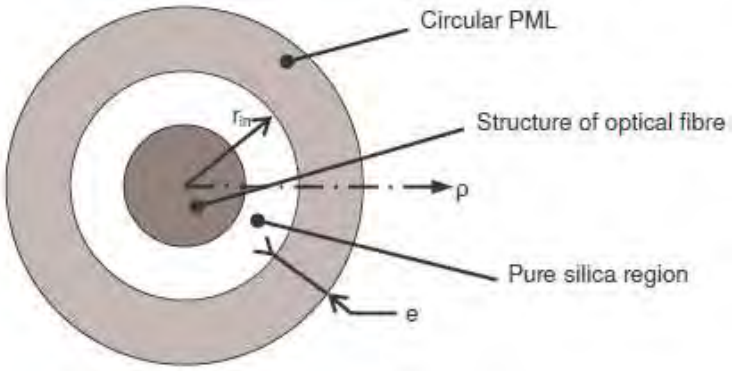

Fig. 2.2 PML region surrounding the waveguide structure.

Formulation of wave equations in the PML region can be done after rigorous analysis,

$$\bar{n}\times\bar{H} = jwn^2 s\bar{E}$$
$$\bar{n}\times\bar{E} = -jw\mu_0 s\bar{H}$$
$$s = 1 - j\frac{\sigma_e}{wn^2\varepsilon_0} = 1 - j\frac{\sigma_m}{w\mu_0} \qquad (2.14)$$

Where,
E: Electric Field
H: Magnetic Field
σ_e and σ_m**:** Electric and magnetic conductivities of PML, respectively.

e is the thickness of the PML layer which is ideally a multiple of the operating wavelength. To avoid numerical reflection, conductivity in the PML region is graded to a peak value rather than an abrupt rise as shown in Fig. 2.2.

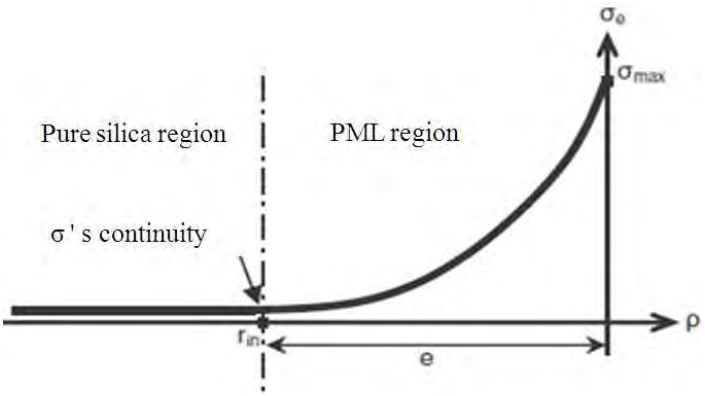

Fig. 2.3 Grading of PML conductivity.

PML parameter s becomes,

$$s = \begin{cases} 1 - j \cdot \kappa \cdot \left(\dfrac{\rho - r_{in}}{e} \right)^2, & \text{in PML region} \\ 1, & \text{in others regions} \end{cases}$$

where κ is defined for λ (wavelength) by

$$\kappa = \frac{3\lambda}{4\pi n e} \cdot \ln\left(\frac{1}{R}\right) \tag{2.15}$$

where R is the reflection coefficient of electromagnetic field from the interface to be minimized. For a perfectly matched condition to secure zero reflection from the interface, we can write,

$$\frac{\sigma_e}{\varepsilon_0 n^2} = \frac{\sigma_m}{\mu_0} \tag{2.16}$$

Now reflection coefficient is defined as below [50],

$$R = \exp\left[-2 \frac{\sigma_{max}}{\varepsilon_0 c n} \int_0^d \left(\frac{\rho}{d} \right)^m d\rho \right] \tag{2.17}$$

From this, maximum conductivity is defined as below,

$$\sigma_{\max} = \frac{m+1}{2}\frac{\varepsilon_0 cn}{d}\ln\left(\frac{1}{R}\right) \tag{2.18}$$

Here, *m* is the order of polynomial for grading conductivity. These equations imply that, a minimum reflection will occur for a maximum conductivity. However, numerical error terms imply that there is an optimum magnitude of reflection for accurate propagation constant. A stable value of complex effective index can be obtained by altering the thickness of PML and distance of PML from centre of the PCF.

CHAPTER 3
BEND LOSS FORMULA FOR OPTICAL FIBERS

In many practical applications, optical fibers encounter bends and twists. It is also well known that when a fiber is bent, the modal field shifts in the outward direction and suffers from radiation loss.

To study arbitrary bends in PCFs, various methods are used. Among them conformal transformation [27] is the most famous. In this transformation, a curved dielectric waveguide is converted to its equivalent straight one with a modified index profile. The coordinate transformation maps the refractive index profile of a bent optical fiber *n(x,y)* to its equivalent straight optical fiber's refractive index $n_{eq}(x,y)$ using the following formula,

$$n_{eq}(x,y) = n(x,y)[1+\frac{x}{R}] \tag{3.1}$$

Here, R is the radius of the curvature and x is the distance from the center of the waveguide. This equation is valid for the range $x \ll R$, which is well within the ranges considered in this paper. When a waveguide is bent, change in the refractive index due to the stress-optic effect should also be taken into account. This can be done by replacing the bending radius R by effective bend radius, R_{eff} where, $\frac{R_{eff}}{R}$ = 1.28 [27]. Thus, Eqn. (3.1) can be rewritten as,

$$n_{eq}(x,y) = n(x,y)[1+\frac{x}{R_{eff}}] \tag{3.2}$$

3.1 Simplified Bend Loss Formula

The simplified bend loss formula (the word 'simplified' indicates that this formula is a simplified form of a more complex one) for step index optical fibers reported by Marcuse is as follows,

$$2\alpha = \frac{\pi^{\frac{1}{2}}\kappa^2 \exp\left(-\frac{2\gamma^3 R}{3\beta_z^2}\right)}{2R^{\frac{1}{2}}\gamma^{\frac{3}{2}}V^2 K_{m-1}(\gamma a)K_{m+1}(\gamma a)} \tag{3.3}$$

Here, a is the core radius, 2α is the power loss coefficient, κ and γ are the field decay rates in the core and cladding defined as,

$$\kappa = \sqrt{k_{core}^2 - \beta_z^2} \tag{3.4}$$

$$\gamma = \sqrt{\beta_z^2 - k_{clad}^2} \tag{3.5}$$

and the K terms are modified Bessel functions, V is the normalized frequency, k_{core} is the core propagation constant, k_{clad} is the cladding propagation constant and β_z is the effective propagation constant of the fundamental mode (the z- axis being the direction of propagation). Bend loss in units of dB/length is obtained by multiplying 2α by the factor 4.343.

3.2 Modification of Simplified Bend Loss Formula

Schermer et. al. argues in [27] that the bending radius R in Eqn. (3.3) should be replaced by R_{eff} to include the elastooptic effect due to bending resulting in,

$$2\alpha = \frac{\pi^{\frac{1}{2}} \kappa^2 \exp\left(-\frac{2\gamma^3 R_{eff}}{3\beta_z^2}\right)}{2R_{eff}^{\frac{1}{2}} \gamma^{\frac{3}{2}} V^2 K_{m-1}(\gamma a) K_{m+1}(\gamma a)} \tag{3.6}$$

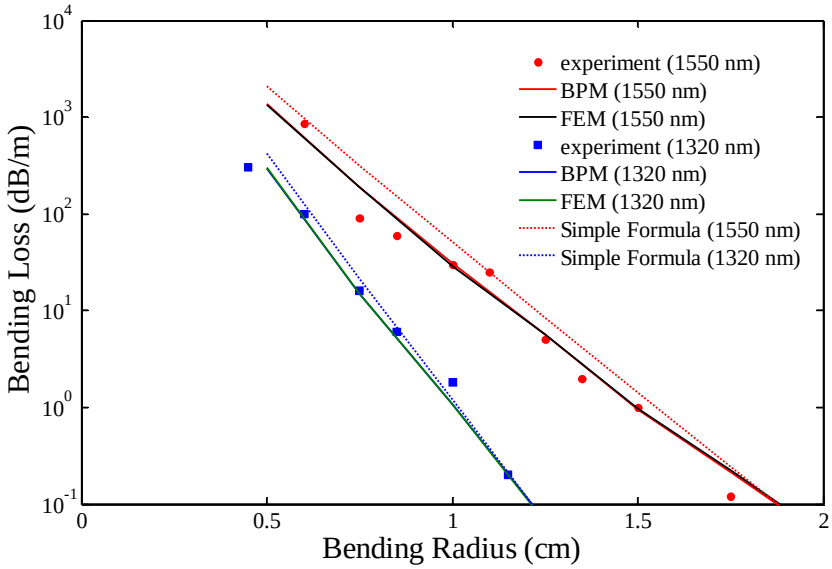

Fig. 3.1 Comparison of FEM calculated bend losses with those of experimental, BPM calculated and simple formula generated values for SMF-28 fiber.

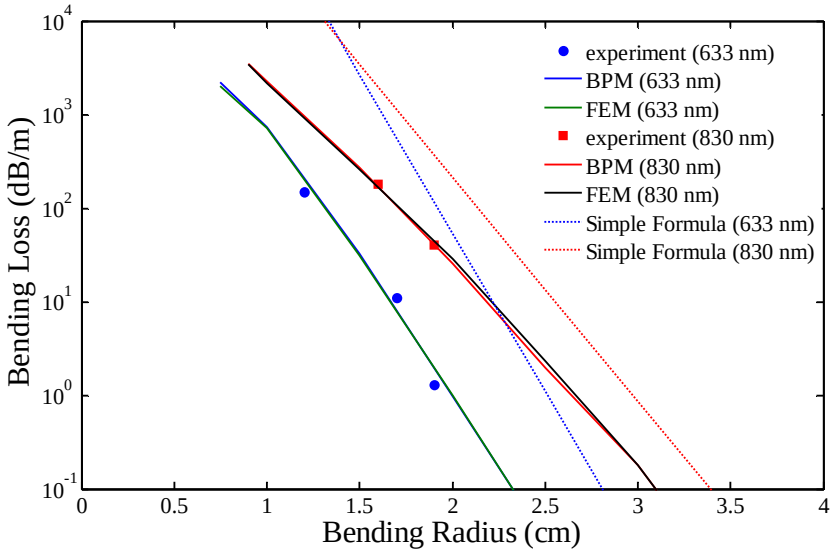

Fig. 3.2 Comparison of FEM calculated bend losses with those of experimental, BPM calculated and simple formula generated values for Liekki passive 25/240DC fiber.

They calculated the bend loss of SMF-28 (a single mode fiber) and Liekki passive 25/240DC (a multi-mode fiber) numerically by beam propagation method (BPM), also obtain these values experimentally and finally compared these bend loss values with those calculated from Eqn. (3.6). The accuracy of their BPM was established as the bend loss calculated by BPM matched those of obtained from experiment. In this thesis, the bend loss of SMF-28 and Liekki passive 25/240DC are calculated by using the FEM based software [48] and its accuracy is established too as the calculated bend loss very closely match those of experimental values shown by [27]. In Figs. (3.1) and (3.2) these comparisons are shown, It can be seen from Fig. 3.1 that the simple formula of Eqn. (3.6) overestimates the bend losses for lower values of bending radii although it approximately matches the actual bend losses at higher bending radii. Though this slight overestimation is not dealt with much importance in the literatures [27], it will be worth reducing this difference to increase the accuracy of the formula.

In the case of multi-mode fiber, it can be seen from Fig. 3.2 that the simple formula of Eqn. (3.6) overestimates the bend losses to a much larger extent than in the case of single mode fiber. This overestimation is even larger at the lower values of bending radii. Clearly, a modification in the formula of (3.6) is essential to reduce this difference for multimode fibers.

It is clear from [25] that in Eqn. (3.6), effective refractive index of a straight fiber is used. But, when the fiber is bent, Eqn. (3.2) is used to obtain the index distribution of the equivalent straight fiber. Thus, the effective index of the fundamental mode of interest is

now different from that of a straight fiber. Thus, the effective index of the bent fiber should be used in (3.6) for the corresponding bending radius. This is one source of overestimating bend loss by the simplified formula identified by Schermer.

Another simplifying assumption that was made by Marcuse in the process of derivation of Eqn. (3.6) is, he assumes the mode field distribution does not change due to bending. To account for this change in mode field distribution in bent fibers, Schermer derived the following formula by expanding the fields on the boundary cylinder, defined by x = a, as a superposition of outgoing cylindrical waves in the cladding.

$$2\alpha = \frac{\pi^{\frac{1}{2}} \kappa^2 \exp\left(-\frac{2\gamma^3 (R+a)_{eff}}{3\beta_z^2} - 2\gamma a \right)}{2(R+a)_{eff}^{1/2} \gamma^{\frac{3}{2}} V^2 K_{m-1}(\gamma a) K_{m+1}(\gamma a)} \tag{3.7}$$

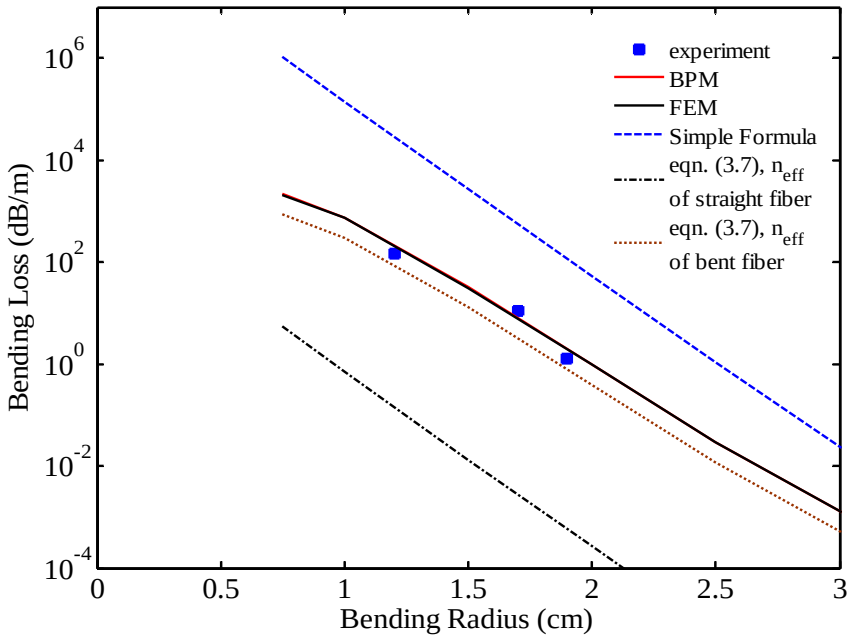

Fig. 3.3 Comparison of eqn. (3.7) generated bend losses with those of experimental, BPM calculated and FEM calculated values for Liekki passive 25/240DC fiber at the wavelength of 633 nm.

These two sources of discrepancies from the actual bend loss were identified by Schermer and they are almost overcome using Eqn. (3.7) where κ and γ are calculated from the actual refractive index of the bent fiber. But, this would weaken the justification of using an analytical formula to calculate bend loss which could otherwise be calculated by any tedious numerical method such as BPM or FEM.

To increase the accuracy of the modified formula, the modified formula of Schermer should be re-modified. For this, the simplified assumption by Schermer should be dealt with proper care. Schermer derived Eqn. (3.7) by expanding the fields on the boundary cylinder, defined by x = a. The reason is, the peak of mode field distribution shifts towards the bend direction from the center of the core and taking x = a implies that the shift distance is equal to the core radius. But actually it should be dependent upon the bending radius according to the rule that the lower the bending radius, the larger becomes the shift distance.

Usually, the field along a line through the center of the fiber follows the Gaussian distribution. But when the fiber is bent, the field deviates from the Gaussian shape and resembles the shape of Chi-square distribution.

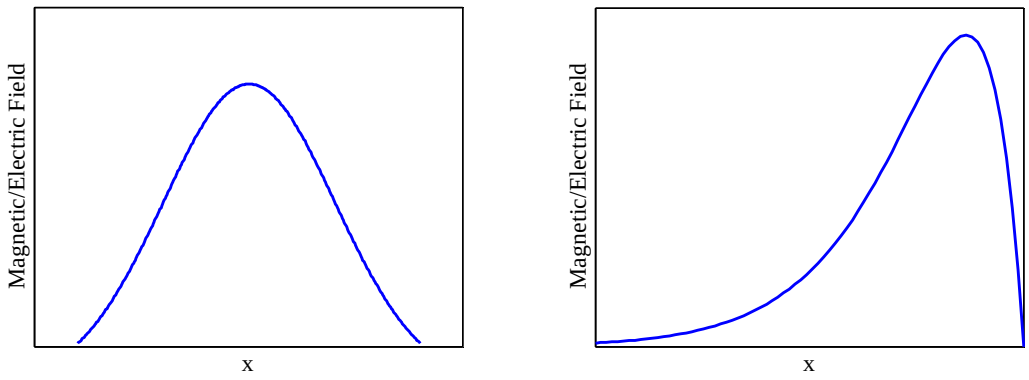

(a) (b)

Fig. 3.4 Qualitative field distribution along a line going through the center of the cross section for a (a) straight fiber and (b) for a bent fiber.

In this thesis, firstly we argue that the value, x = a, should not be used to derive Eqn. (3.7) as it will underestimate the loss to a large extent. Rather, by expanding the fields on the point where the peak of the field occurs, defined by x = x_{peak} the resulting bend loss equation becomes,

$$2\alpha = \frac{\pi^{\frac{1}{2}}\kappa^2 \exp\left(-\frac{2\gamma^3\left(R+x_{peak}\right)_{eff}}{3\beta_z^2} - 2\gamma x_{peak}\right)}{2\left(R+x_{peak}\right)_{eff}^{1/2}\gamma^{\frac{3}{2}}V^2 K_{m-1}\left(\gamma x_{peak}\right)K_{m+1}\left(\gamma x_{peak}\right)} \tag{3.8}$$

But, it is observed that Eqn. (3.8) underestimates the bend loss too though the values are closer to the actual ones this time than those determined by eqn. (3.7), as shown in Fig. 3.5. So, taking x = x_{peak} cannot be the solution. To determine the value of x, a quasi- analytical

technique is adopted. It is to be noted that the calculated bend loss from eqn. (3.7) gets lower with the decrease of x. So, a value smaller than x_{peak}, will return the accurate result.

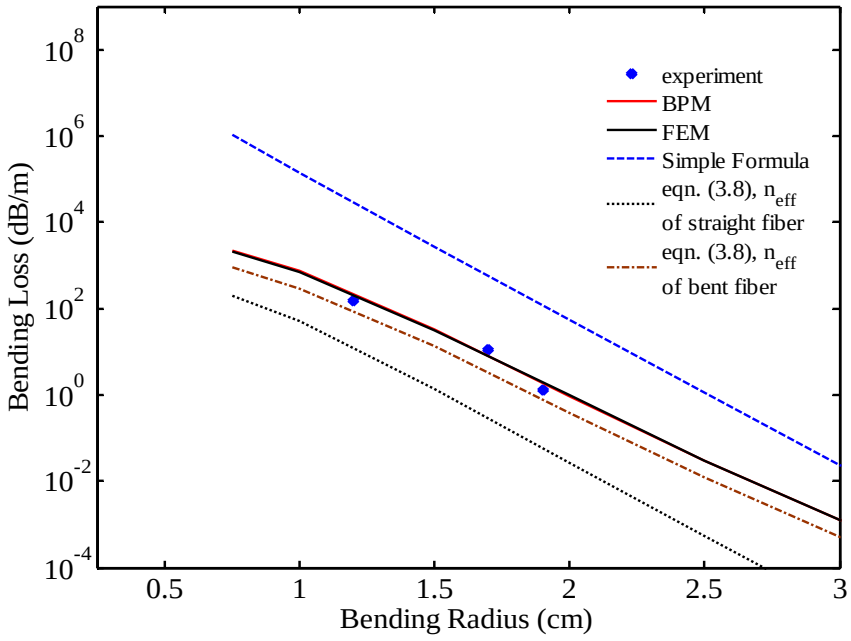

Fig. 3.5 Comparison of eqn. (3.8) generated bend losses with those of experimental, BPM calculated and FEM calculated values for Liekki passive 25/240DC fiber at the wavelength of 633 nm.

The area under the Gaussian curve of Fig. 3.4(a) is divided into two equal halves at x = x_{peak}. But, for the Chi-square like distribution, the area under the curve is divided into two equal halves for a value of $x < x_{peak}$. This value of x is determined by a computer program and symbolized as $x_{eq.area}$. If this $x_{eq.area}$ is put into the eqn. (3.7) instead of the core radius a, we get,

$$2\alpha = \frac{\pi^{\frac{1}{2}}\kappa^2 \exp\left(-\frac{2\gamma^3\left(R+x_{eq.area}\right)_{eff}}{3\beta_z^2} - 2\gamma x_{eq.area}\right)}{2\left(R+x_{eq.area}\right)_{eff}^{\frac{1}{2}}\gamma^{\frac{3}{2}}V^2 K_{m-1}\left(\gamma x_{eq.area}\right)K_{m+1}\left(\gamma x_{eq.area}\right)} \tag{3.9}$$

In Fig. 3.7, eqn. (3.9) generated bend loss values are compared with those calculated using the BPM, FEM and simple formula of Marcuse. The formula given by eqn. (3.9) is shown to estimate bend loss with a very high accuracy. So, the quasi-analytic assumption x = $x_{eq.area}$ is a valid one.

Next, it has to be checked that whether the eqn. (3.9) works well enough too for single mode SI fibers or not. Fig. (3.8) shows the comparisons among eqn. (3.9) generated bend

losses with those of experimental, BPM calculated and FEM calculated values for SMF-28 fiber used by Schermer et. al. It can be seen from this figure that like a multimode fiber, the accuracy of bend loss estimation for a single mode fiber using eqn. (3.9) is very high too.

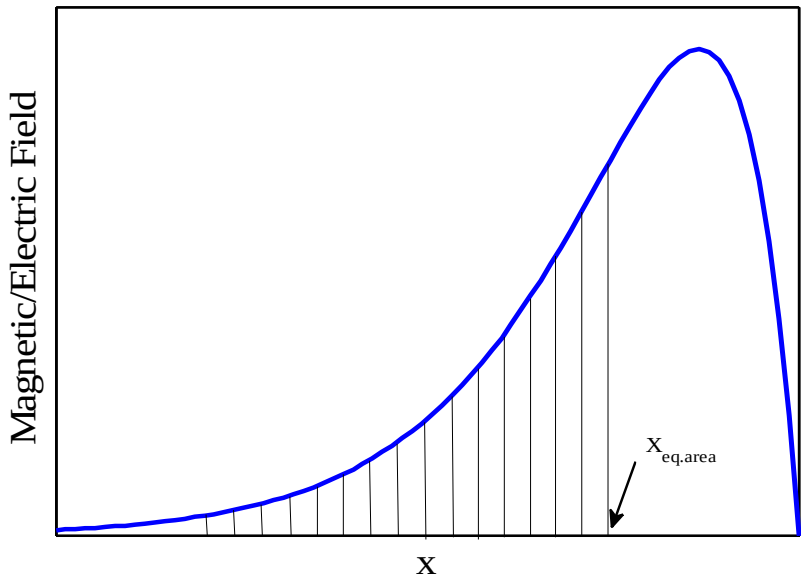

Fig. 3.6 The area under the curve is divided into two equal halves at $x_{eq.area}$.

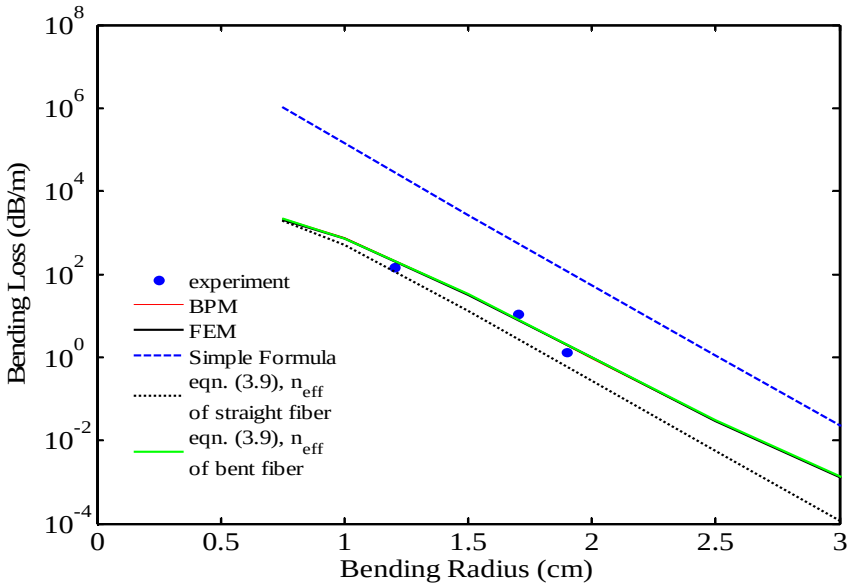

Fig. 3.7 Comparison of eqn. (3.9) generated bend losses with those of experimental, BPM calculated and FEM calculated values for Liekki passive 25/240DC fiber at the wavelength of 633 nm.

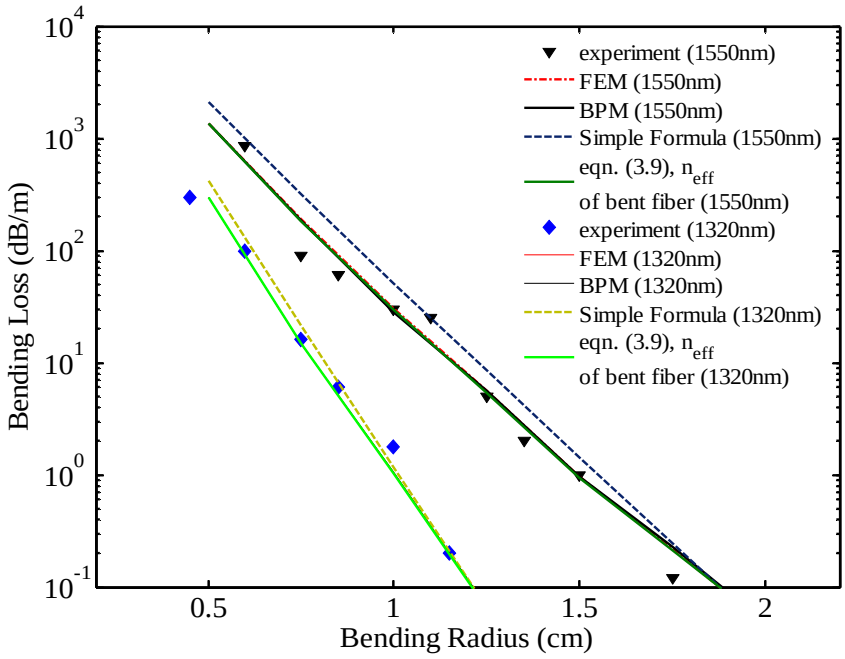

Fig. 3.8 Comparison of eqn. (3.9) generated bend losses with those of experimental, BPM calculated and FEM calculated values for SMF-28 fiber.

3.3 Bend Loss Formula for PCFs

The applicability of Marcuse's simplified bend loss formula for PCFs has not been addresses in the literature much. In this thesis, an attempt has been made to modify Marcuse's formula for bend loss prediction of PCFs in the telecommunication wavelength bands (usually lies between 1350 nm 1700 nm). Unlike SI fibers, bend loss of PCFs shows a peak in the lower wavelength range (between 500 nm to 850 nm) [43] along with another peak in the telecommunication wavelength bands. Whereas, SI fiber has a single peak in its bend loss curve only in the telecommunication wavelength bands. That is why Marcuse's formula which was originally developed for SI fibers is difficult to apply on PCFs.

Here, an attempt to apply the modified Marcuse's formula of eqn. (3.9) has been made in the wavelength range 1450 nm to 1650 nm. Eqn.(3.9) is applied directly on PCFs with the only exception that k_{clad} in eqn. (3.5) is calculated from the fundamental space filling mode, n_{FSM} adopting a technique described in [47]. The core radius is taken to be $\Lambda/\sqrt{3}$ [47] for calculating the normalized frequency V, where Λ is the pitch of the PCF.

It can be seen from Figs. 3.9-3.11 that the modified bend loss formula developed for SI fibers in eqn. 3.9 can predict the bend loss in PCFs too. Though the accuracy is not similar

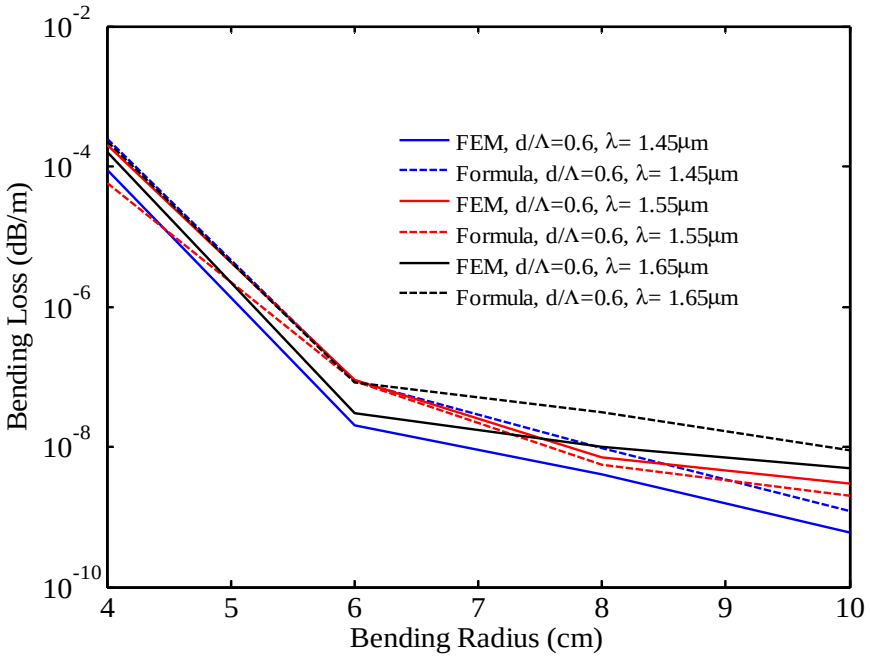

Fig. 3.9 Comparison of eqn. (3.9) generated bend losses with those FEM calculated values for an H-PCF having Λ = 18μm and d/Λ = 0.6 at different wavelengths.

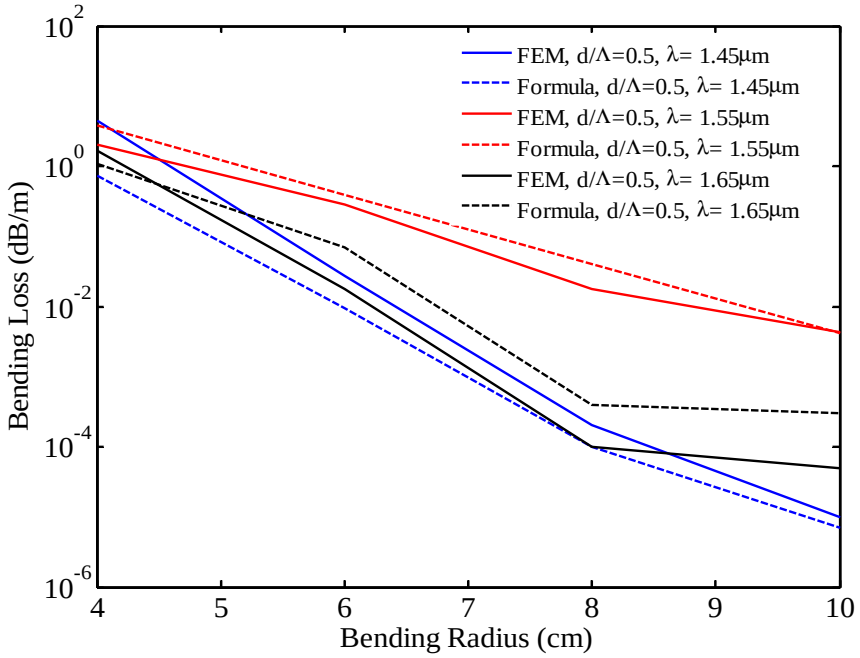

Fig. 3.10 Comparison of eqn. (3.9) generated bend losses with those FEM calculated values for an H-PCF having Λ = 18μm and d/Λ = 0.5 at different wavelengths.

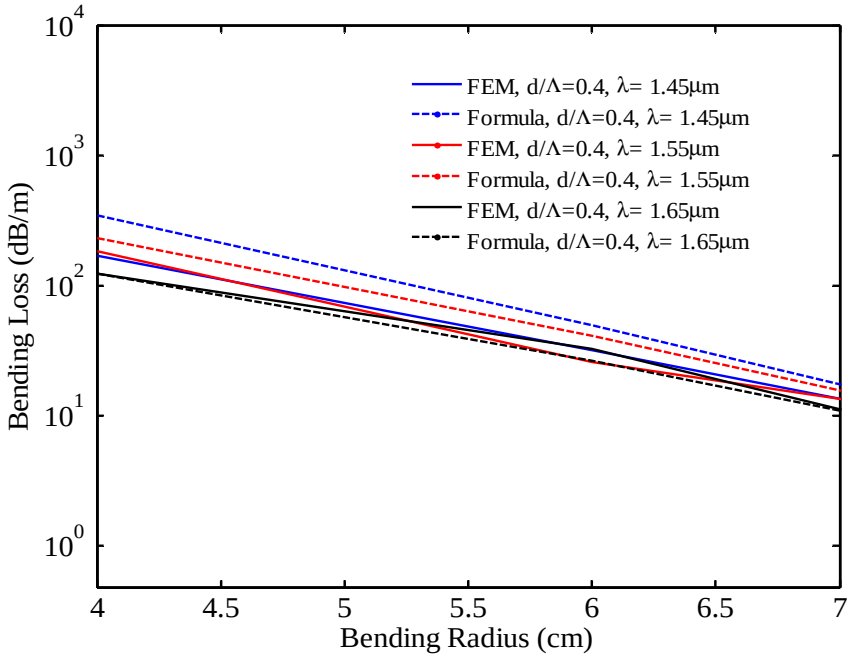

Fig. 3.11 Comparison of eqn. (3.9) generated bend losses with those FEM calculated values for an H-PCF having Λ = 18μm and d/Λ = 0.4 at different wavelengths.

to the case of SI fibers, the values are close enough to the actual ones calculated by FEM. It is intuitive that the differences are due to the bend induced coupling [40] between the fundamental mode and leaky cladding mode, which is totally unpredictable and depends on wavelength strongly. Thus, the formula of (3.9) finds its applicability for PCFs over a limited range of wavelength.

3.4 Comments

A modified bend loss formula has been proposed in this chapter for step index fibers and its applicability is verified through numerical simulations using FEM. Before this, the accuracy of FEM in calculating bend loss is confirmed through a comparison with the previously published results. Moreover, this modified formula is also shown to be applicable for PCFs, though in a limited extent. It is expected that this formula will ease the computation of bend loss both for SI fibers and PCFs.

CHAPTER 4
DESIGN AND ANALYSIS OF PHOTONIC CRYSTAL FIBERS

A conventional design of PCF has a hexagonal lattice where three parameters such as, pitch, air hole diameter and number of air hole rings, can be varied to obtain useful properties. On the contrary, an ES-PCF has more than three parameters to vary like variable pitch, air hole diameter, number of air hole rings, angular difference between rings, increase factor of air hole diameter etc. Thus, an ES-PCF offers more design flexibility to obtain valuable properties in fiber optic communication systems. In this chapter, several such designs of ES-PCF have been shown.

4.1 Residual Dispersion Compensating ES-PCF

In section 2.3.1, several design based on H-PCF have been shown for residual dispersion compensation over the telecommunication wavelength bands [31]-[33]. In this thesis, an ES-PCF has been investigated for this application for the first time to my knowledge. The polarization issue has been considered here simultaneously. Among the several developed designs, the first one has an elliptical air hole at the core region which is employed to achieve a flattened and larger negative dispersion to obtain dispersion compensation over *E+S+C+L+U* wavelength bands. The structure also exhibits a very high value of birefringence.

4.1.1 ES-PCF design

The proposed residual dispersion compensating fiber (RDCF) design is based on the equiangular spiral PCF [20]. In this design process, a full-vectorial finite element method (FEM) has been used to characterize the proposed ES-PCF as described in chapter three. An anisotropic perfectly matched layer (PML) was used to accurately account for the confinement losses. Chromatic dispersion caused by the combined effects of material and waveguide dispersions in an optical fiber, can be calculated by the formula,

$$D = -\frac{\lambda}{c}\frac{\partial^2(\mathrm{Re}(n_{eff}))}{\partial\lambda^2}, \tag{4.1}$$

where λ is the wavelength of, c is the velocity of light, n_{eff} is the effective refractive index of the fundamental mode and Re(·) indicates the real part. The birefringence is determined by taking the difference of the real parts of the effective indices of two fundamental polarization modes (slow and fast axis modes) [51],

$$\mathrm{B} = |n_{\mathrm{x}} - n_{\mathrm{y}}|. \tag{4.2}$$

Fig. 4.1 shows the air hole arrangement in the proposed design. In this design, there are N_r air holes in each ring. The first ring has a radius of r_o and the radii of the subsequent rings increase by geometric progression. Each air hole of the first ring is

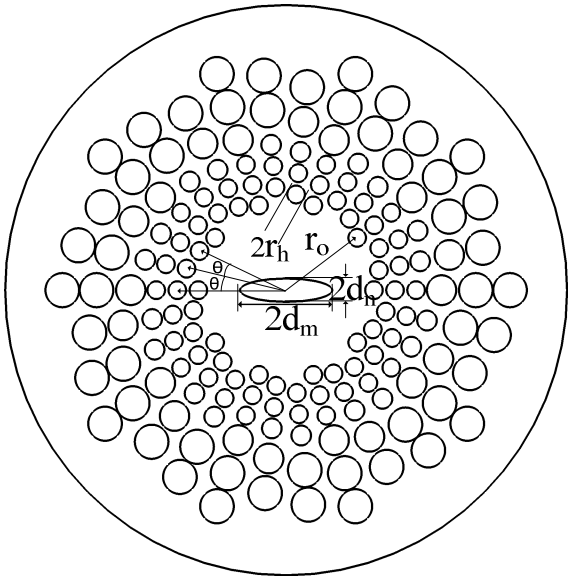

Fig. 4.1 Cross section of the proposed ES-PCF.

the starting point of a spiral arm. There are N circular air holes in each arm. The first nine of them has a radius of r_h. The angular position of each air hole in an arm is increased by θ than the previous one. The major and minor semi axes lengths of the central defect air hole are d_m and d_n, respectively.

4.1.2 Simulation results

A full-vectorial finite element method (FEM) described in chapter three has been used to characterize the ES-PCF design. About 20512 second-order triangular elements arranged in an irregular mesh over the cross section have been used to represent the fiber structure. A single simulation run on a 64-bit dual core Intel Pentium desktop computer took about 90 s. The numerical results are reported for an optimized structure with N_r=10, N=16, r_o=1.4µm, θ=12◦, r_h=0.15µm, d_m=0.735µm and d_n=0.1838µm for an RDCF having numerical aperture around 0.65. The minimum and average distances between air holes are 0.02 µm and 0.18 µm, respectively. The material dispersion is taken into account by using the Sellmeier equation to obtain the refractive index of silica at different wavelengths. An RDCF should have a flat negative chromatic dispersion of high magnitude in the wavelength band of interest.

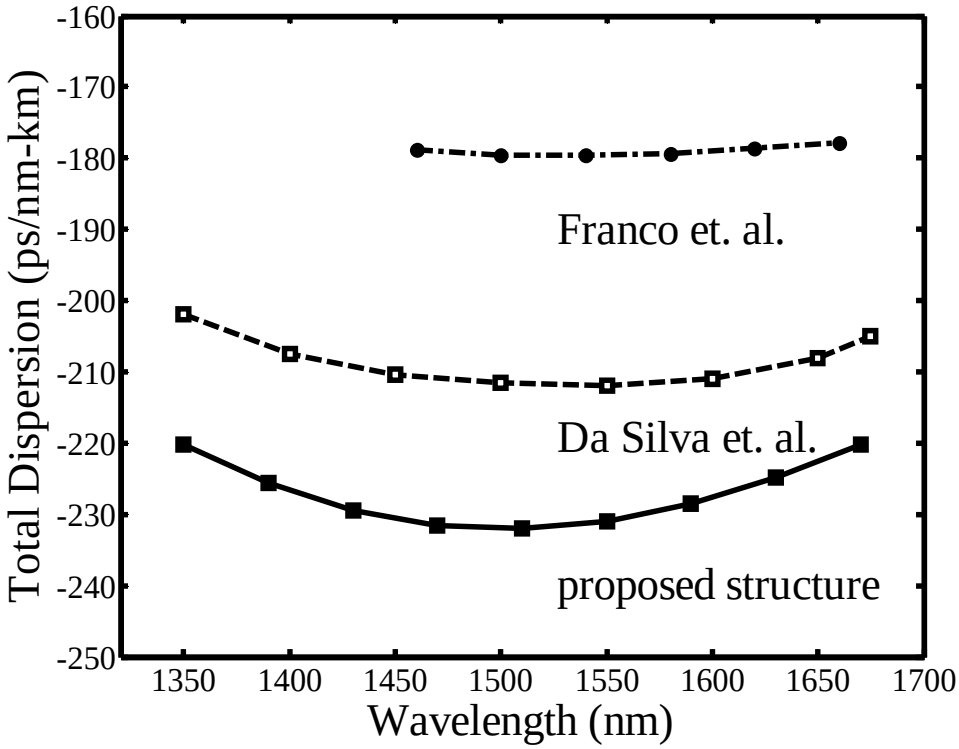

Fig. 4.2 Comparison of the dispersion profile with those reported in recent literature.

In this work, the design shows an average value of chromatic dispersion equal to −227 ps/nm-km with a dispersion variation of 11 ps/nm-km (between −220.2 ps/nm-km and −232.1 ps/nm-km) in the wavelength range 1350nm to 1675nm for the fundamental

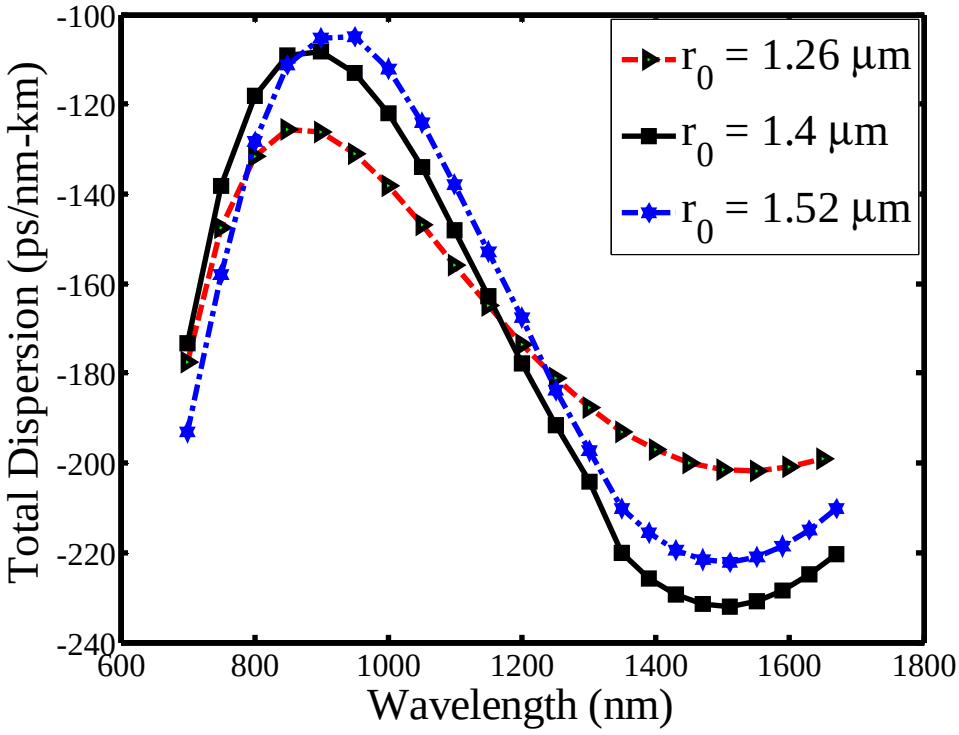

Fig. 4.3 Total dispersion versus wavelength as a function of r_o.

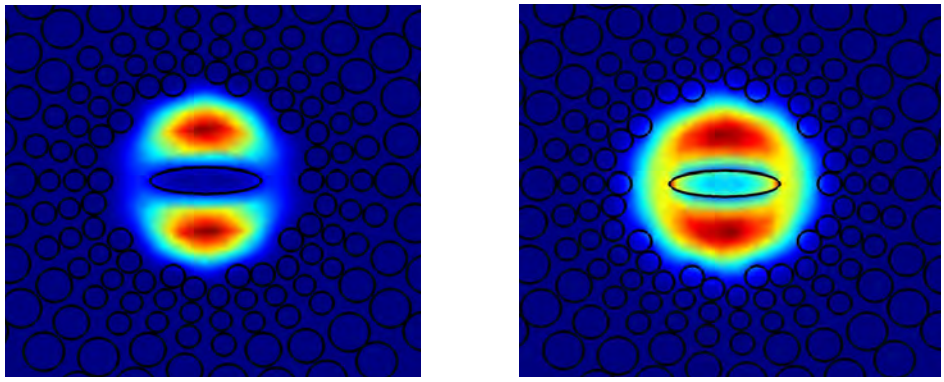

(a) (b)

Fig. 4.4 Electric field of the fundamental slow axis mode of the proposed ES-PCF, (a) at 800 nm, (b) at 1550 nm.

slow axis mode. In Fig. 4.2, we have compared our result of total dispersion with those obtained by Franco et. al. [31] and Da Silva et. al. [32]. For our design, we have obtained negative dispersion with higher amplitude than those of Franco et. al. and Da Silva et. al. In Fig. 4.3 we show the total dispersion versus wavelength as a function of r_o over a wide band (from 700nm to 1700nm) while the other parameters are unchanged. It can be seen here that at lower wavelengths, the dispersion increases with wavelength as the field spreads in the central silica region and effective index decreases rapidly as the field interacts with the first ring of air holes as shown in Fig. 4.4(a). As the field spreads out further and interacts with the silica cladding in the

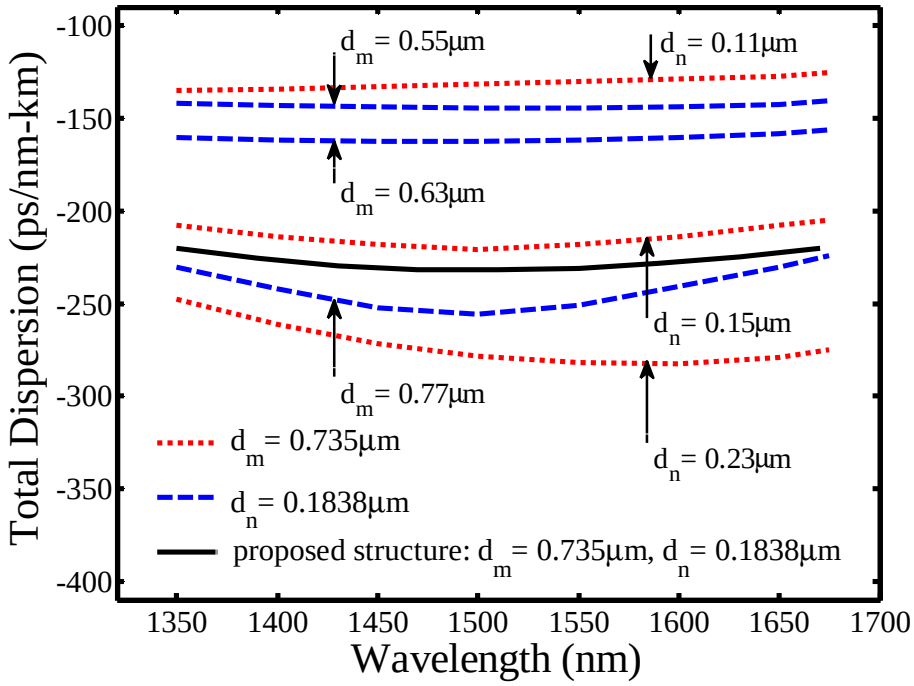

Fig. 4.5 Total dispersion variation for different values of d_m and d_n.

region beyond the first ring of air holes, the change in refractive index reduces and dispersion becomes nearly flat at the wavelength near 1000 nm. With further increase in wavelength, the field comes under the influence of the second ring of air holes as shown in Fig. 4.4(b) and causes to increase the change in refractive index and thus leads to large negative dispersion. At higher wavelengths near 1500 nm, the field again interacts with silica cladding beyond the second ring of air holes and again the change in refractive index slows down. It leads to a flat negative dispersion of interest for dispersion compensation. It can also be seen that some small fraction of power, about 1.3% at 800nm and about 6% at 1550nm, stays in the elliptical air hole in the core.

In Fig. 4.5, we show the total dispersion variation as a function of different values of d_m and d_n. A change in anyone of the semi axes (d_m or d_n) causes a significant variation in total dispersion. However, the structure is optimized to obtain a large negative and flat dispersion profile and high birefringence simultaneously. A change in orientation of the defect air hole however does not alter the dispersion curves much. It has been found that the birefringence is of the order of 10^{-2} over the wavelength range considered here and at 1500nm it is about 0.017 when r_o=1.4µm. At r_o=1.26µm it is even higher as to obtain a polarization maintaining fiber in comparison with the values presented earlier in the literatures [51]-[55]. Here, it has also been found that the high birefringence of the proposed structure is due to the central elliptical air hole alone.

Next, to ensure the stability of the proposed designs, tolerance study was performed based on different structural parameters. Total dispersion and birefringence are shown

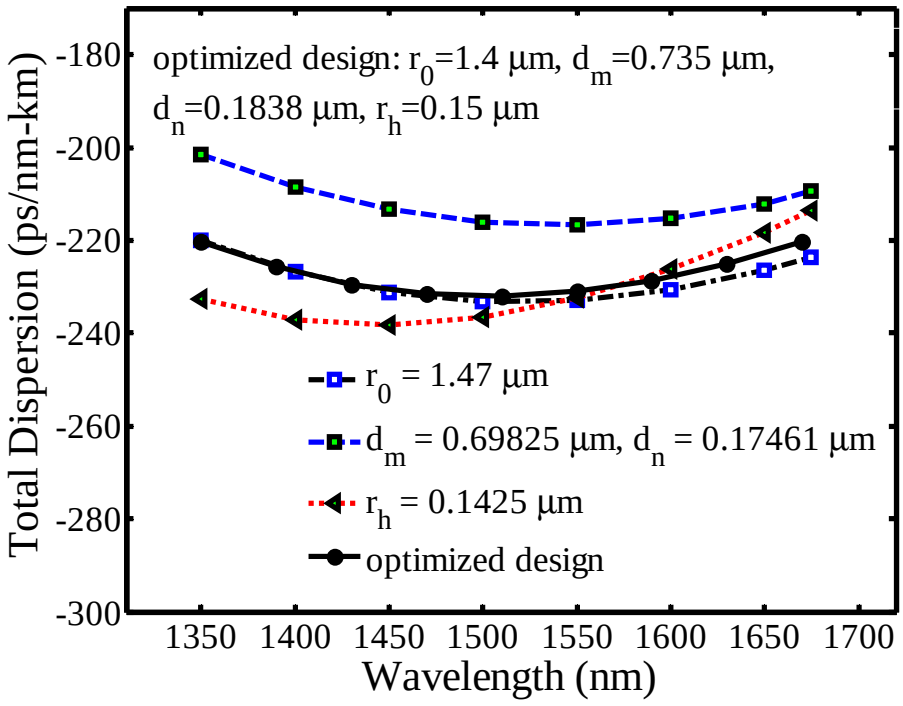

Fig. 4.6 Sensitivity of total dispersion for different structural parameters.

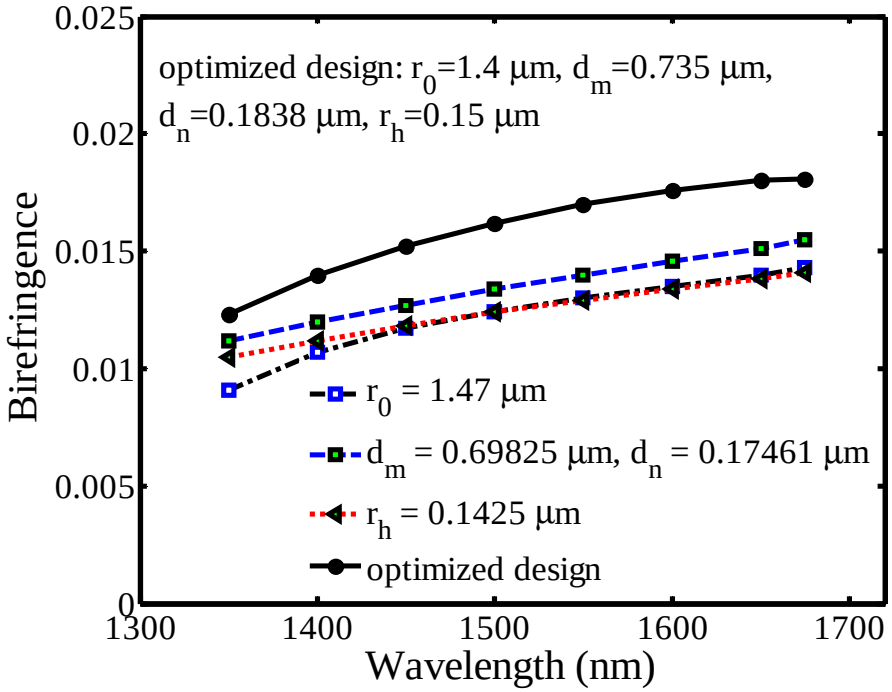

Fig. 4.7 Sensitivity of birefringence for different structural parameters.

in Fig. 4.6 and Fig. 4.7, respectively, where the results of the optimized design are compared with the results obtained by changing only one parameter at a time. It is seen that a variation of about 5% in the structural dimension does not alter the average dispersion and birefringence much. The curves with the dark circle show the results of the optimized design.

4.1.3 Outcomes

Here, an ES-PCF is investigated as a polarization maintaining residual dispersion compensating fiber in the telecommunication frequency bands. Apart from dispersion compensation, the proposed design in this work also maintains single polarization. Its birefringence value is fairly high and even higher than most of the polarization maintaining fiber reported earlier. These dual characteristics make this fiber a promising candidate in its application in the fiber optic communication link in the telecommunication window.

4.2 Residual Dispersion Compensating ES-PCF with Modified Design

In this section, the dispersion profile and birefringence of the ES-PCF are investigated by introducing more than one air holes in the core region to obtain a dispersion profile even flatter than that discussed in section 4.1, with less dispersion variation over the wavelength range 1350 nm to 1650 nm. Dispersion profiles having average dispersion of about −293.5 ps/nm-km and −393 ps/nm-km over the wavelength range of interest

have been reported here with dispersion variation of only 8.6 ps/nm-km and 10.4 ps/nm-km, respectively. Also, a further investigation has been carried out to obtain a higher birefringence in the order of 10^{-2} over the wavelength range1350 nm to 1650 nm (0.0278 at 1550 nm.). Furthermore, the higher order modes (HOMs) of this ES-PCF are suppressed by introducing a secondary annular core in the outer cladding region.

4.2.1 Modified design of ES-PCF

The structure of the proposed residual dispersion compensating fiber (RDCF), which is basically an ES-PCF having air hole arrangement in silica background is shown in Fig. 4.8. There are N_r air holes in each ring, the first ring has a radius of r_o and the radii of the rings in the same arm increase by geometric progression. There are N

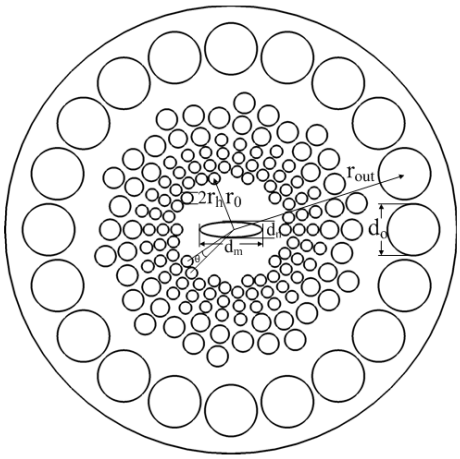

Fig. 4.8 Geometrical model of the proposed residual dispersion compensating fiber, where r_o = the radius of the first air hole ring in the cladding, θ = angular increment of each air hole in spiral arms, $2r_h$ = the diameter of the air holes in the first nine rings.

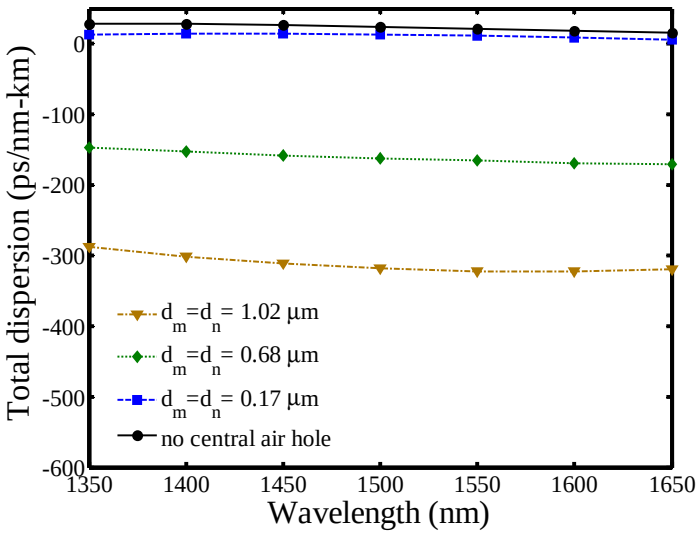

Fig. 4.9 Total dispersion versus wavelength for circular air hole of different radius in the core.

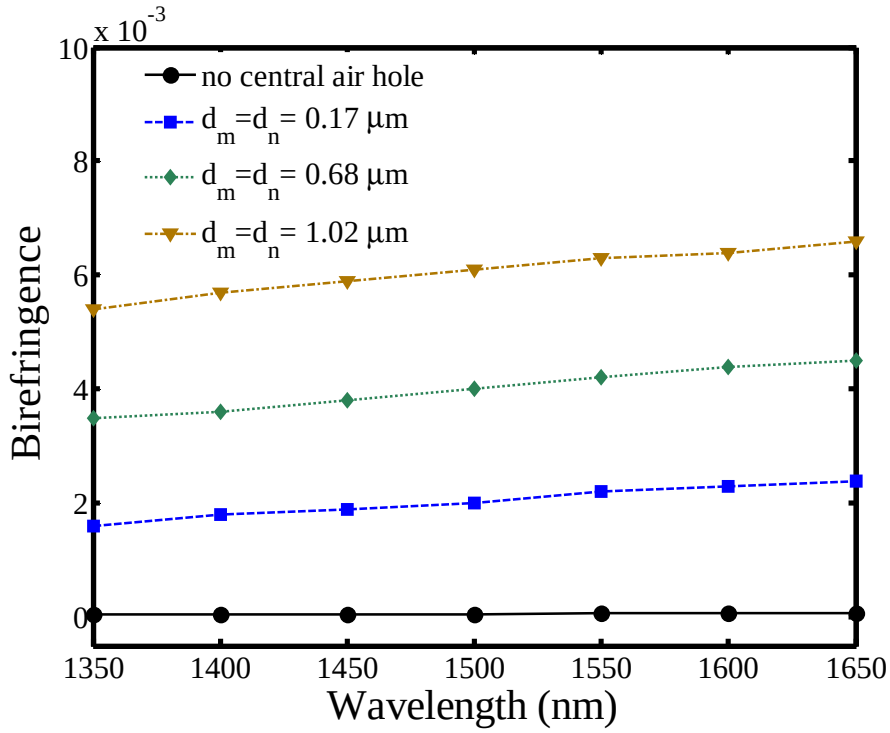

Fig. 4.10 Birefringence versus wavelength for circular air hole of different radius in the core.

circular air holes in each arm. The first seven of them have a radius of r_h. The radii of the subsequent air holes in the same arm are increased gradually. The angular position of each air hole in an arm is increased by θ than the previous one. Here, d_m and d_n are

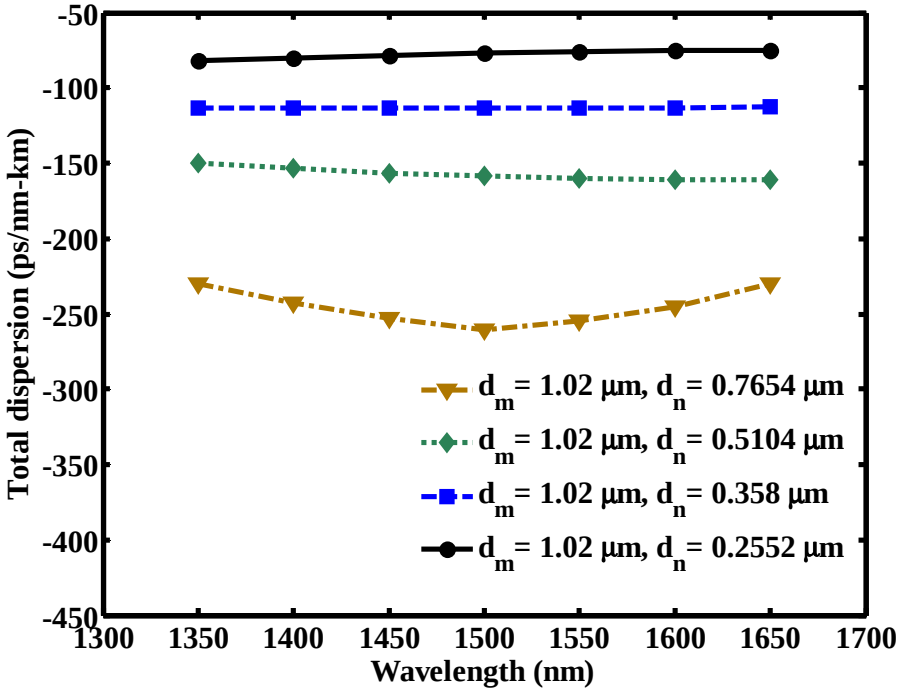

Fig. 4.11 Total dispersion versus wavelength for one elliptical air hole of different ellipticity in the core.

major and minor axes of the elliptical air hole at the center of the core. The dispersion properties are shown for the fundamental slow axis mode. Material dispersion that refers to the wavelength dependence of the refractive index of the material and is caused by the interaction between the optical mode and ions, molecules, or electrons in the material and is taken into account here by using the Sellmeier equation to obtain the refractive index of silica at different wavelengths. In most cases, the following structural parameters are kept unchanged unless otherwise stated: N_r=10, N=16, r_o=1.4µm, θ=12◦ and r_h=0.148µm.

As shown in Fig. 4.8, a secondary annular core is introduced in the outer cladding by employing an air hole ring having radial distance from the center, r_{out} = 5.88 µm resulting in a dual core ES-PCF. The diameter of the air holes of this ring is d_0 = 1.68 µm. The values of r_{out} and d_0 are so optimized that the resulting secondary core modes occur as degenerate modes with the higher order modes (HOMs) of the central core. Coupling of energy between the secondary core modes and the central HOMs makes these HOMs very lossy over the entire wavelength range of interest [57]. It is observed that the HOMs of the central core have confinement loss more than 1dB/m and thus, they can be effectively suppressed to realize the single mode (SM) condition in ES-PCF. It should be noted here that single modedness in H-PCF has been realized similarly in [42].

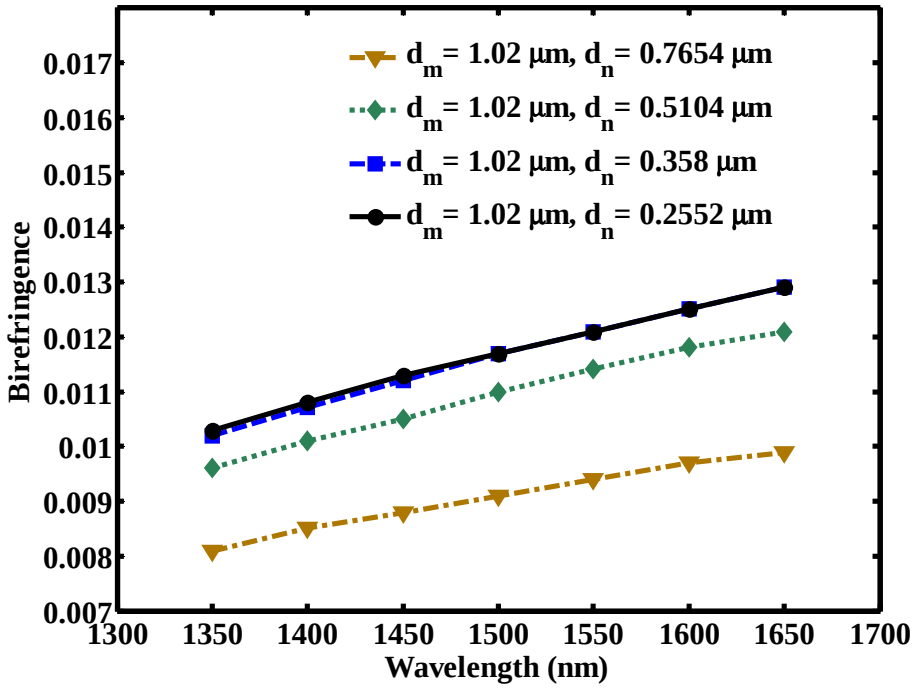

Fig. 4.12 Birefringence versus wavelength for one elliptical air hole of different ellipticity in the core.

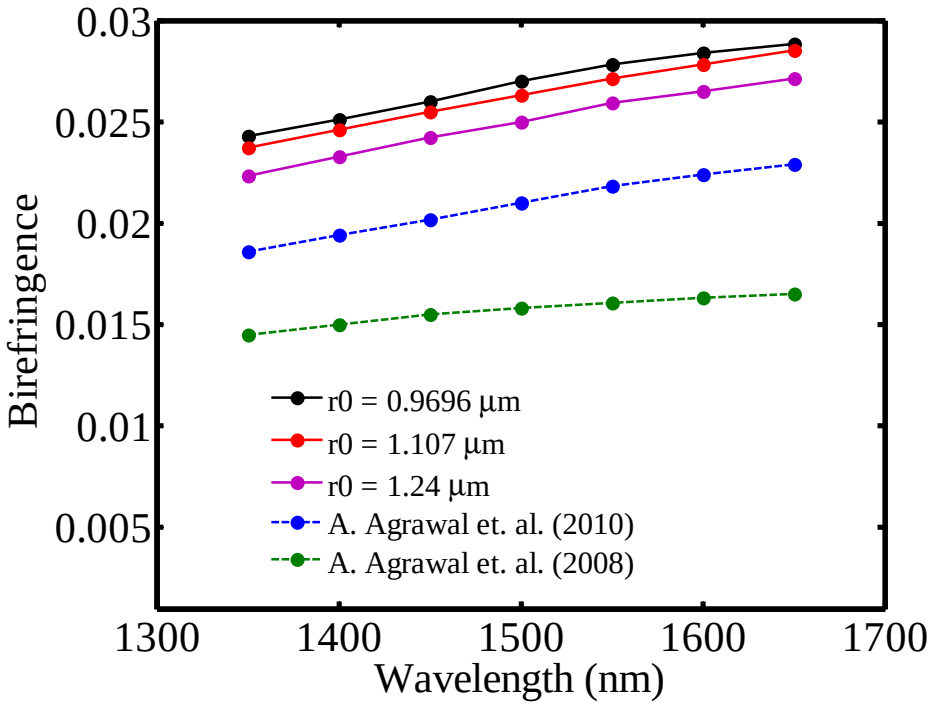

Fig. 4.13 Birefringence versus wavelength as a function of r_o.

4.2.2 Simulation results and discussion

The dispersion and birefringence properties of the ES-PCF structure with one circular air hole ($d_m = d_n$) in the center of the core are shown in Figs. 4.9 and 4.10, respectively. In Fig. 4.9, we can see that the dispersion becomes more negative with the introduction of air hole in the core and the value increases further with the increase of its radius. Here, the blue line shows a flattened profile of average dispersion about 10 ps/nm-km over 1350 nm to 1650 nm wavelength bands when the diameter of the central hole, $d_m = d_n = 0.17$ µm. For $d_m = d_n = 1.02$ µm, the average dispersion is −300 ps/nm-km with a flat profile having a dispersion variation of 35 ps/nm-km around the mean value. This is a large negative value as compared to those reported in [31]-[33], but the flatness should be improved. We can also notice from Fig. 4.9 that the more negative the dispersion goes, the less flat its profile becomes. A trade-off has to be made between the flatness and higher negative values of dispersion. From Fig. 4.10, we can see that the birefringence of the ES-PCF increases after introducing a circular air hole in the core. The birefringence also increases with the increase of diameter of this air hole. It is perhaps due to the fact that the symmetry of the structure is disturbed more due to the increase in diameter of the central air hole.

Now, we consider a single elliptical air hole in the core and show the dispersion and birefringence properties in Figs. 4.11 and 4.12, respectively. The effect of ellipticity (defined as the ratio of major axis length to minor axis length) on dispersion and

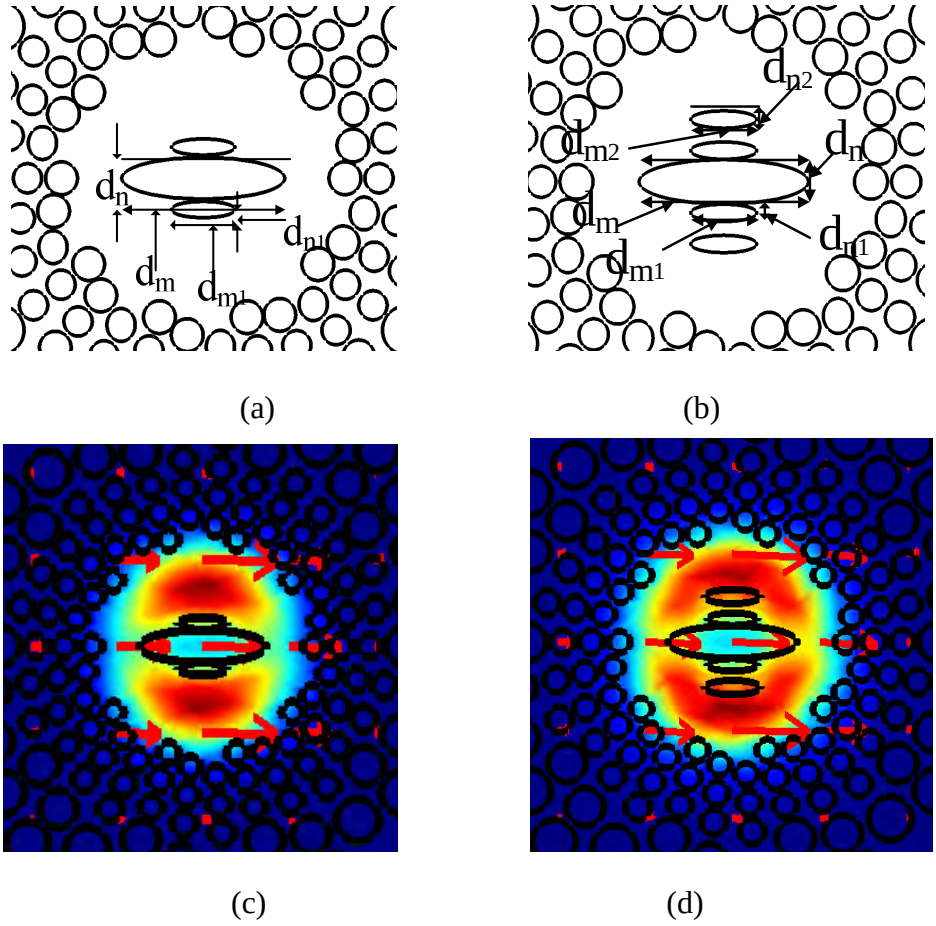

Fig. 4.14 Different number of elliptical air holes in the core with their dimensions, in (a) three air holes, (b) five air holes and (c) electric field distribution for three air holes, (d) electric field distribution for five air holes.

birefringence has been demonstrated here. In Fig. 4.11, we can see that the dispersion becomes more negative for lower ellipticity that results in larger size of the air hole as expected [46]. Here, for d_m= 1.02 µm and d_h=0.7654 µm, the gray line with triangular marker shows an average dispersion of −245 ps/nm-km over 1350 nm to 1650 nm wavelength bands with a dispersion variation of about 30 ps/nm-km. This value is less negative but slightly flatter than that shown in Fig. 4.9, where the dispersion variation is about 34.6 ps/nm-km for a circular central air hole with d_m= d_n= 1.02 µm, although the flatness should be improved more to be used effectively as a DCF. A more flat profile with less negative dispersion values has been achieved by optimizing the structural parameters for the same structure as reported in [58]. It can be seen in Fig. 4.11 that an ultraflattened dispersion profile can be obtained when d_n= 0.358 µm as shown by the blue line with square markers. In this case an average dispersion of −113 ps/nm-km over 1350 nm to 1650 nm wavelength bands with a dispersion

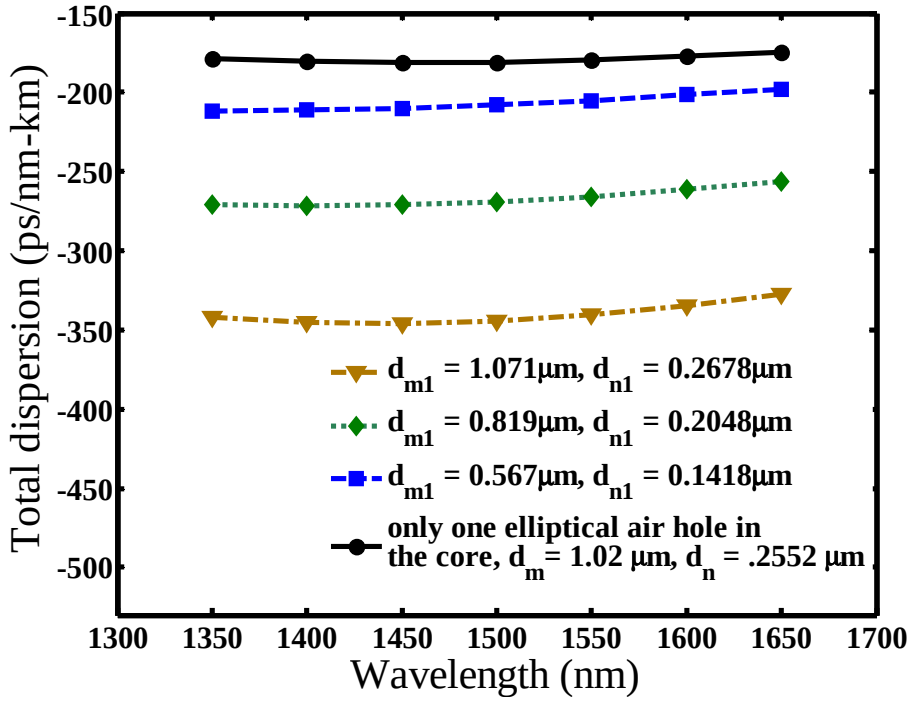

Fig. 4.15 Total dispersion versus wavelength for additional two elliptical air holes of different size in the core.

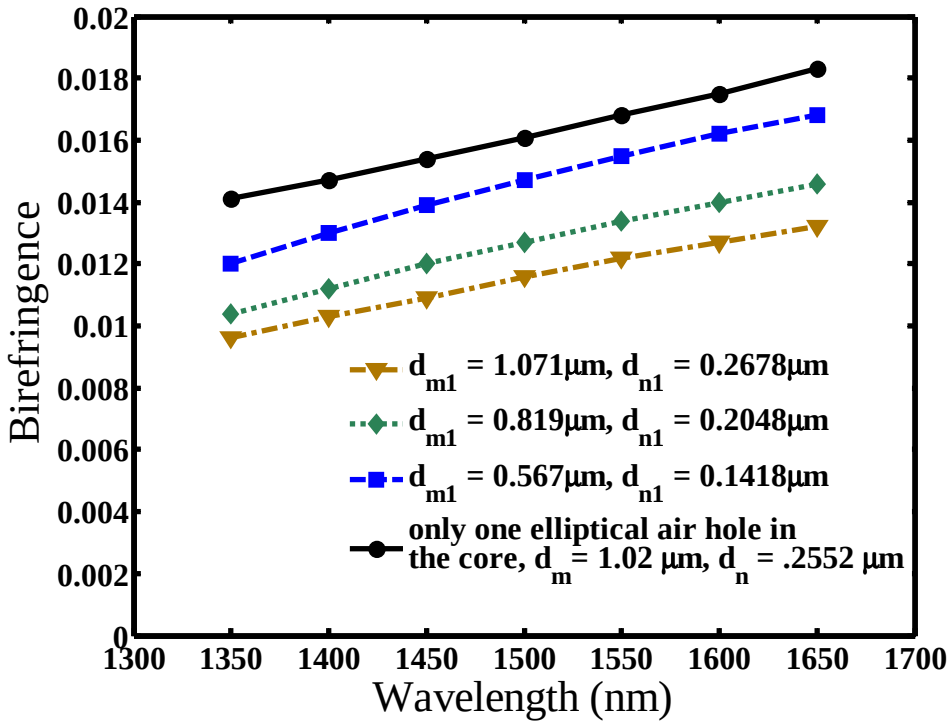

Fig. 4.16 Birefringence versus wavelength for additional two elliptical air hole of different size in the core.

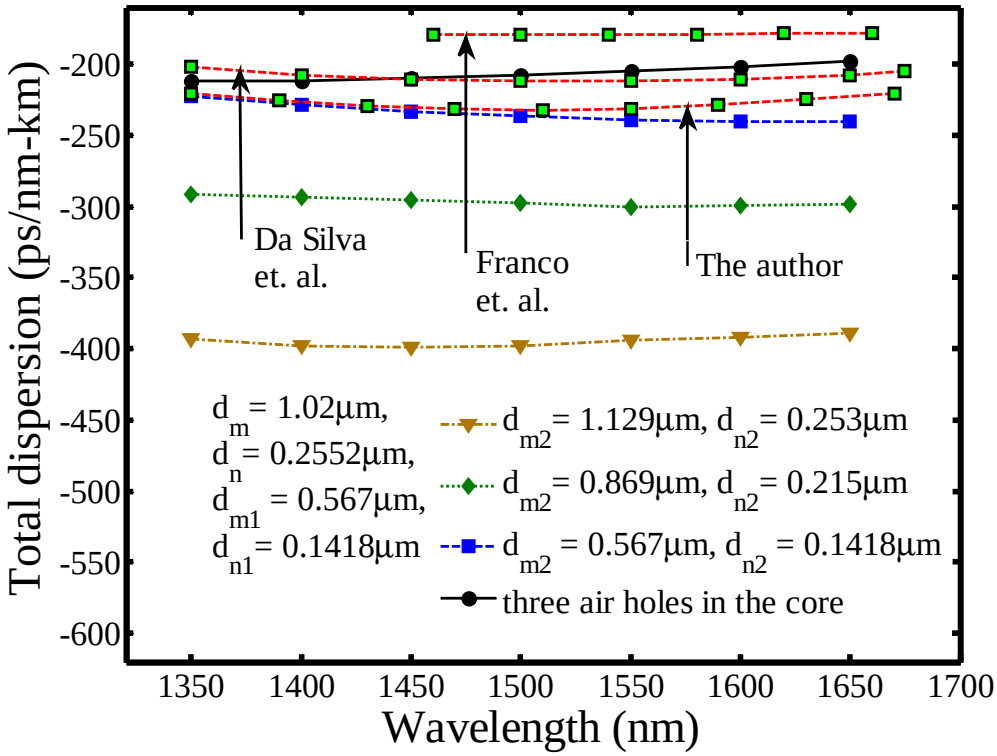

Fig. 4.17 Total dispersion versus wavelength for additional four elliptical air holes of different size in the core.

variation of only ~0.5 ps/nm-km between ~13.25 ps/nm-km and ~12.75 ps/nm-km can be obtained.

From Fig. 4.12, we can see that the birefringence becomes higher with the increase in ellipticity, although the dispersion becomes less negative. This is because higher asymmetry is encountered by the field with the increased ellipticity of the central air hole. If we optimize the structural parameters to obtain a higher birefringence, we get even higher value of birefringence over the wavelength bands of interest. The birefringence increases with the decrease of r_0 when other dimensions are unchanged as shown in Fig. 4.13. The highest value of birefringence is found to be 0.0278 at the wavelength of 1550 nm for the parameters d_m= 1.3089 µm, d_n= 0.3272 µm, r_0= 0.9696 µm and r_h= 0.115 µm shown in Fig. 4.13. This birefringence is very high, even higher than the values reported in [54]-[55]. However, this structure shows an average dispersion of −113 ps/nm-km with a variation of about 14 ps/nm-km over the wavelength range 1350 nm to 1650 nm.

We have observed that large negative dispersion with high birefringence can be achieved with even one elliptical air hole in the core by increasing the size of the hole.

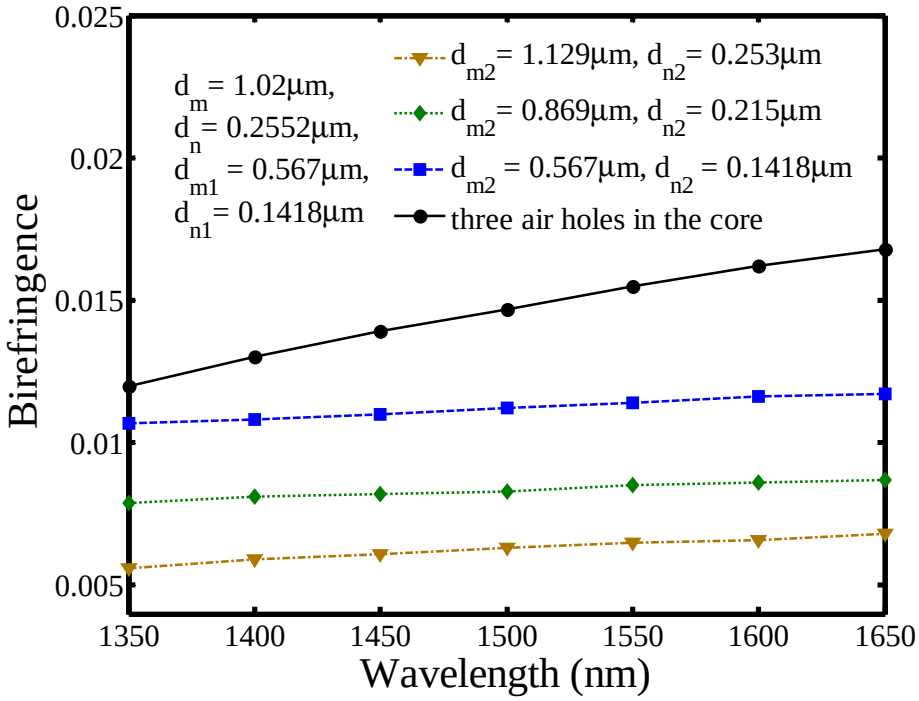

Fig. 4.18 Birefringence versus wavelength for additional four elliptical air hole of different size in the core.

But, as the dispersion gets more negative, it becomes less flat. Now, we introduce more air holes in the core region as shown in Fig. 4.14 and study dispersion and birefringence properties for each case separately to obtain large negative as well as flat dispersion profile with high birefringence. In Fig. 4.15, the dispersion properties are shown for the structure of Fig. 4.14(a), where for additional holes, the major and minor axes are d_{m1} and d_{n1}, respectively. The size of central air hole is kept fixed at d_m= 1.02 µm, d_n= 0.2552 µm because at values greater than these, the modal effective area becomes very small resulting in high splice loss with an standard SMF. The sizes of the additional two elliptical air holes are varied keeping their ellipticity (d_{m1}/d_{n1}) fixed at 4 because birefringence is seen to be maximum around this value. It can be seen that the dispersion gets more negative with the introduction of two more elliptical air holes. Also, as the size of these extra air holes increase, the dispersion becomes more negative. The gray line with triangular marker in Fig. 4.15 has an average dispersion of about −340 ps/nm-km with a dispersion variation of ~16 ps/nm-km over the wavelength bands of interest, and this value is far more negative than those reported in [31]-[33] though the curve is slightly less flat. However, for these structures the birefringence remains in the order of 10^{-2} and is seen to be decreasing after introducing the two additional air holes in the core and also with the increase of the size of these two air holes as shown in Fig. 4.16.

With the intuition of obtaining a large negative as well as flat dispersion profile over the wavelength band of interest, we consider another structure shown in Fig. 4.14(b). The additional two air holes have major and minor axes of d_{m2} and d_{n2}, respectively. The sizes of previous three air holes are kept fixed at d_m= 1.02 µm, d_n= 0.2552 µm,

d_{m1}= 0.567 µm, d_{n1}= 0.1418 µm and the sizes of the newly introduced two are varied keeping their ellipticity fixed at 4 for the same reason stated previously. From Fig. 4.17, we can see that the dispersion gets more negative after employing those extra two air holes and becomes even more negative for increased size. The curves shown by the gray line with triangular marker has an average dispersion of about −396 ps/nm-km with a dispersion variation of only 10.4 ps/nm-km and the green line with

TABLE 4.1
Summary of Proposed ES-PCF designs

Design No.	Structural parameters	Dispersion and Birefringence properties
1.	r_0= 0.9696 µm, r_h= 0.115 µm d_m= 1.3089 µm and d_n= 0.3272 µm	B = 0.0278 at λ = 1.55 µm, D = −115 ps/nm-km, ΔD = 14 ps/nm-km over λ = 1.35 to 1.65 µm
2.	r_0= 1.4 µm, r_h= 0.148 µm, d_m= 1.02 µm, d_n= 0.2552 µm, d_{m1}= 0.567 µm, d_{n1}= 0.1418 µm, d_{m2}= 1.129 µm and d_{n2}= 0.253 µm	B = 0.0065 at λ = 1.55 µm, D = −393 ps/nm-km, ΔD = 10.4 ps/nm-km over λ = 1.35 to 1.65 µm
3.	r_0= 1.4 µm, r_h= 0.148 µm, d_m= 1.02 µm, d_n= 0.2552 µm, d_{m1}= 0.567 µm, d_{n1}= 0.1418 µm, d_{m2}= 0.869 µm and d_{n2}= 0.215 µm	B = 0.0085 at λ = 1.55 µm, D = −293.5 ps/nm-km, ΔD = 8.6 ps/nm-km over λ = 1.35 to 1.65 µm

D = Average dispersion, ΔD = Dispersion variation

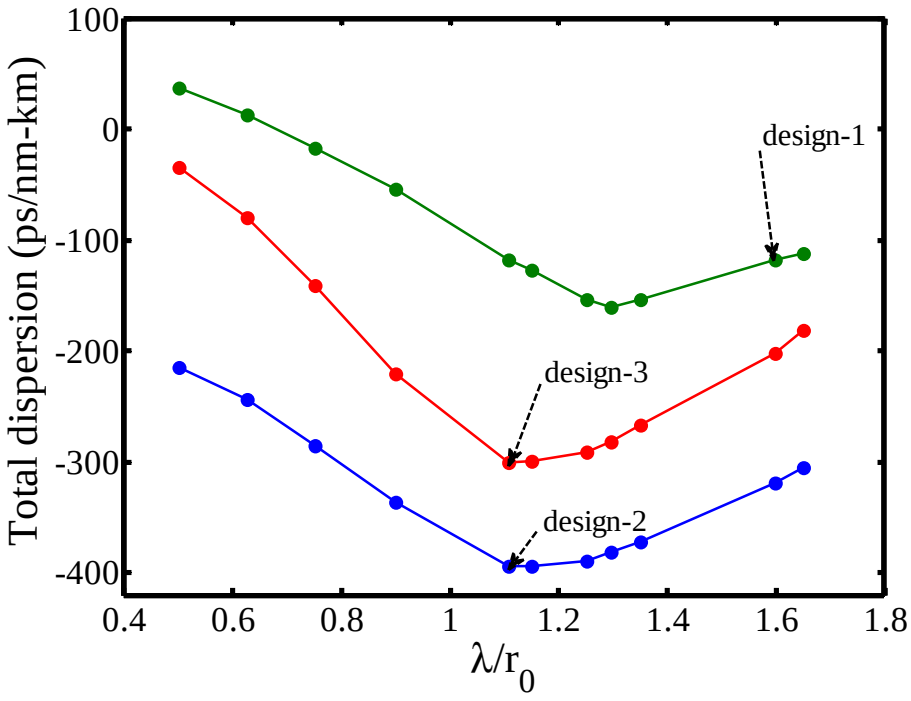

Fig. 4.19 Total dispersion as a function of r_0.

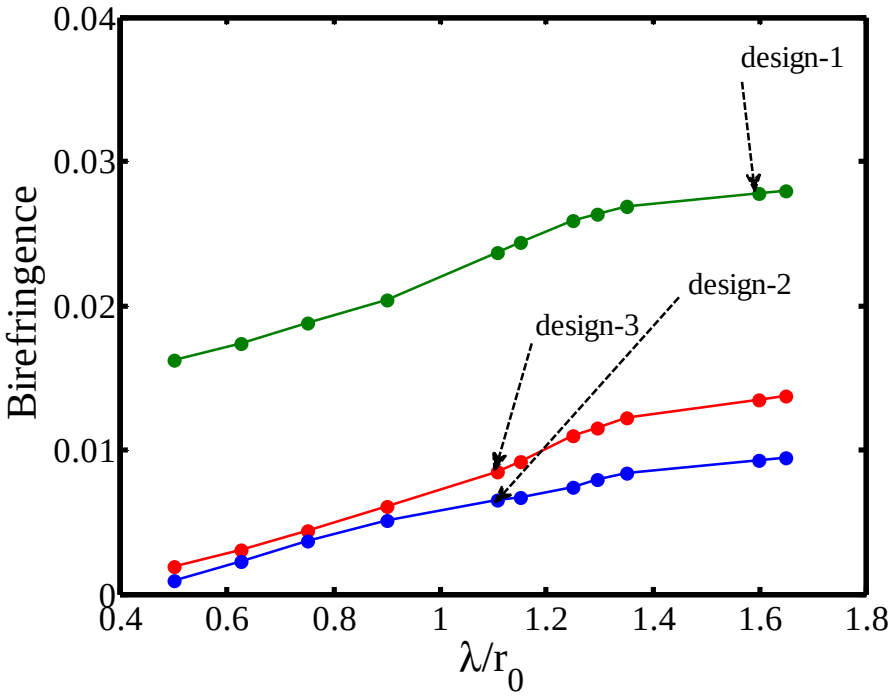

Fig. 4.20 Birefringence as a function of r_0.

diamond marker has an average dispersion of about −296 ps/nm-km with a dispersion variation of only around 8.6 ps/nm-km over the wavelength bands of interests are even far more negative than those reported in [31]-[33] and also more flat or flat almost as like as that of [58]. However, the birefringence remains between the orders of 10^{-3}~10^{-2} for these structural parameters and is seen to be decreasing when these two additional air holes are introduced in the core and also with the increase of the size of these two air holes as shown in Fig. 4.18. It is observed and also can be deduced from Figs. 4.10, 4.12, 4.16, 4.18 that the birefringence is maximum for the structure of Fig. 4.8 with hole ellipticity around 4 and it decreases with the introduction of more holes in the core resulting in structures of Fig. 4.14(a)-(b). It is also observed that the introduction of more elliptical air holes in the core in the structure of Fig. 4.14(b) does not result in significant improvement in birefringence and in the dispersion profile to be used for dispersion compensation. So, the analysis is shown for a maximum of five air holes in the core.

In Table 4.1, the optimized designs of the proposed ES-PCFs are summarized. The main focus of design no.1 is to obtain an ES-PCF with high birefringence while the main focus of the other two designs, no. 2 and 3 is to obtain ES-PCFs with flat large negative dispersion profile over the wavelength range 1350 nm to 1650 nm. Design 2, however, provides more negative dispersion with less flatness than design 3. In Figs. 4.19 and 4.20, the total dispersion and the birefringence, respectively, are shown

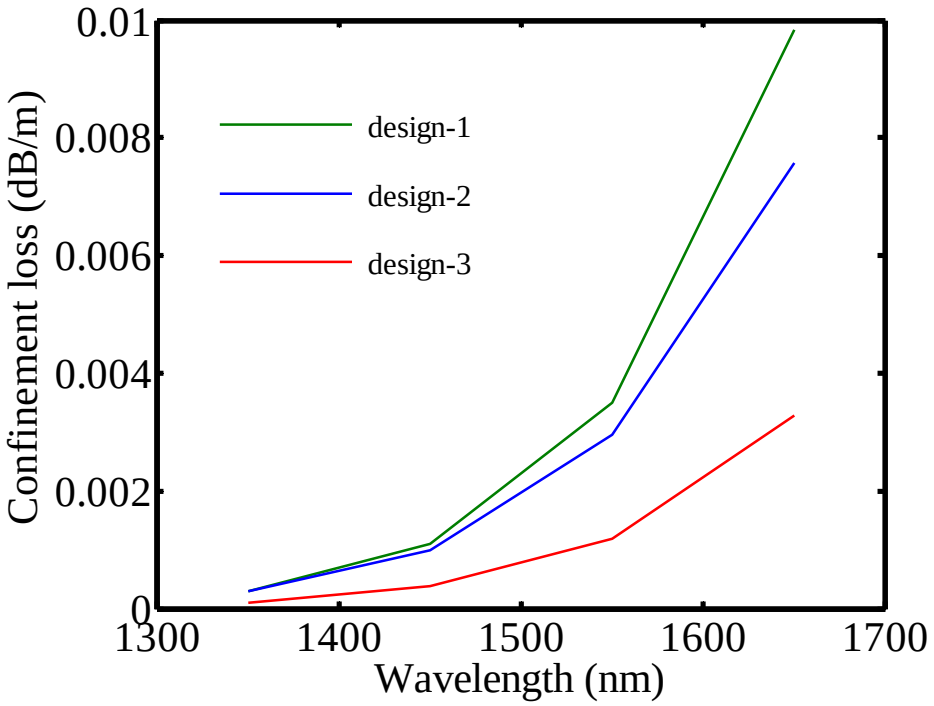

Fig. 4.21 Confinement loss versus wavelength of the fundamental mode for the proposed ES-PCF designs.

as functions of r_0 at λ= 1550 nm. Here, in these figures, by varying r_0, the whole structure is scaled up or down. In Fig. 4.19, it can be seen that the minima of the total dispersion curves of color blue and red occur at those r_0 corresponding to design no. 2 and 3, respectively as expected. As design no. 1 is optimized to obtain a very high birefringence and the focus was not on obtaining a large negative dispersion, the minima of the green line in Fig. 4.19 is not at the r_0 corresponding to design no. 1. In Fig. 4.20, one could expect that the maxima of the green curve should occur at the r_0 corresponding to design no. 1. But, the maxima occurs for a value of r_0 which is obviously smaller than that of design no. 1. This implies that higher birefringence can be achieved for lower r_0 values than the optimized one. But for r_0 lower than 0.9696 µm (design no. 1), the confinement loss becomes very high as is evident from Fig. 4.21, where the confinement losses of the optimized designs are shown as a function of λ. The confinement loss can be calculated from the imaginary part of the complex effective index [17],

$$\text{Confinement Loss} = \frac{40\pi}{\ln(10)\lambda}\,\mathrm{Im}(n_{eff})\times 10^3\ , \text{[dB/km]} \qquad (4.3)$$

where $\mathrm{Im}(n_{\mathrm{eff}})$ is the imaginary part of n_{eff}. The other two designs, design no. 2 and 3, are not optimized to obtain the highest birefringence rather they are optimized to obtain very large negative dispersion over the wavelength bands of interest. So, it is not unexpected that the maxima of the blue and red curves do not occur at those r_0 corresponding to design no. 2 and 3 respectively. Here, all the ES-PCF designs are

optimized so that the confinement loss of the fundamental mode lie within an acceptable limit of 0.01 dB/m over the entire wavelength range of interest. As shown in Fig. 4.21, the confinement loss increases with the decrease of structural dimensions. The confinement loss is the highest for design no. 1 because it has the lowest r_0 among the three designs. Also, design no. 2 has higher confinement loss than that of design no. 3. This is because the effective core index is lower in design no. 2 as it has elliptical air holes of larger size than those of design no. 3 resulting in reduced difference between the effective core index and effective cladding index. It is observed that confinement loss for all the designs increases if the number of air hole rings, N in the cladding is decreased as expected. For this reason, a large number of N=16 has to be employed to obtain confinement losses within the limit 0.01 dB/m over the entire wavelength range of interest.

Here, the single modedness of the ES-PCF is another important issue. We defined the single mode operation of the ES-PCF in a way that the confinement loss of the first higher-order mode (HOM) should be greater than 1 dB/m [16]. Also, the confinement losses of the fundamental modes are about 1.15×10^4, 1.25×10^4 and 2.1×10^4 times lower than those of the first HOMs of the design no. 1, 2 and 3, respectively, at 1.55 µm ensuring single mode operation. One can see from Fig. 4.22 that the first HOMs have cut-off wavelengths around 925 nm, 1195 nm and 1290 nm for design no. 1, 2 and 3, respectively, which are well below the wavelength range of interest (1350 nm to 1650 nm).

The issue of splice loss becomes very critical when the PCF has to be jointed with a conventional SMF in a communication link for residual dispersion compensation and maintaining polarization. The splice loss due to mode field diameter (MFD) mismatch can be calculated from MFDs of two fibers using [59],

$$\text{Splice Loss [dB]} = 20\log\left[\frac{1}{2}\left(\frac{MFD1}{MFD2}+\frac{MFD2}{MFD1}\right)\right], \tag{4.4}$$

where $MFD1$ and $MFD2$ are the MFDs of the two fibers. The transverse extent of the optical intensity distribution of a mode of an optical cavity or a waveguide is usually specified as a mode radius, which is defined like a Gaussian beam radius. For non-Gaussian mode shapes, it is also common to use a Gaussian fit and take its radius as the result. The MFD is simply twice the mode radius. Splice loss depends mostly on the difference of MFDs of the two fibers of interest. Thus, from equation (4), average splice loss for both directions can be calculated. The splice loss increases with the increase of difference between these two MFDs. The average MFD of a typical SMF is taken to be 10µm [59]. The MFDs of the proposed ES-PCF designs are calculated from $A_{\text{eff}} = \pi w^2$, where A_{eff} is the effective modal area and w is the mode field radius which is half of MFD. The A_{eff} of the ES-PCF is calculated from the following equation [43],

$$A_{\text{eff}} = \frac{\iint \left(\left|E^2\right| dxdy\right)^2}{\iint \left|E^4\right| dxdy}. \tag{4.5}$$

The A_{eff} and average splice loss between a typical SMF and the ES-PCF designs as functions of wavelength are shown in Fig. 4.23. Though the splice losses shown in Fig. 4.23 are high, they can be minimized by the technique proposed in [26]. This loss

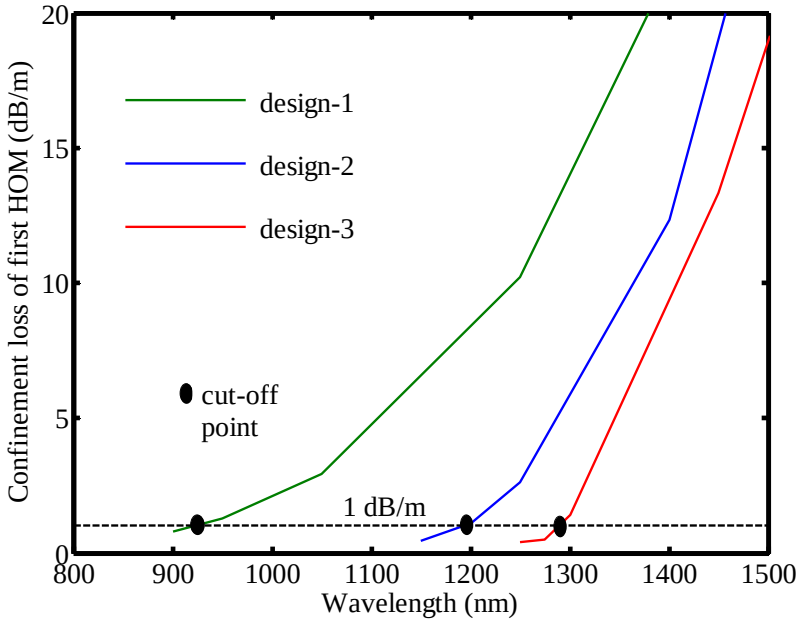

Fig. 4.22 Confinement loss of the first HOM versus wavelength for the proposed ES-PCF designs.

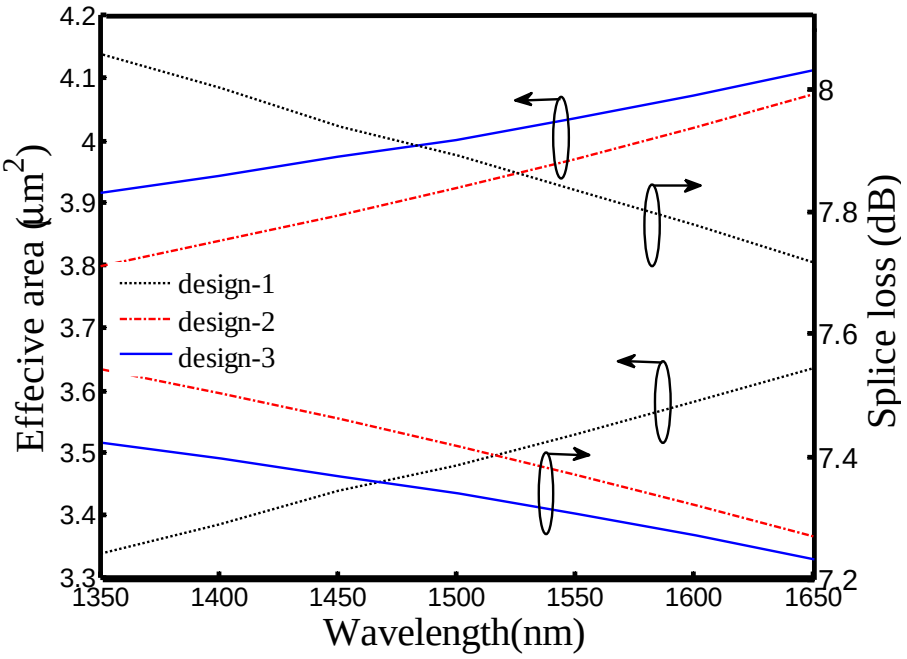

Fig. 4.23 Effective area and splice loss versus wavelength for the proposed ES-PCF designs.

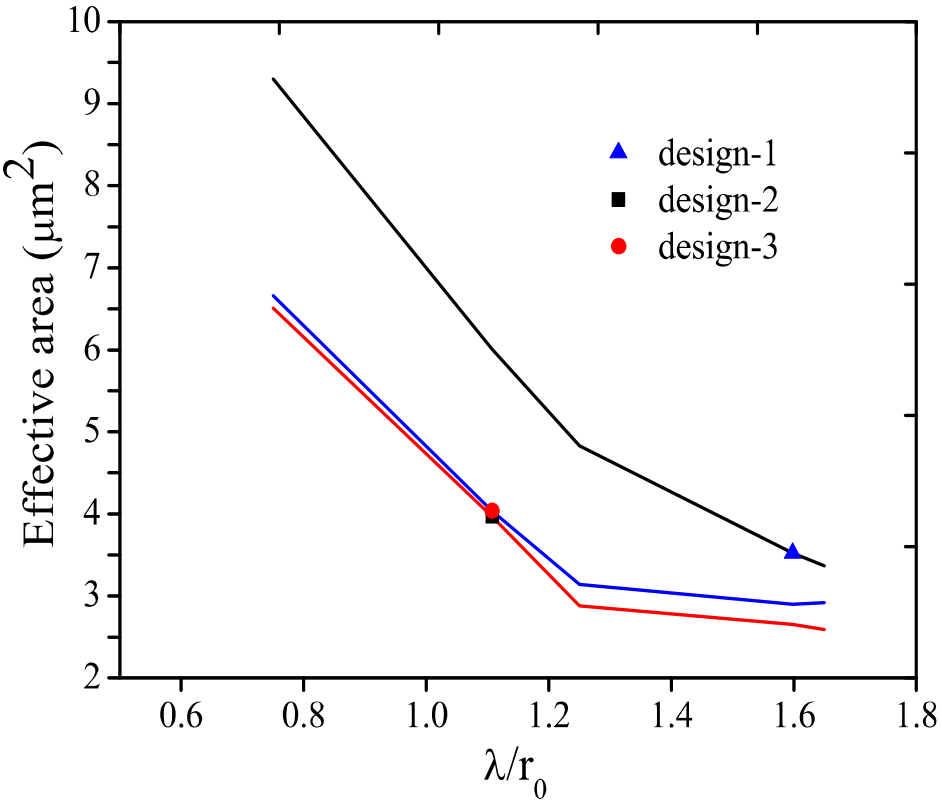

Fig. 4.24 Effective area as a function of r_0.

will also be reduced if an SMF to be spliced with the ES-PCF is used having MFD less than 10μm.

In Fig. 4.24, effective areas of the ES-PCF designs as functions of r_0 are shown. It can be deduced that at higher values of r_0, the effective area approaches that of a typical SMF resulting in reduced splice loss. But, for these values of r_0, the desired dispersion and birefringence cannot be obtained as is evident from Figs. 4.19 and 4.20. So, a trade-off has to be made between low splice loss and large negative dispersion with high birefringence. A large negative dispersion and high birefringence normally yields low effective area and vice versa.

4.2.3 Outcomes

In this section, ES-PCF is investigated as a polarization maintaining residual dispersion compensating fiber in the telecommunication wavelength bands. It is numerically shown to exhibit an average dispersion of −293.5 ps/nm-km and −393 ps/nm-km for two different designs with dispersion variation of only 8.6 ps/nm-km and 10.4 ps/nm-km, respectively. To our knowledge, this dispersion profile is more negative than the residual dispersion compensating fibers reported earlier. Another unique feature of these designs is their high birefringence along with the property of dispersion compensation. An optimized structure exhibits a birefringence as high as 0.0278. The structural dependence as presented in the paper also shows that large negative and flattened dispersion and high birefringence can be obtained over a wide

wavelength range and this structure can be considered to be robust with respect to small variations in structural parameters which are unavoidable during fabrication. The dual characteristics of dispersion compensation and high birefringence make this fiber a promising candidate in its application in the fiber optic communication link in the telecommunication window.

4.3 Liquid Crystal Infiltrated Residual Dispersion Compensating ES-PCF

Here, two more elliptical air holes than the design presented in section 4.1 in the core as shown in Fig. 4.8, have been used and the elliptical air holes are surrounded by a circular region containing nematic liquid crystal. An average dispersion of −259 ps/nm-km with dispersion variation about 4.58 ps/nm-km has been obtained over the

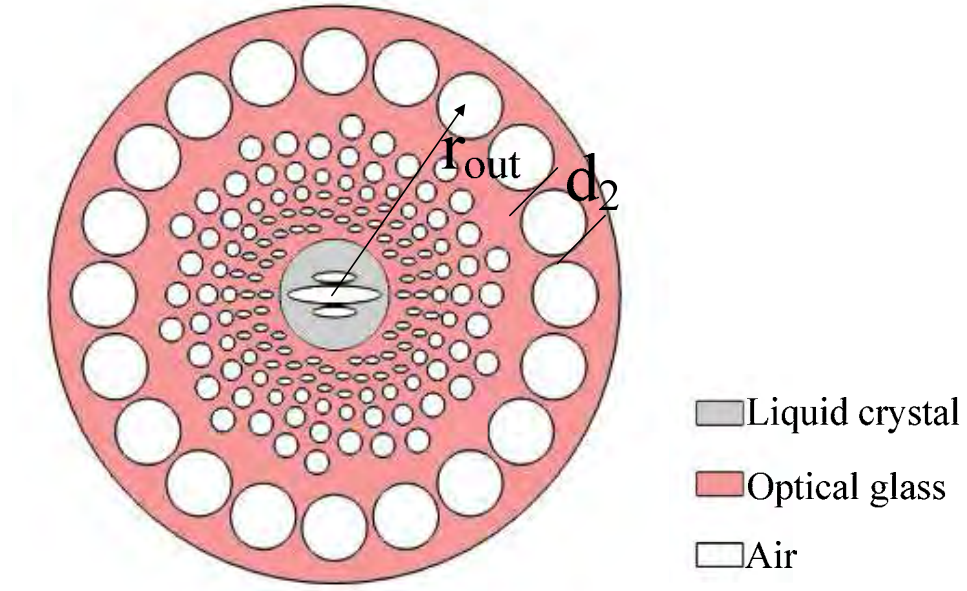

(a)

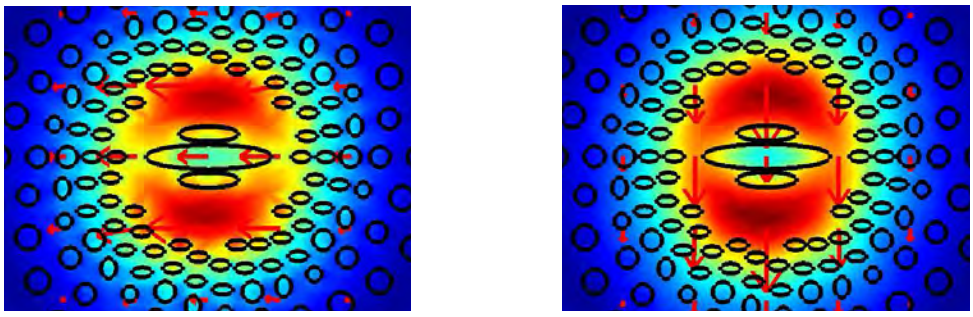

(b) (c)

Fig. 4.25 (a) Cross section of the proposed ES-PCF with infiltration of liquid crystal, (b) electric field distribution and (c) magnetic field distribution of the fundamental mode.

wavelength range 1.35 µm to 1.675 µm. Also the proposed fiber shows single polarization with one of its two degenerate fundamental modes completely suppressed and its single modedness is ensured. Also, the dispersion is more negative than those of recently published works [31]-[33], [58]. Although the dispersion compensating fibers of section 4.1 and 4.2 shows very high birefringence, complete achievement of single polarization was not possible there.

4.3.1 Design of liquid crystal (LC) infiltrated ES-PCF

Fig. 4.25 shows the air hole arrangement in the proposed design in a optical glass background with refractive index, n_g. In this design, there are N_r air holes in each ring. The first ring has a radius of r_0 and the radii of the subsequent rings increase by geometric progression. Each air hole of the first ring is the starting point of a spiral arm. There are N circular air holes in each arm. The first seven of them are elliptical having major axis length d_{ma} and minor axis length d_{na}. The angular position of each air hole in an arm is increased by θ than the previous one. The major and minor axes lengths of the central defect air hole are d_m and d_n, respectively. The elliptical air holes just below and above the central one have major axes length d_{m1} and minor axes length d_{n1}.

The single-modedness of the proposed ES-PCF is difficult to achieve as its fundamental space filling mode, n_{FSM} is much lower than the effective core index, n_{core}. This can be inferred from the compactness of the air holes surrounding the core. The single-modedness is thus achieved by employing a unique technique discussed in [57]. For this purpose, a secondary annular core is introduced at the outer cladding of the ES-PCF. as shown in Fig. 4.25. This secondary core has radial distance from the center, r_{out} and the diameter of the air holes of this ring is d_2. The values of r_{out} and d_2 are so optimized that the resulting secondary core modes occur as degenerate modes with the higher order modes (HOMs) of the central core. Coupling of energy between the secondary core modes and the central HOMs makes these HOMs very lossy over the entire wavelength range of interest [57]. It is observed that the HOMs of the central core have confinement loss more than 1dB/m and thus, they can be effectively suppressed [42] to realize the single mode (SM) condition in ES-PCF. There is a cylindrical region in the core having a radius of r_{lc} filled with a typical nematic LC material.

Nematic liquid crystals are anisotropic materials consisting of rod-like molecules whose axis coincides with the anisotropy's optical axis. When confined in closed cylindrical cavities in the absence of external stimuli, the liquid crystal's director distribution is determined by the physics of elastic theory and the anchoring conditions at the cavity's surface [35]. Under the application of a static electric field the director's orientation can be controlled, since the liquid crystal molecules tend to align their axis according to the applied field. In an alternative approach, the properties of nematic liquid crystals can be tuned thermally owing to the dependence of the refractive index values on temperature. The above features have favored their

utilization in a number of recently proposed photonic crystal based optoelectronic devices [35].

The nematic liquid crystal (LC) material in the core is characterized by ordinary and extraordinary refractive indices of n_o and n_e, respectively. The anisotropic refractive index of nematic LC is utilized to obtain a single polarization behavior of the proposed ES-PCF over the entire bands of wavelength of interest. The ES-PCF is analyzed for a uniform distribution of the nematic director along x- or y-axis (the direction of propagation is along the z-axis). Though this condition is somewhat ideal, it can be achieved under the influence of the appropriate homeotropic anchoring conditions or by controlling the nematic director through the application of an external electric (or magnetic) static field [35]. The fiber material is chosen such that its index, n_g is slightly lower than the extraordinary index of the LC material n_e. Among the various types of available fiber glasses for which $1.5 < n_g < 1.8$ are the high-lead silicate, barium crown, lanthanum crown, or barium flint fiber glasses [35]. The refractive index of these glasses can b\e tuned, for instance, by adjusting the doping percentage of metal oxides such as lead (PbO) or lanthanum (La2O3) oxides. For the purposes of the present analysis, we selected the common nematic material E7 with n_e and n_o around 1.68 and 1.5, respectively and barium flint as fiberglass with n_g around 1.66. The material dispersion is taken into account by using the Sellmeier equation to obtain the refractive index of barium flint and LC E7 at different wavelengths. The fiber is considered to be uniform along the z-axis, which coincides with the axis of the cylindrical defect core. It is to be noted that LC E7 has melting point around 70° C. So, it is possible to have air holes inside the LC region of the central core.

4.3.2 Simulation results

An RDCF should have a flat negative chromatic dispersion of high magnitude in the wavelength band of interest. In this work, the optimized structural parameters are: r_0= 1.4 µm, r_{lc}= 1.4 µm, d_m= 1.91 µm, d_n= 0.384 µm, d_{m1}= 0.91 µm, d_{n1}= 0.2275 µm, d_{ma}= 0.31 µm, d_{na}= 0.15 µm and θ = 12°. The design shows an average value of chromatic dispersion equal to −259 ps/nm-km with a dispersion variation of 4.58 ps/nm-km (between −256.96 ps/nm-km and −261.54 ps/nm-km) in the wavelength range 1350nm to 1675nm for the fundamental x-polarized mode. In Fig. 4.26, we have compared the results of total dispersion with those obtained by Franco et. al.

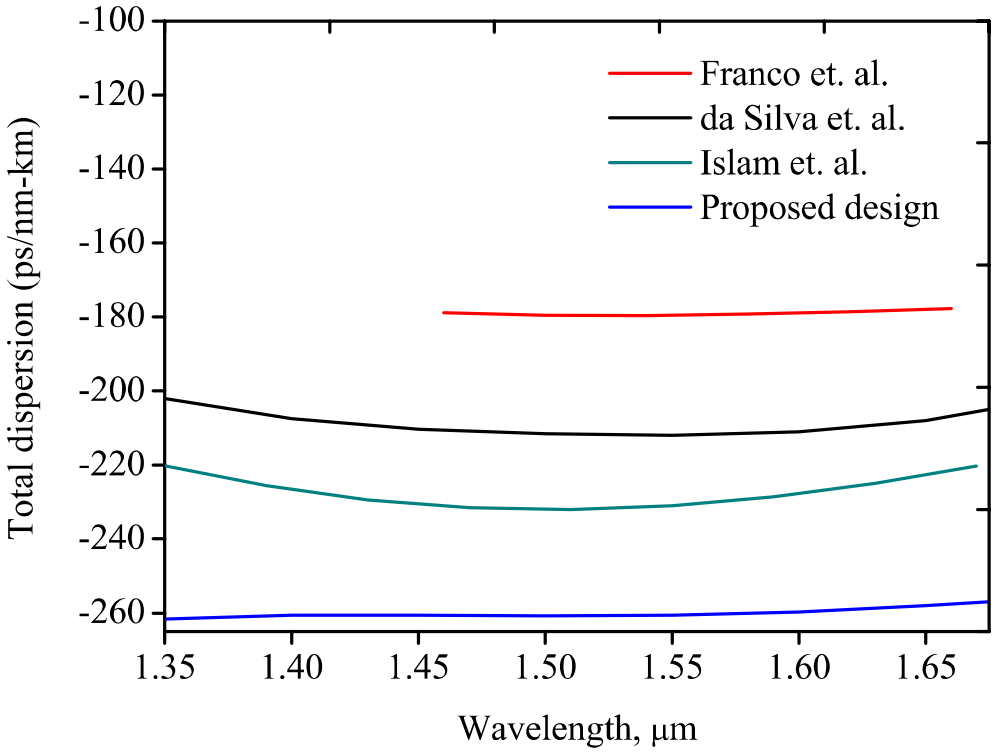

Fig. 4.26 Dispersion profile of the Proposed ES-PCF in comparison with other profiles reported in the literatures.

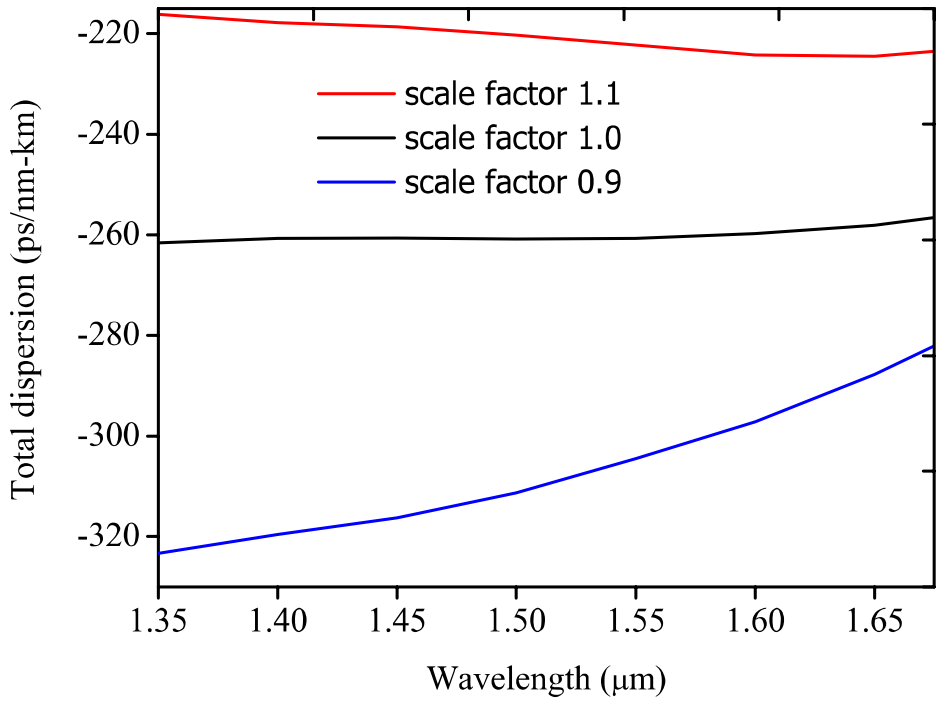

Fig. 4.27 Dispersion profile of the Proposed ES-PCF for different scale factors applied over the whole geometry.

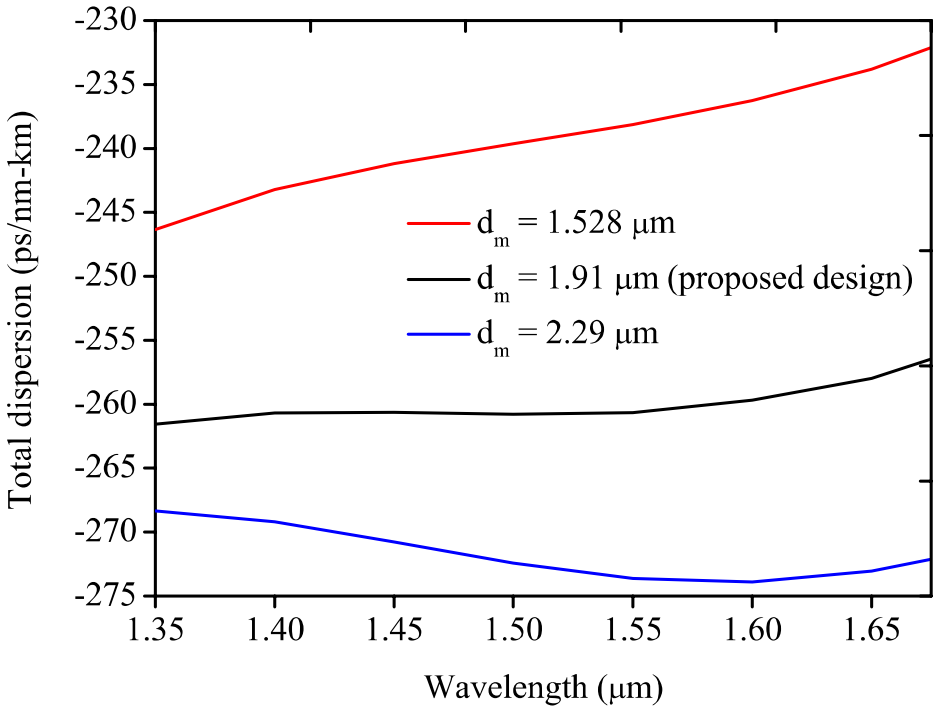

Fig. 4.28 Dispersion profile of the Proposed ES-PCF as a function of d_m.

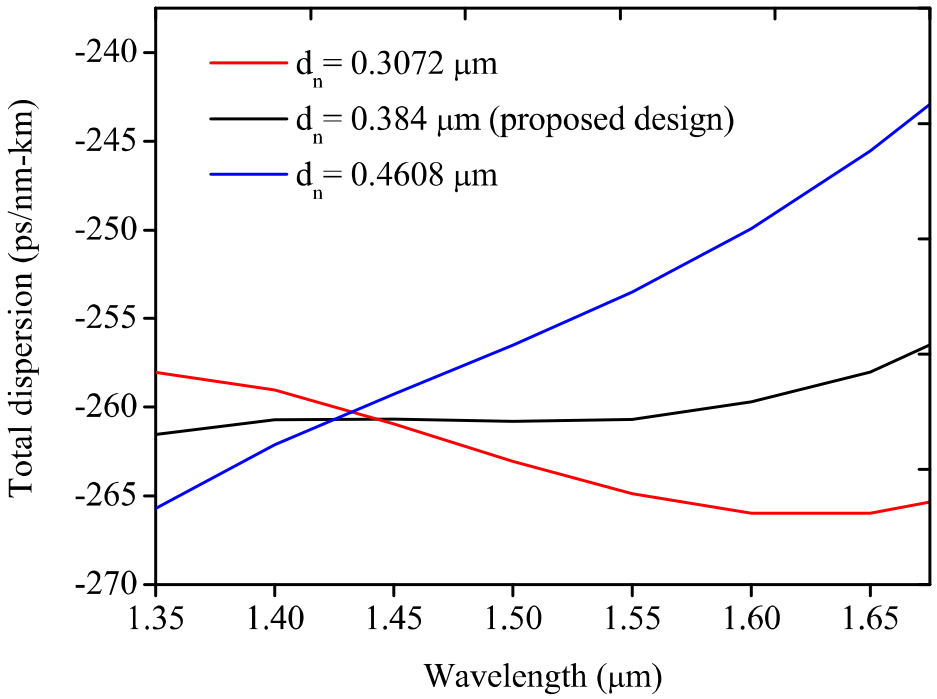

Fig. 4.29 Dispersion profile of the Proposed ES-PCF as a function of d_n.

[31], da Silva et. al. [32] and the author [58]. The proposed design exhibits more negative and also more flat dispersion profile than these literatures except [31]. Though the dispersion variation of [31] is slightly less than the present design,

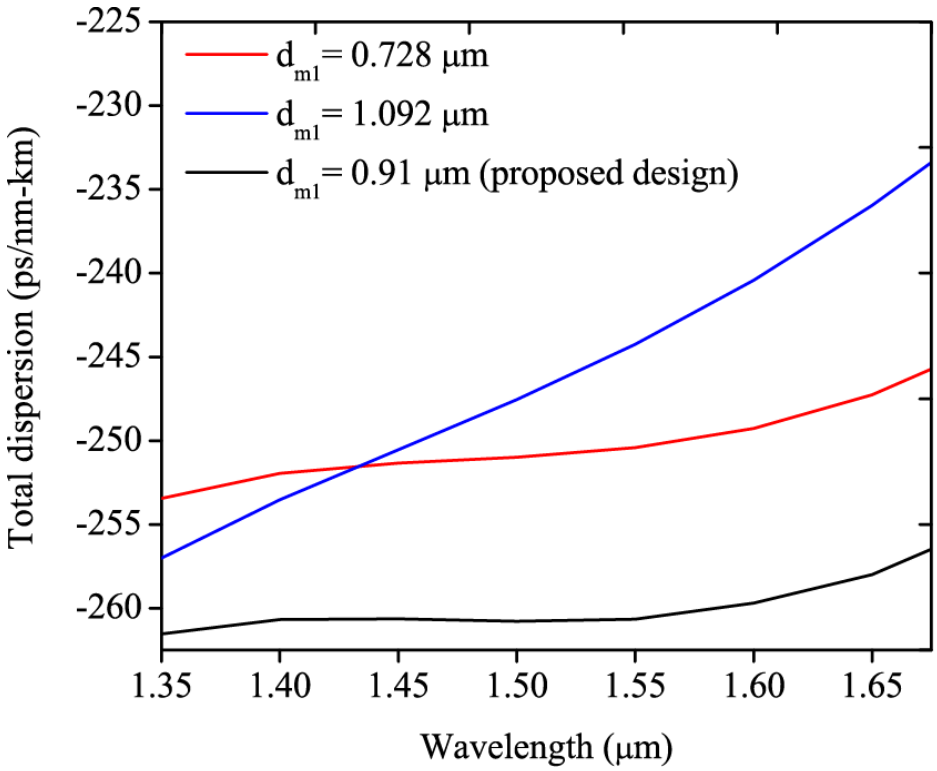

Fig. 4.30 Dispersion profile of the Proposed ES-PCF as a function of d_{m1}.

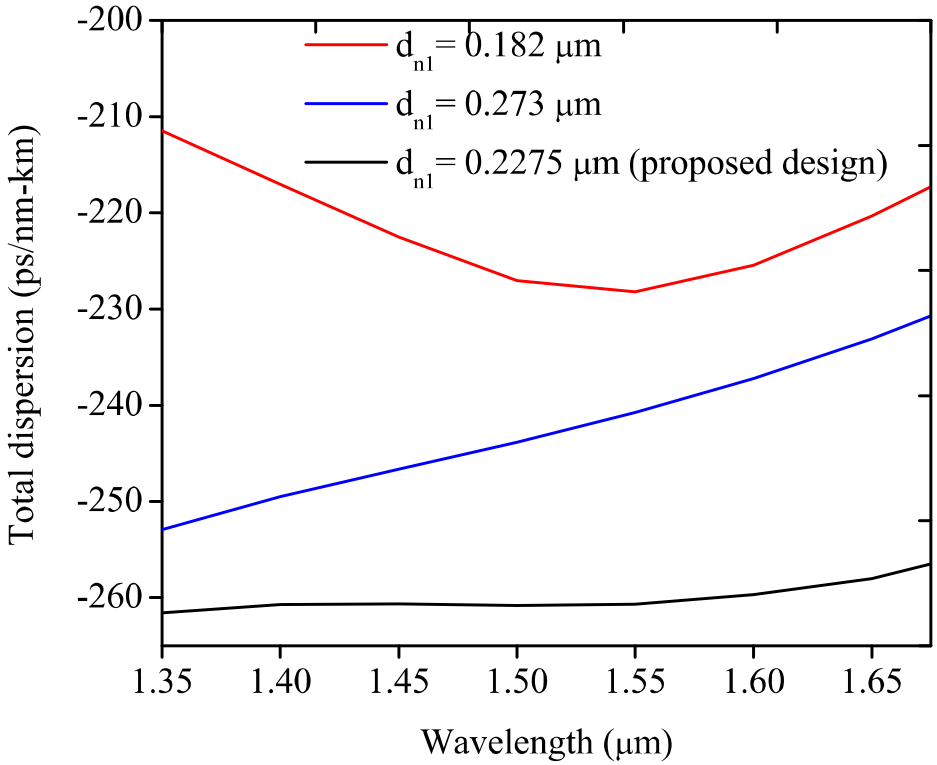

Fig. 4.31 Dispersion profile of the Proposed ES-PCF as a function of d_{n1}.

its dispersion value is less negative. Also, it shows a dispersion profile for a shorter range of wavelength.

In Fig. 4.27, we show the total dispersion versus wavelength for three values of scale factor applied to all over the cross sectional geometry of the fiber. The scale factor can be used to scale up or down the overall cross sectional geometry of the ES-PCF. It can be seen here that smaller scaling factor yields more negative dispersion profile but with larger variation of it. On the other hand, for larger scaling factor, the dispersion profile shifts upward.

In Figs. 4.28 and 4.29, the total dispersion versus wavelength as a function of d_m and d_n are shown, respectively. Though dispersion profiles more negative than the proposed design can be achieved for higher values of d_m and d_n than those of proposed design, the proposed design has the most flat dispersion profile than that of others as evident from Figs. 4.28 and 4.29.

The total dispersion versus wavelength for different values of d_{m1} and d_{n1} are shown in Figs. 4.30 and 4.31, respectively. Here, it is shown that the total dispersion is the most negative and flat for the d_{m1} and d_{n1} of the proposed structure.

The confinement and bend losses are also very important features to be considered during fiber design. High confinement or bend loss is a limiting factor for a fiber to be used efficiently as a part of the communication system. Here, the ES-PCF design is optimized so that the confinement loss of the fundamental mode of the central core remain within an acceptable limit of 0.01 dB/m over the entire wavelength range of interest. The confinement losses of the HOMs of the central core is greater than 10 dB/m for the entire wavelength range of interest. Thus, the HOMs are effectively suppressed. The bending loss of the proposed ES-PCF is found to be 0.02 dB/m around bending radius 500 µm which is lower than that of hexagonal lattice PCF having similar structural dimensions. This low value of bending radius is attributed to the compactness of air holes surrounding the central core. It is also found that the average effective area of this ES-PCF is around $5\mu m^2$ and the calculated splice loss is around 6.5 dB. This loss can be reduced using fusion splicing reported in [60].

4.3.3 Outcomes

Here, an ES-PCF is investigated to obtain a more negative flat dispersion profile than that of the recently published literature. With a change in the background material from silica into fiber glass, it exhibits a more negative dispersion profile having an average value of −259 ps/nm-km with much smaller dispersion variation than those of recently published results over the wavelength range 1.35 µm to 1.675 µm. Two additional elliptical air hole are employed in the central core with the previous one to get this lowered dispersion profile. Also, the previous ES-PCF structure is further modified by introducing a cylindrical region in the central core containing nematic LC material having anisotropic index. This feature allows the suppression of one of the two degenerate fundamental modes resulting in single polarized operation of the proposed ES-PCF. Moreover, the apparently unavoidable HOMs of the central core are effectively suppressed by an ingenious technique. To the best of our knowledge, this is the first single polarization residual dispersion compensating fiber with a large

negative flat dispersion profile. These novel characteristics make this fiber a promising candidate in its application in the fiber optic communication link in the telecommunication window.

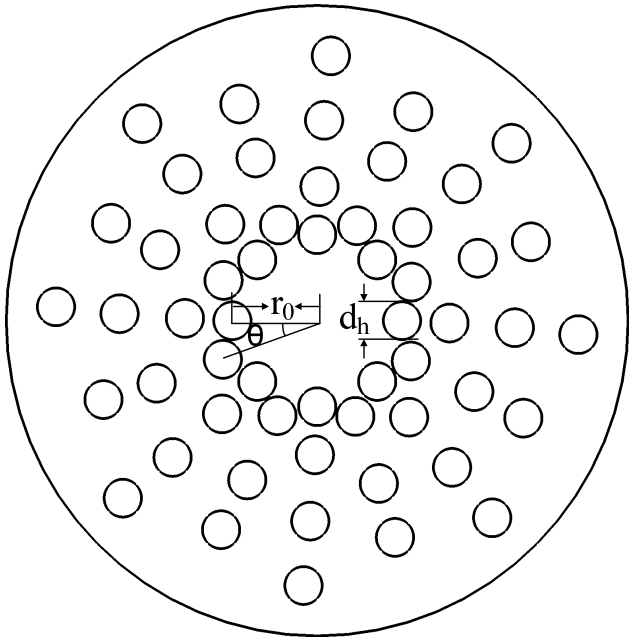

Fig. 4.32 Geometrical model of the proposed ES-PCF.

4.4 Mode Degeneration in ES-PCF

As ES-PCF is found to be a potential candidate to achieve useful properties in fiber optic communication system, many important properties of this type of PCF like confinement loss, bending loss, mode degeneration of core mode with the cladding modes etc. need to be investigated thoroughly to explore different possible applications. In the practical applications of PCFs, one cannot avoid bends, twists and stresses on the fiber. When a fiber is bent, the modal field shifts in the outward direction and radiation loss occurs. One of the main disadvantages suffered by standard silica fibers has been that significant bending loss arises due to the low index contrast between the core and cladding when compared to that of a PCF [40]. However, sometimes the need for a small bending radius may be unavoidable in a specific application. Also, bending effects have also been exploited to design functional devices such as ring resonators, arrayed waveguide filters, optical delay lines, bend attenuators, to suppress higher order modes etc. [40].

To study the arbitrary bends in PCFs, various methods are used. Among them conformal transformation is widely used [27]. In this transformation, a curved dielectric waveguide is converted to its equivalent straight one with a modified index

profile. The coordinate transformation maps the refractive index profile $n(x,y)$ of a bent PCF to its equivalent straight fiber's refractive index $n_{eq}(x,y)$ using the following formula [27],

$$n_{eq}(x,y) = n(x,y)\left[1+\frac{x}{R}\right], \quad \text{where } 2x \ll R \tag{4.6}$$

Here, R is the radius of the curvature and x is the distance from the center of the waveguide. The wavelength dependent refractive index of silica material is obtained by using the Sellmeier equation.

4.4.1 ES-PCF design

Fig. 4.32 shows the air hole arrangement in a silica background of the proposed ES-PCF design. In this design, there are N_r air holes in each ring. The first ring has a radius of r0 and the radii of the subsequent rings increase by geometric progression. Each air hole of the first ring is the starting point of a spiral arm. There are N circular air holes in each arm having diameter d_h each. The angular position of each air hole in an arm is increased by θ than the previous one. The d_h is set at a value to obtain the required ASR for each case.

4.4.2 Simulation results

In Figs. 4.33(a)-(c), the comparison of variations of the total loss of the fundamental slow axis mode with the bending radius R between H-PCF and ES-PCF are shown for the wavelength 1550 nm. Here, N_r = 8, N = 4, and θ = 22°. At first, total loss is determined for r0 = 2.6 µm. Then the whole ES-PCF structure is scaled up to obtain higher structural dimensions with r0 = 3.8 µm and r0 = 5 µm and total loss is determined for these cases. This procedure is repeated for three values of ASRs: 0.1686, 0.2092 and 0.2332. The curves having the same color are similar structures of ES-PCF and H-PCF and are subject to comparison of their total losses. Here, for H-PCF, the number of air hole rings is N_h = 3 and the air hole diameter d is set at a value to obtain the required ASR. Here, the total losses for the fundamental fast axis mode are not shown as these are seen to be similar to those of the slow axis mode.

It is known that at lower structural dimensions, a PCF operates closer to its modal cut-off than its higher structural dimensions. When a PCF operates close to its modal cut-off, the leakage loss becomes high which is evident in Fig. 4.33 at lower structural dimensions (for $R = 10^4$ µm the total loss contains mainly the confinement loss, as the pure bending loss is nearly zero). As the bending radius is reduced, the bending loss increases gradually and as a result the total loss also increases. The rate of increase is more for higher structural dimensions which is obvious according to eqn. (4.6). For higher structural dimensions the term x in eqn. (4.6) becomes more dominant than that for lower dimensions and the total loss increases.

Though PCFs having higher values of structural dimensions are used in many applications for their lower total loss for large bending radii, they show high total loss for low bending radii [40]. This loss may become even higher than that of PCFs

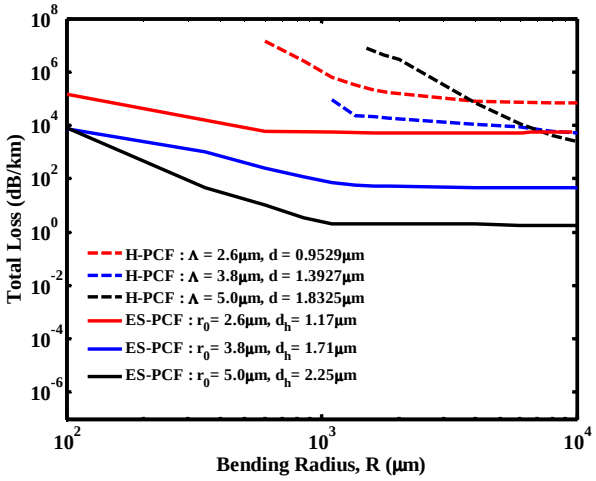

(a)

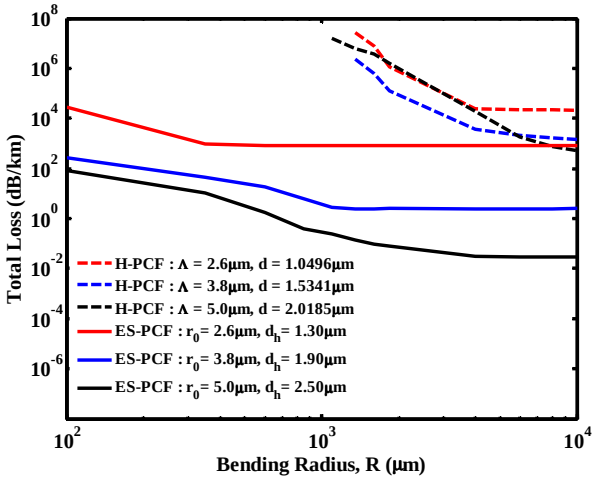

(b)

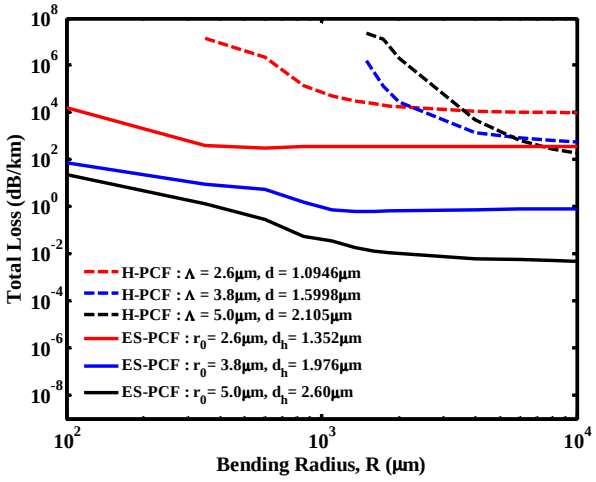

(c)

Fig. 4.33 Comparison of leakage loss as a function of bending radius between H-PCF and ES-PCF, (a) ASR = 0.1686, (b) ASR = 0.2092 and (c) ASR = 0.2332.

having lower values of structural dimensions as shown in Fig. 4.33. But, in ES-PCF, this is less likely to occur. Also, it can be seen from Fig. 4.33 that at higher bending radii the confinement loss is 10^2 to 10^3 times lower in ES-PCF than in H-PCF. At lower bending radii this total loss becomes even lower in ES-PCF than that of H-PCF (10^3 to 10^6 times on the average). In [40], the degeneration of the cladding modes with the fundamental core mode is discussed for a conventional H-PCF. The degeneration occurs at $R \approx 1445$ µm for $\Lambda = 5$µm, d = 2.5 µm and $N_h = 3$ which is also confirmed in our calculation. At *R* larger than this value, the effective index of the fundamental core mode is greater than that of the highly dispersive first cladding mode. But when *R* is smaller than this value, the effective index of the first cladding mode becomes larger. Coupling between the fundamental core mode and cladding mode, occurring at the point of degeneration, is responsible for a sudden rise in leakage loss for conventional H-PCFs according to [57]. But, as seen in this work, for ES-PCF, no such cladding mode exists for the structures considered here. This may be due to the less number of air hole rings which cannot confine cladding modes. So, the sudden rise in leakage loss like that in H-PCF, was not observed in ES-PCF for similar bending radii. Although at a very low value of *R*, the power distribution of the fundamental core mode shifts far from the center along the bending direction and a significant amount of power leaks out of the core.

In Fig. 4.34, the power distribution is shown for three different bending radii for the proposed ES-PCF with ASR = 0.2092, r0= 5 µm and d_h= 2.5 µm. It can be observed from here that the distribution shifts more to the direction of bending (along x axis in this case) as the bending radius gets lower. But, the field as well as power does not leak into the cladding like that of H-PCF [40].

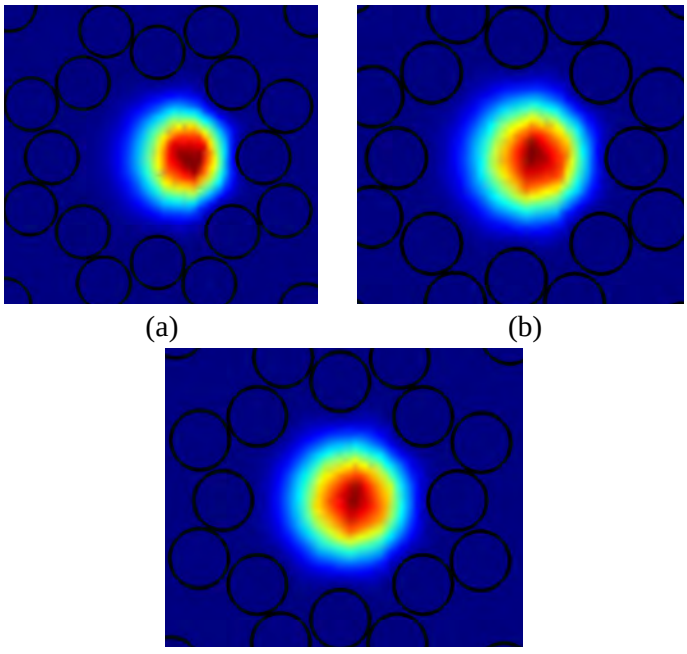

(a) (b)

(c)

Fig. 4.34 Power distribution of the fundamental mode of the ES-PCF at bending radii, (a) 500 µm, (b) 1000 µm and, (c) 1500 µm.

From Fig. 4.35, it can be observed that the effective area values of ES-PCF are almost similar at higher bending radii to those of H-PCF for similar dimensions. But, at lower bending radii, effective area decreases for ES-PCF whereas for H-PCF it increases. This is because the field of fundamental core mode is highly confined in the core even at lower bending radii for ES-PCF and cannot leak in the outer cladding much as the air holes of the first two cladding rings are very compact. But, in H-PCF, the field for fundamental core mode easily leaks in the outer cladding as the bending radius gets lower.

To understand the abrupt increase of total loss, we show the total loss and n_{eff} at lower bending radii in Fig. 4.36, where the structural dimensions are same as those of blue dotted line in Fig. 4.33(b). Here both n_{eff} and total loss increase very rapidly as R is reduced from 280µm. This can be attributed to the term x of eqn. (4.6), from where one can deduce that the difference of effective refractive indices of the core and cladding reduces even more rapidly at lower values of R. Thus, it accelerates the rise of total loss at the same R as the n_{eff} starts to grow rapidly even though there is no coupling between fundamental core mode and cladding mode.

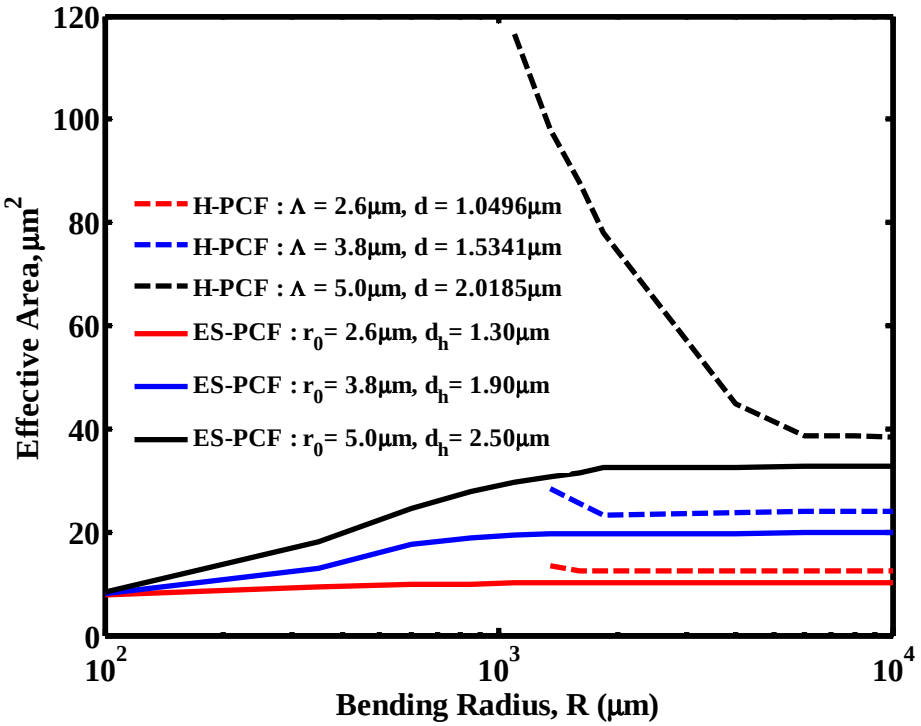

Fig. 4.35 Comparison of effective area as a function of bending radius between H-PCF and ES-PCF for air-silica ratio 0.2092.

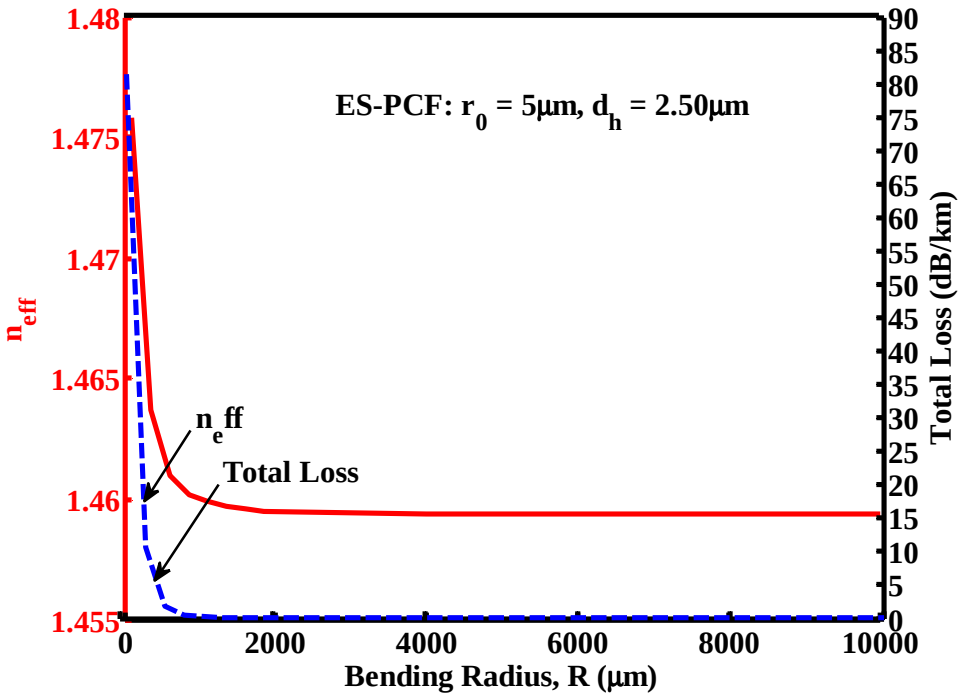

Fig. 4.36 The effect of reducing bending radius on effective index and total loss of the fundamental core mode.

4.4.3 Outcomes

In conclusion, it can be said that for similar dimensions an ES-PCF shows confinement losses almost 2 to 3 order of magnitude lower than that of an H-PCF at higher bending radii. At lower radii, ES-PCF shows even lower bending loss (10^3 to 10^6 times on the average) than H-PCFs. Also we have found no mode degeneration between fundamental core mode and first cladding mode like H-PCFs in ES-PCFs as there was no significant cladding modes for the structural dimensions considered here. This phenomenon is related to the very low bending loss of ES-PCFs. Now, it can be said that ES-PCFs are less sensitive to bending than H-PCFs. The reason of rapid rise of total loss at lower bending radii (much lower than that of H-PCF) is also discussed. The ES-PCF can thus play a significant role in the optical communication system as a low loss optical fiber.

4.5 Bend Insensitive Single Mode Spiral PCF with Large Effective Area

The high leakage loss of a bent PCF can be minimized to an acceptable level by appropriately choosing the air hole diameters. But, apart from low bending loss, other two conditions are to be met simultaneously. These are, the higher order modes which are usually unavoidable in a low bending loss PCF, should be suppressed and the effective mode area of the fundamental mode of the PCF should be very close to that of a typical single mode fiber (SMF) to minimize the splice loss. This is a challenge to meet these three conditions simultaneously as they are usually conflicting. However,

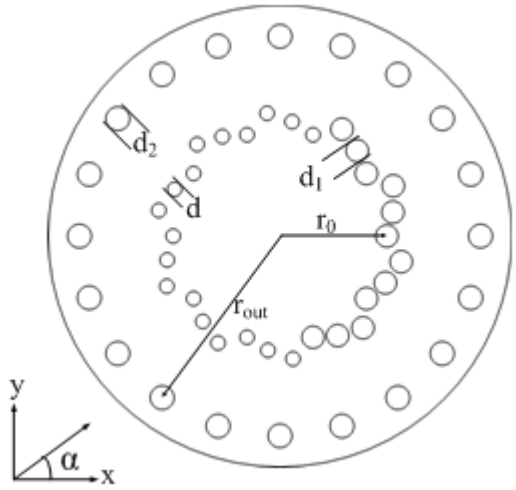

Fig. 4.37 Cross section of the proposed ES-PCF.

several such designs have been reported in the literatures [42]-[45] for hexagonal lattice PCFs.

In this section, an equiangular spiral photonic crystal fiber (ES-PCF) with a very low bending loss, suppressed higher order modes (HOMs) and large effective modal area close to that of a standard SMF is proposed. The ES-PCF has an asymmetric cladding structure with air holes of larger diameter in one side and air holes of smaller diameter in the opposite side. If the fiber is bent to a particular direction (along x axis or around, in Fig. 4.37), the propagating modes will become more confined upto a certain bending radius resulting in reduced leakage loss even lower than that of the same straight ES-PCF. This phenomenon is unique as compared to that of other literatures. The proposed ES-PCF exhibits a leakage loss of about 8.32×10^{-4} dB/turn (0.033 dB/m) at the wavelength of 1.55 µm for a bending radius as low as 4 mm, effective modal area 80.78 μm^2 at the same wavelength for a straight fiber resulting in a very low splice loss of about 0.00086 dB, and the cut-off frequency of the HOMs below 1.35 µm.

4.5.1 ES-PCF design

Fig. 4.37 shows the air hole arrangement in silica background. In this design, there are 10 air holes in each ring. The first ring has a radius of r_0 and the radii of the subsequent rings increase by geometric progression. Each air hole of the first ring is the starting point of a spiral arm. There are 3 circular air holes in each arm. Among the 10 spiral arms, 6 arms have air holes of diameter d and the remaining 4 have air holes of diameter d_1 where $d_1 > d$ to ensure lower leakage loss due to bent in a particular direction (along x axis or around in this case). The angular position of each air hole in an arm is increased by $\theta = 12°$ than the previous one.

As shown in Fig. 4.37, a secondary core is introduced in the cladding region beyond the third air hole ring by employing another ring of air holes at a distance r_{out} from the

center and diameter of air holes d_2. As will be shown later, these secondary core modes appear as degenerate modes with the HOMs of the central core. Thus these HOMs become lossy and effectively can be suppressed [57]. A HOM is suppressed if the associated leakage loss is greater than 1 dB/m [44].

4.5.2 Simulation Results

A full-vectorial finite element method (FEM) has been used to characterize the proposed ES-PCF. An anisotropic perfectly matched layer (PML) has been used to accurately account for the leakage losses. The material dispersion is taken into account here by using the Sellmeier equation to obtain the refractive index of silica at different wavelengths. Here, r_0 of the ES-PCF corresponds to the parameter Λ (hole to hole spacing) of a hexagonal lattice PCF and in this section, a change in r_0 implies change in every parameter of the ES-PCF structure by the same factor.

For a low splice loss the mode field diameter (MFD) of the ES-PCF should be as close as possible to that of a standard SMF to which it is to be spliced [58]. It is observed here that the MFD of the ES-PCF depends much on r_0 and less on d_1/d. At first, r_0 is chosen for which the MFD is close to that of a standard SMF (10 µm) and then, d_1/d and d_2 are optimized to achieve suppression of HOMs and low bending loss simultaneously. Fig. 4.38 shows how MFD and splice loss vary for different r_0 as a function of d_1/d. Here, it is obvious that splice loss is minimum for r_0 = 6.5 µm and does not change much with the change of d_1/d. So, this value of r_0 is chosen for the structure and d_1/d is optimized to obtain single modedness with low bending loss simultaneously. Here, d = 0.878 µm, r_{out} = 12.2 µm and d_2 = 1.452 µm are set fixed for r_0 = 6.5 µm. d_1 is varied to obtain the desired features of the ES-PCF.

It is observed that the leakage loss of both the straight and bent fibers increase with the increase of wavelength. To obtain a low bending loss large effective area ES-PCF with HOMs suppressed over the wavelength range1.35 µm to 1.65 µm, the cut-off frequency of the first HOM should be below 1.35 µm over the range of bending radii of interest. Also, the leakage loss of the fundamental mode (FM) should be very low at 1.65 µm which will ensure lower leakage loss below 1.65 µm. In Figs. 4.39 and 4.40, leakage loss of first HOM at 1.35 µm and FM at 1.65 µm are shown, respectively, over the bending radii 2 mm to 10 mm for r_0 = 6.5 µm with $\alpha = 0°$ when the cladding air holes with radius d_1 remains at the outside of the bend. Here, α is the angle of bending orientation.

It can be seen from Fig.4.39 that the first HOM is suppressed for all three d_1/d values (leakage loss greater than 1 dB/m) over the bending radii 2 mm to 10 mm. As the leakage loss of the first HOM is decreasing with the increase of bending radius, one may expect that it will fall below 1dB/m line for a certain value of the bending radius. But, it has been found that, the minima of the leakage losses of the first HOM are 1.86 dB/m, 1.81 dB/m and 1.76 dB/m, which occurs at bending radius around 10 mm for

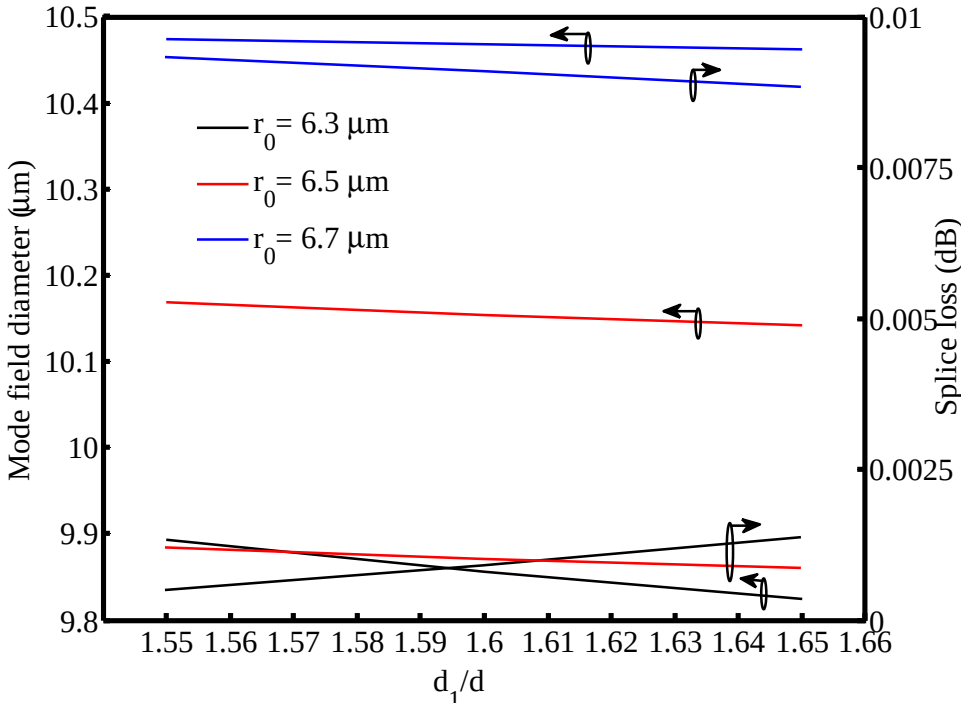

Fig. 4.38 Mode field diameters and corresponding splice losses as functions of d_1/d at 1.55 μm for straight fiber.

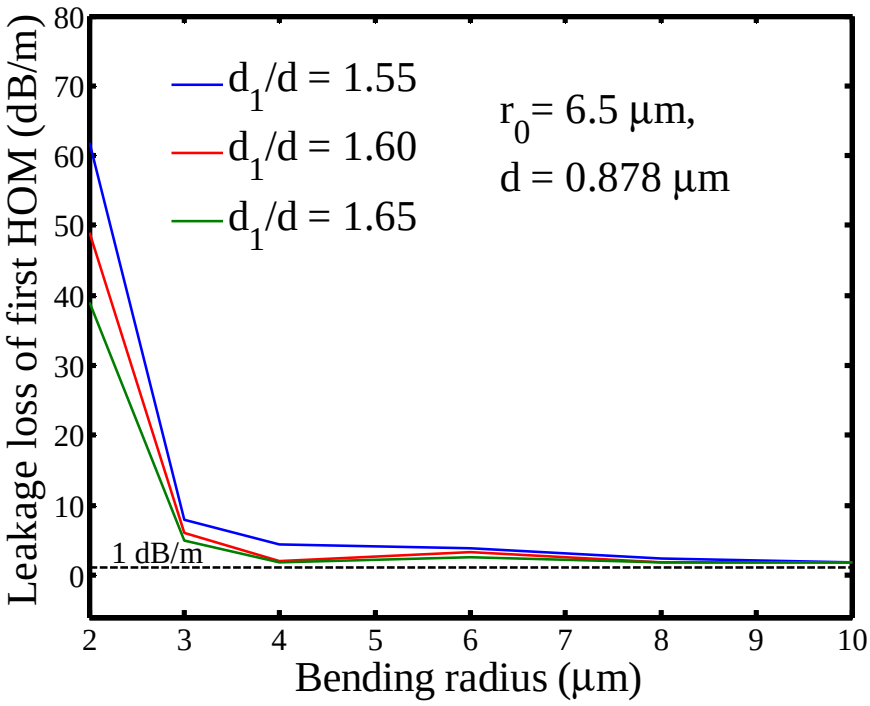

Fig. 4.39 Leakage loss versus bending radius of the first HOM at 1.35 μm.

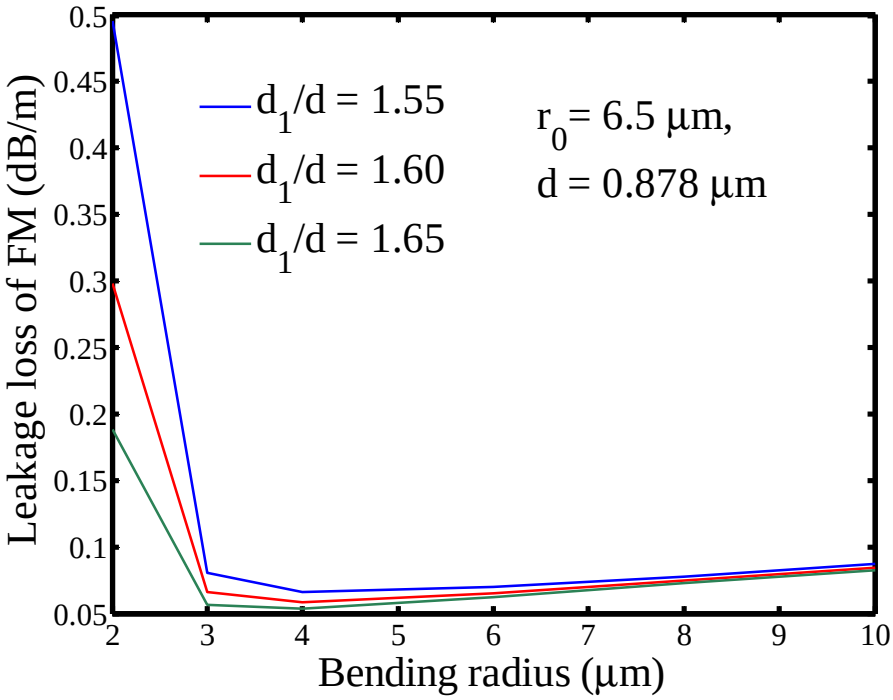

Fig. 4.40 Leakage loss versus bending radius of the fundamental mode at 1.65 μm.

d_1/d = 1.55, 1.60 and 1.65, respectively. Also, the leakage losses of a straight fiber are 3.4 dB/m, 3.3 dB/m and 3.2 dB/m for d_1/d = 1.55, 1.60 and 1.65, respectively. It is unusual to have bent fiber leakage losses less than those of straight ones.

From Fig. 4.40, it can be seen that the ES-PCF exhibits a very low leakage loss of the FM when it is bent at bending radii 2 mm to 10 mm having a leakage loss as low as 0.0536 dB/m at a bending radius 4 mm for d_1/d = 1.65 and this loss decreases with the increase of d_1/d. It may be expected that d_1/d can be further increased to reduce the leakage loss of the FM maintaining the condition that the leakage loss of the first HOM should be greater than 1dB/m. But this will lead to a structure having spacing between the air holes of the first and second ring of the same arm smaller than 50 nm (it is 50 nm for d_1/d = 1.65). The fabrication of an ES-PCF of such a structure will be very difficult. Thus, the structural parameters of the proposed large mode area, low leakage loss single mode ES-PCF are: r_0 = 6.5 μm, d = 0.878 μm, d_1/d = 1.65, d_2 = 0.726 μm.

It is to be noted that the leakage losses of the FM for a straight fiber are 0.187 dB/m, 0.183 dB/m and 0.178 dB/m, for d_1/d = 1.55, 1.60 and 1.65, respectively. So, the leakage losses of the FM are lower in a bent fiber than those of a straight one when bent in a specific direction. This unconventional phenomenon can be explained in a way that the ES-PCF has $d_1 > d$. So, when the fiber is bent at $\alpha = 0°$ (along positive x axis) and around as will be seen later, the propagating modes become more confined as shown in Fig. 4.41, where power confinements of the FM of a straight and bent fiber are shown. It is worth mentioning here that if we calculate the bending losses of

this fiber, obviously it will return negative values. The leakage loss rapidly increases at bending radii lower than 3 mm in both Figs. 4.39 and 4.40, where the effect of bending dominates the higher mode confinement due to $d_1 > d$. Thus, the proposed ES-PCF can be used upto bending radius as low as 3 mm.

From Fig. 4.42, the leakage losses of the first HOM and FM as a function of α are seen to be increasing with the increase of α. The increase of leakage loss of the first HOM suppress it more which is desirable. But, the increase of leakage loss of the FM should be minimized. Although, leakage losses increase with the increase of α, its value is within acceptable limit upto α = 40° where the leakage loss of FM is 0.303 dB/m at 1.65 µm. To control the angular rotation of the fiber, a precise fiber rotator can be employed with an accuracy of 2° [45]. The ES- PCF behaves similarly for negative values of α. A previously reported PCF with bending loss dependent on α [45] had permissible value of α = ±7° only.

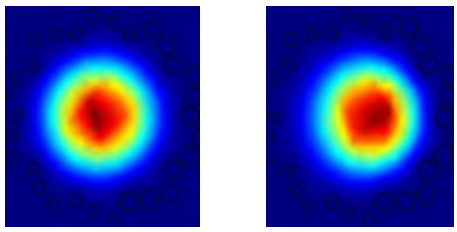

(a) (b)

Fig. 4.41 Power confinement of the fundamental mode of the proposed ES-PCF, (a) for straight fiber (b) for bent fiber with bending radius 4mm.

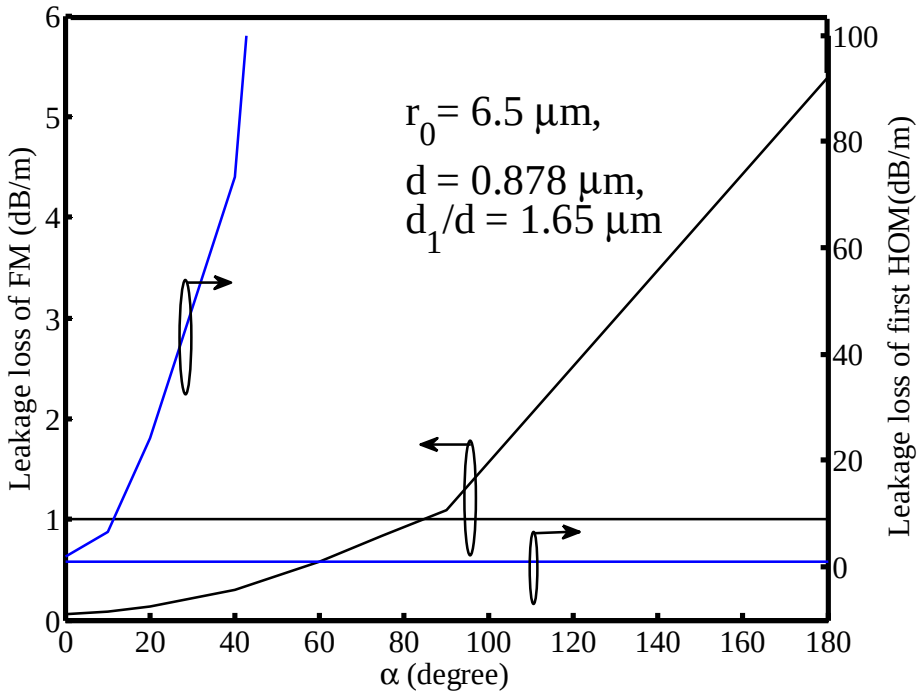

Fig. 4.42 Leakage loss as a function of bending orientation.

4.5.3 Outcomes

In this section, the compactness of cladding air holes in an ES-PCF is utilized to achieve low leakage loss over a wide wavelength range 1.35 µm to 1.65 µm and above. But, this results in HOMs in the core. However, a useful technique is employed to suppress these HOMs. The optimized structure also exhibits a very low splice loss if spliced with a conventional SMF. The proposed structure shows leakage loss as low as 8.32×10^{-4} dB/turn (0.033 dB/m) at 1.55 µm for bending radius 4 mm, single-modedness over 1.35 µm and splice loss 0.00086 dB with a typical SMF. Moreover, the proposed structure has a unique property that it shows lower leakage loss as it is bent upto a certain radius than that of the same straight fiber. Thus, the proposed ES-PCF can be a very good candidate for the fiber-to-the home usage.

4.6 A Novel Design on Bend Insensitive Single Mode Circular PCF with Ultralarge Effective Area

In WDM transmission systems, dispersion and nonlinearity are of major concern as it may degrade the system performance to a large extent [42]. Dispersion compensation techniques have been developed and are extensively used in high speed transmission systems [42]. Due to higher nonlinearity, the optical input power must be restricted below a level. To increase this level, fibers having higher effective area, A_{eff} are always necessary. Several such designs with a large A_{eff} have been developed [42]-[45].

The high leakage loss of a bent PCF can be minimized to an acceptable level by appropriately choosing the air hole diameters. But, apart from low bending loss, other two conditions are to be met simultaneously. These are, the higher order modes which are usually unavoidable in a low bending loss PCF, should be suppressed and A_{eff} of the fundamental mode of the PCF should be high. But, fibers with higher A_{eff} usually have more number of higher order modes (HOMs).

In this section, a bend insensitive large effective area circular PCF (C-PCF) has been proposed over the wavelength range 1300 nm to 1700 nm for WDM transmission (design-1). This proposed C-PCF exhibits bend loss in the order of 10^{-3}-10^{-4} dB/turn, effective area around 250 µm^2 and higher order mode leakage loss over 22 dB/m in the range 1300nm to 1700nm. Also, the whole structure of the same C-PCF is scaled down to obtain a bend insensitive large effective area C-PCF for fiber to the home application over the same wavelength range (design-2). This design shows bend loss in the order of 10^{-4} dB/turn, effective area very close to 80 µm^2 that ensures near zero splice loss with a typical SMF and higher order mode leakage loss over 10 dB/m in the same wavelength range. These dual characteristics make this fiber very attractive to be used in fiber optic communication systems.

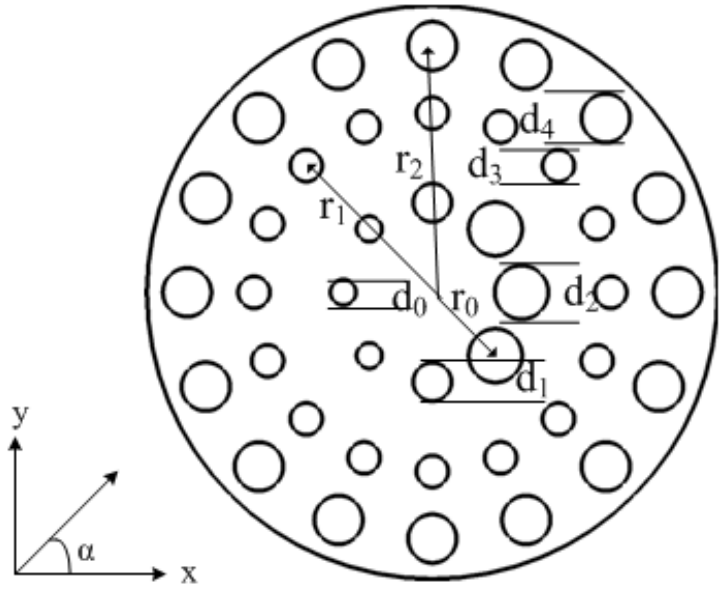

(a)

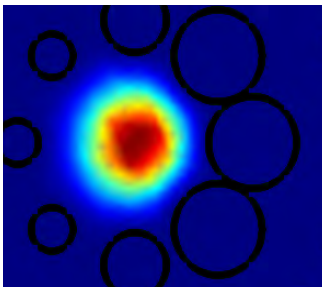

(b)

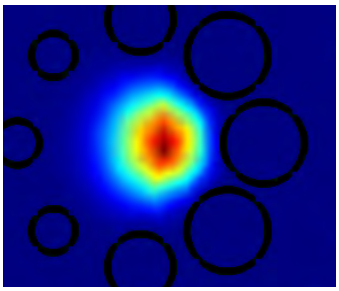

(c)

Fig. 4.43 (a) Geometry of the proposed C-PCF and electric field distribution at 1550nm (b) for first design at *R* = 30mm, (c) for second design at *R* = 4mm.

4.6.1 C-PCF design

The proposed C-PCF consists of three circularly arranged air hole rings in the cladding with a silica background. The first of them has eight air holes. Three of these eight have a diameter of d_2, two of them have that of d_1 and the remaining three have that of d_0 where $d_2>d_1>d_0$ to ensure lower leakage loss due to bending in a particular direction (along x axis or around in this case). The radii of the first, second and third air hole rings are r_0, r_1 and r_2, respectively. When the fiber is bent in the direction of positive x-axis, the angle of bending orientation, α (shown in Fig. 1) is equal to zero. A full-vectorial finite element method (FEM) has been used to determine optical modes of this design. A perfectly matched layer (PML) has been used at the outer boundary to account for the leakage loss correctly. Sellmeier equation has been used

to calculate the wavelength dependent index of silica. Leakage losses of bent fibers are calculated using the technique of conformal mapping [27]. The optimized structural parameters for the design-1 are: d_0= 6µm, d_1= 9µm, d_2= 12.6µm, r_0= 16.8µm, r_1= 33.6µm, r_2= 46.2µm. Those for design-2 can be obtained by multiplying each parameters of design-1 with 0.5. It is observed that variation of ~5% of these parameters does not yield significant deviation from the characteristics shown here.

4.6.2 Simulation results

In this work, we take a limiting value of 0.5 dB/100 turns at a bending radius of 30 mm as assumed in [42] which is described in ITU-T recommendations G.655 and 656. The bending loss of the proposed C-PCF should be lower than this for the entire range of wavelength. It can be seen from Fig. 2 that the bending loss is lower than 0.5dB/100turns for the bending radius, *R* = 26mm-34 mm. In fact, the highest bending loss is 0.0019 dB/turn at 1300 nm for *R* = 30mm. Also, the bending loss of design-1 is lower for the corresponding wavelength range keeping the effective area higher than those of [42]. Apart from this, it shows lower bending loss over a wider range of wavelength.

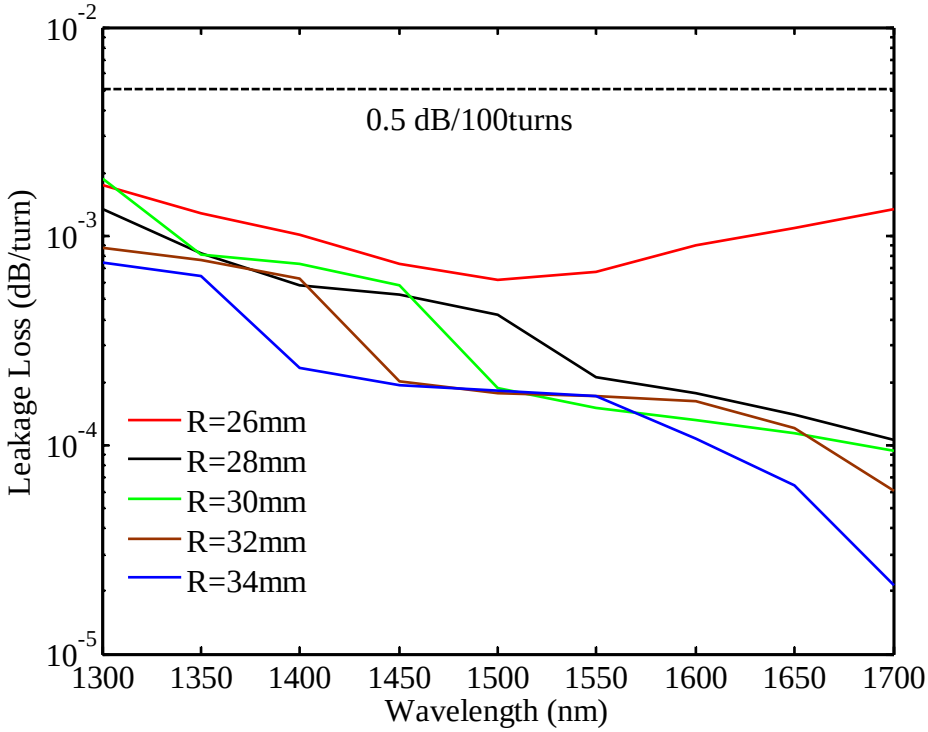

Fig. 4.44 Leakage loss of the proposed C-PCF for design-1 for different bending radius.

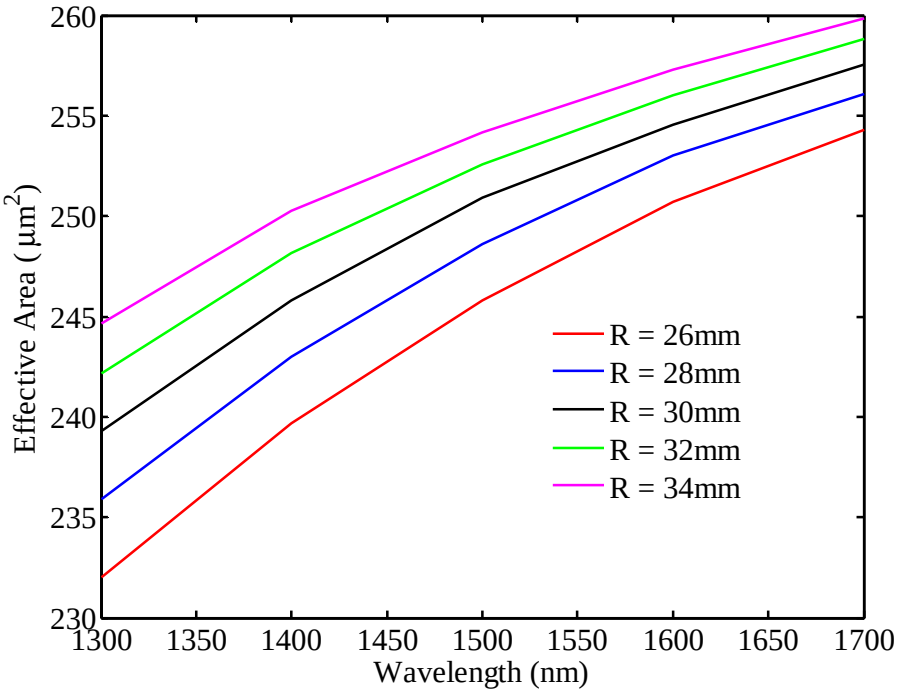

Fig. 4.45 Effective area of the proposed C-PCF for design-1 for different bending radius.

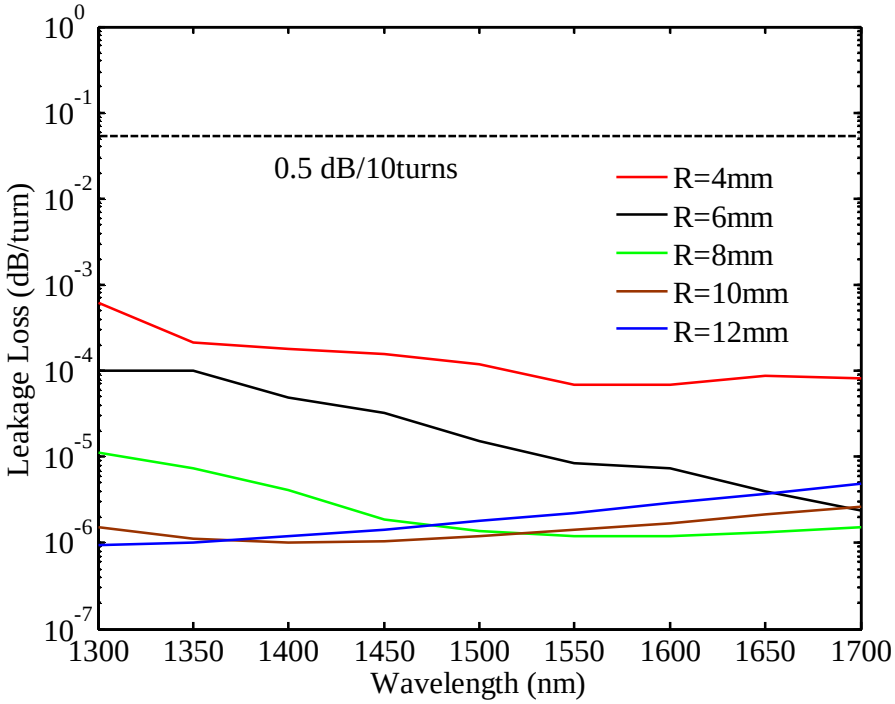

Fig. 4.46 Leakage loss of the proposed C-PCF for design-2 for different bending radius.

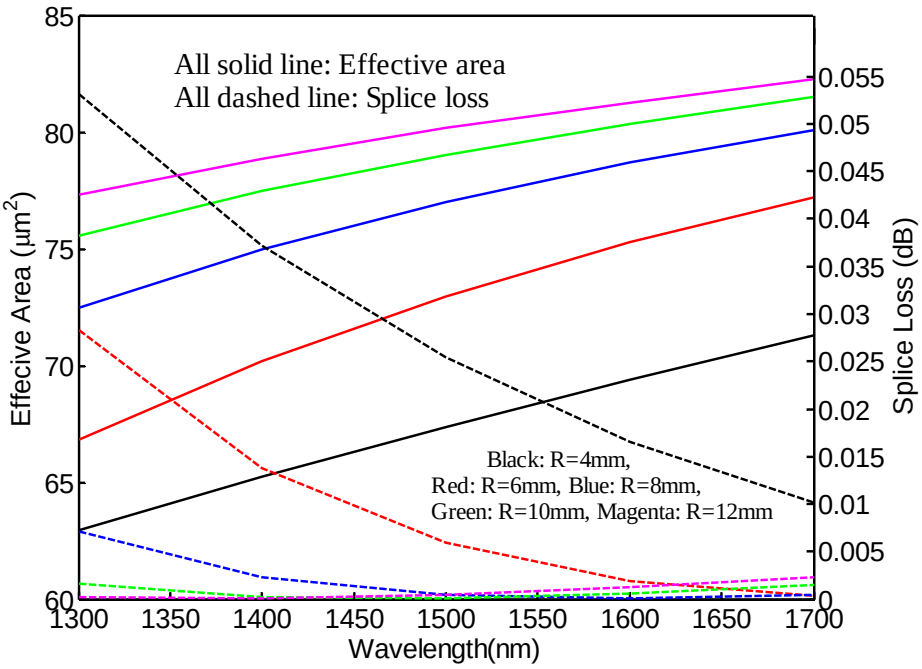

Fig. 4.47 Effective area and corresponding splice loss of the proposed C-PCF for design-2 for different bending radius.

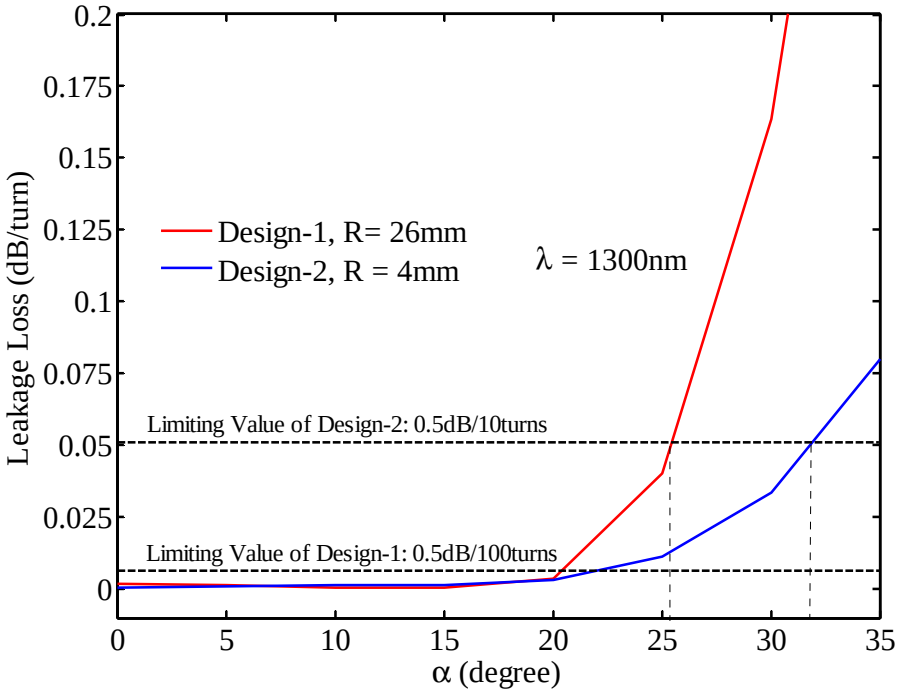

Fig. 4.48 Leakage loss as a function of bending orientation.

It is shown in Fig. 3 that the A_{eff} varies from 239.26 μm^2 to 257.55 μm^2 for R = 26mm-34 mm in the range 1300nm-1700nm. These A_{eff} are higher than those in [42]. From Fig. 4, it can be seen that for design-2, the leakage loss is very low over the wavelength range 1300nm to 1700nm for R = 4mm to 12 mm. The highest leakage

loss is 6.13×10^{-4} dB/turn at 1300nm for R = 4mm which is much lower than that reported in [44] for a holey fiber (HF) at R = 5mm. Also, in [44] the acceptable leakage loss was taken as 0.5 dB/10turns. In design-2 of the proposed C-PCF, the leakage loss is at least 10^2 times lower than this over the wavelength range 1300nm-1700nm.

Fig. 4.47 shows the A_{eff} and corresponding splice loss vs. wavelength curves for R = 4mm-12mm for design-2. For low splice loss with a standard SMF (mode field diameter = 10μm), the effective area of the C-PCF should match closely that of a standard SMF. Here, the highest splice loss 0.0532 dB occurs for R = 4mm at 1300nm which is lower than that reported in [44]. For R = 8mm and above, the splice loss is near zero for the wavelength over 1450nm.

It is evident from table 1 and table 2 that for both design-1 and design-2, the leakage loss the first four HOMs are well above 1 dB/m which ensures that the HOMs are effectively suppressed [42]. The uneven nature of the leakage loss may be due to the fact that the degree of coupling between the leaky cladding modes and core HOMs varies with the wavelength and bending radius. Though the leakage loss of the HOMs are not shown in the continuous range between 1300nm-1700nm, it is thoroughly checked and confirmed that the leakage loss does not fall below the limiting values for both designs. Also, the leakage loss of the other HOMs are also observed to be higher than the limiting values and thus effectively suppressed. It is observed that the cut-off wavelength for any HOM is below 1200nm for design-1 and 700nm for design-2.

Both the designs show single mode operation even when the fiber is not bent (straight fiber). For straight fibers, the highest confinement loss of the HOMs we observed are just over 1 dB/m making it effectively suppressed in this case too. However, the confinement losses of the fundamental modes are more than 10^3 times lower than this.

Table 4.2 Leakage Loss of the first four HOM at R = 30 mm for Design-1

	1300nm	1400nm	1500nm	1600nm	1700nm
4th HOM	4.7538	7.37	9.72	9.87	8.86
3rd HOM	4.3577	9.43	13.28	11.60	16.44
2nd HOM	8.8550	51.20	53.72	41.80	72.93
1st HOM	12.7345	48.32	68.67	52.23	56.54

Table 4.3 Leakage Loss of the first four HOM at R = 4 mm for Design-2

	1300nm	1400nm	1500nm	1600nm	1700nm
4^{th} HOM	23.33	53.45	67.47	91.98	225.03
3^{rd} HOM	29.60	77.67	83.44	86.45	149.77
2^{nd} HOM	81.67	225.78	187.54	217.34	312.13
1^{st} HOM	69.54	152.45	160.77	189.76	241.37

Although, leakage losses increases with the increase of α as shown in Fig. 6, their values remain within acceptable limit upto α = 32° for design-1 and α = 25.6° for design-2. To control the angular rotation of the fiber, a precise fiber rotator can be employed with an accuracy of 2° [45].

4.6.3 Outcomes

A very low bending loss large mode area index guided PCF design has been presented in this paper. The same fiber design can be exploited in two different applications if scaled up or down. The designs are single moded as the HOMs bending losses exceed over certain limiting values. There are also about 10^4 times differences between bending loss of fundamental mode and HOMs. These characteristics make this C-PCF a useful candidate in WDM transmission and fiber to the home application.

CHAPTER 5
CONCLUSION

5.1 Conclusion of the Work

Different properties of equiangular spiral (ES) PCF have been numerically investigated in this thesis. The higher number of degrees of freedom in ES-PCF, yields greater flexibility in tailoring dispersion, birefringence, confinement, bending loss etc. than that in more conventional hexagonal lattice PCF. Thus, it is worth predicting that very useful results may be obtained by tuning the structural parameters of an ES-PCF. In this thesis, several designs of PCFs have been done for numerous applications in fiber optic communication systems. Among these designs, an ES-PCF has been proposed to obtain large negative flat dispersion over the telecommunication wavelength bands for dispersion compensation with high birefringence. This design is further modified by employing more elliptical air holes in the core to obtain even more negative dispersion profile. This dispersion profile is much more negative than the existing literatures on residual dispersion compensating fibers. Also, the birefringence issue along with dispersion compensation is addressed for the first time to my knowledge. Based on a similar structure, another design of ES-PCF containing liquid crystal infiltration in the core region to yield complete suppression of one degenerate mode form the two fundamental modes along with large negative flat dispersion profile is also showed. This design exhibits a very flat dispersion profile flatter than those of the existing literatures. The mode degeneration phenomenon between the fundamental core mode and cladding mode is investigated next. It is shown that ES-PCFs do not show significant mode degeneration between core and cladding modes like that of hexagonal lattice PCFs. A single mode bend insensitive ES-PCF with large effective area for fiber to the home application is shown subsequently. It offers lower bending loss with single modedness having splice loss near zero with a typical SMF. The single modedness is achieved with an ingenious technique of introducing a secondary core in the outer cladding. Other than ES-PCF, a new structure of circular PCF has been proposed to obtain a single mode bend insensitive fiber with large effective area for both WDM transmission and fiber to the home application. This new structure is confirmed to be largely single moded over a wide range of wavelengths and bending radii.

Prior to the numerical investigations, a modified bend loss formula have been developed that can predict bend loss more accurately than the previous literatures for a very wide range of bending radius and wavelength for step index fibers. Also, this formula is applied to predict bend loss of PCFs. Though this formula shows moderately accurate estimation of bend loss of PCFs for a limited range of structural parameters, wavelength and bending radius, it can be very useful in bypassing the conventional cumbersome numerical calculations involved in predicting bending loss.

5.2 Scope for the Future Work

Though a number of useful designs on PCFs have been proposed, they are not tested experimentally. The fabrication of conventional hexagonal lattice PCF is done through stack and draw process [40]. But, the complex irregular structures of ES-PCF and C-PCF are difficult to fabricate using this process, though not impossible as suggested by [21]. These designs are most likely to be fabricated by extrusion or drilling technique which has already been proposed to fabricate a golden spiral PCF [40]. Also, the sol-gel technique has some potential to fabricate irregular structures where all the structural parameters can be adjusted independently [46]. Thus, one of these two methods can be opted to fabricate the designs shown in this thesis. After fabricating such structures, the numerical results may be verified experimentally that can strengthen the findings.

Though, endlessly single mode behavior of conventional H-PCFs is well established, this feature is yet to be investigated for ES-PCFs. To analyze this property, it seems that the concept of 'unit cell' for an ES-PCF should be defined as a starting point. The boundary conditions are also another aspect which must be treated with care for this purpose.

Large mode area (LMA) limitation in single mode PCFs with low bending loss is addressed extensively during the last few years. For fiber laser applications, the necessity for LMA is evident from the fact that it reduces the nonlinear effects in high power devices. This area of research can be taken into consideration using ES-PCF and C-PCF as they have higher number of degrees of freedom which increases the probability to tune their properties very precisely.

REFERENCES

[1] Knight, J. C., "Photonic crystal fibers," Nature, vol. 424, pp. 847–851, 2003.

[2] Russell, P. St. J., "Photonic crystal fibers," Science, vol. 299, pp. 358–362, Jan. 2003.

[3] Kuhlmey, B. T., McPhedran, R. C., de Sterke, C. M., Robinson, P. A., Renversez, G., and Maystre, D., "Microstructured optical fibers: where's the edge?" Optics Express, vol. 10, pp. 1285–1290, 2002.

[4] Mortensen, N. A., Folkenberg, J. R., Nielsen, M. D., and Hansen, K. P., "Modal cutoff and the V parameter in photonic crystal fibers," Optics Letters, vol. 28, pp. 1879–1881, 2003.

[5] Knight, J. C., Broeng, J., Birks, T. A., and Russell, P. St. J., "Photonic band gap guidance in optical fibers," Science, vol. 282, pp. 1476–1478, 1998.

[6] Reeves, W. H., Knight, J. C., Russell, P. St. J., and Roberts, P. J., "Demonstration of ultra-flattened dispersion in photonic crystal fibers," Optics Express, vol. 10, pp. 609–613, 2002.

[7] de Matos, C. J. S., Taylor, J. R., Hansen, T. P., Hansen, K. P., and Broeng, J., "All-fiber chirped pulse amplification using highly-dispersive air-core photonic bandgap fiber," Optics Express, vol. 11, pp. 2832–2837, 2003.

[8] Limpert, J., Schreiber, T., Nolte, S., Zellmer, H., and T¨unnermann, A., "All fiber chirped-pulse amplification system based on compression in airguiding photonic bandgap fiber," Optics Express, vol. 11, pp. 3332–3337, Dec. 2003.

[9] de Matos, C. J. S. and Taylor, J. R., "Chirped pulse Raman amplification with compression in air-core photonic bandgap fiber," Optics Express, vol. 13, pp. 2828–2834, Apr. 2005.

[10] Humbert, G., Knight, J. C., Bouwmans, G., Russell, P. St. J., Williams, D. P., Roberts, P. J., and Mangan, B. J., "Hollow core photonic crystal fibers for beam delivery," Optics Express, vol. 12, pp. 1477–1484, Apr. 2004.

[11] Kurokawa, K., Tajima, K., Tsujikawa, K., and Nakajima, K., "Reducing the losses in photonic crystal fibres," in Proc. European Conference on Optical Communication ECOC 2005, Glasgow, Scotland, Sept. 25–29, 2005.

[12] Ferrarini, D., Vincetti, L., Zoboli, M., Cucinotta, A., and Selleri, S., "Leakage properties of photonic crystal fibers," Optics Express, vol. 10, pp. 1314–1319, Nov. 2002.

[13] White, T. P., McPhedran, R. C., de Sterke, C. M., Botten, L. C., and Steel, M. J., "Confinement losses in microstructured optical fibers," Optics Letters, vol. 26, pp. 1660–1662, Nov. 2001.

[14] Saitoh, K. and Koshiba, M., "Confinement Losses in air-guiding photonic bandgap fibers," IEEE Photonics Technology Letters, vol. 15, pp. 236–238, Feb. 2003.

[15] Baggett, J. C., Monro, T. M., Furusawa, K., and Richardson, D. J., "Comparative study of large-mode holey and conventional fibers," Optics Letters, vol. 26, pp. 1045–1047, July 2001.

[16] Sorensen, T., Broeng, J., Bjarklev, A., Knudsen, E., and Libori, S. E. B., "Macro-bending loss properties of photonic crystal fiber," Electronics Letters, vol. 37, pp. 287–289, Mar. 2001.

[17] Mortensen, N. A. and Folkenberg, J. R., "Low-loss criterion and effective area considerations for photonic crystal fibers," Journal of Optics A: Pure and Applied Optics, vol. 5, pp. 163–167, May 2003.

[18] Knight, J. C., Birks, T. A., Cregan, R. F., Russell, P. St. J., and de Sandro, J. P., "Large mode area photonic crystal fibre," Electronics Letters, vol. 34, pp. 1347–1348, June 1998.

[19] Nielsen, M. D., Folkenberg, J. R., Mortensen, N. A., and Bjarklev, A., "Bandwidth comparison of photonic crystal fibers and conventional single-mode fibers," Optics Express, vol. 12, pp. 430–435, Feb. 2004.

[20] Agrawal, A., Kejalakshmy, N., Chen, J., Rahman, B. M. A., and Grattan, K. T. V., "Soft glass equiangular spiral photonic crystal fiber for supercontinuum generation," IEEE Photonics Technology Letters, vol. 21, no. 22, pp. 1722-1724, Nov. 2009.

[21] Agrawal, A., Azabi, Y. O., and Rahman, B. M. A., "Stacking the equiangular spiral," IEEE Photonics Technology Letters, vol. 25, no. 3, pp. 291-294, Feb. 2013.

[22] Ebendorff-Heidepriem, H. and Monro, T. M., "Extrusion of complex preforms for microstructured optical fibers," Optics Express, vol. 15, no. 23, pp. 15086-15092, 2007.

[23] Tyagi, H. K., Schmidt, M. A., Sempere, L. P., and Russell, P. S., "Optical properties of photonic crystal fiber with integral micron-sized Ge wire," Optics Express, vol. 16, no. 22, pp. 17227-17236, 2008.

[24] DeHazan, Y., MacChesney, J. B., Stockert, T. E., Trevor, D. J., and Windeler, R. S., U.S. patent 6,467,312 B1, Oct. 2002.

[25] Marcuse, D., "Curvature loss formula for optical fibers," Journal of Optical Society of America, vol. 66, no. 3, pp. 216-220, 1976.

[26] Sharma, A. B., Ai-Ani, A. H., and Halme, S. J., "Constant-curvature loss in monomode fibers: An experimental investigation," Applied Optics, vol. 23, pp. 3297–3301, Oct. 1984.

[27] Schermer, R. T. and Cole, J. H., "Improved bend loss formula verified for optical fiber by simulation and experiment," IEEE Journal of Quantum Electronics, vol. 43, no. 10, pp. 899-909, 2007.

[28] Koplow, J. P., Kliner, D. A. V., and Goldberg, L., "Single-mode operation of a coiled multimode fiber amplifier," Optics Letters, vol. 25, pp. 442–444, Apr. 1, 2000.

[29] Leong, J. Y. Y., Petropoulous, P., Price, J. H. V., Ebendorff-Heiderpriem, H., Monro, T. M., and Richardson, D. J., "High-nonlinearity dispersion-shifted lead-silicate holey fibers

for efficient 1- μm pumped supercontinuum generation," Journal of Lightwave Technology, vol. 24, no. 1, pp. 183–190, Jan. 2006.

[30] Agrawal, G. P., Fiber-Optic Communication Systems, 3rd ed. New York: Wiley, 2002, pp. 15–64.

[31] Franco, M. A. R., Serrão, V. A., and Sircilli, F., "Microstructured optical fiber for residual dispersion compensation over S+C+L+U wavelength bands," IEEE Photonics Technology Letters, vol. 20, no. 9, May 1, 2008.

[32] da Silva, J. P., Bezerra, D. S., Esquerre, V. F. R., da Fonseca, I. E., and Figueroa, H. E. H., " Ge-doped defect-core microstructured fiber design by genetic algorithm for residual dispersion compensation," IEEE Photonics Technology Letters, vol. 22, no. 18, September 15, 2010.

[33] Matsui, T., Nakajima, K., and Sankawa, I., "Dispersion compensation over all the telecommunication bands with double-cladding photonic crystal fiber," Journal of Lightwave Technology, vol. 25, no. 3, pp. 757–762, Mar. 2007.

[34] Du, F., Lu, Y.Q., and Wu, S.T., "Electrically tunable liquid-crystal photonic crystal fiber," Applied Physics Letters, vol. 85**,** pp. 2181–2183, 2004.

[35] Zografopoulos, D. C., Kriezis, E. E., and Rsiboukis, T. D., "Photonic Crystal-Liquid Crystal Fibers for Single-Polarization or High-Birefringence Guidance," Optics Express, vol. 11**,** pp. 2589–2596, 2006.

[36] Little, B. E., Chu, S. T., Haus, H. A., Foresi, J., and Laine, J. P., "Microring resonator channel dropping filters," Journal of Lightwave Technology, vol. 15, pp. 998–1005, 1997.

[37] Hayes, R. R. and Yap, D., "GaAs spiral optical waveguides for delay-line applications," Journal of Lightwave Technology, vol. 11, pp. 523–528, 1993.

[38] Saitoh, K., Florous, N. J., Koshiba, M., and Skorobogatiy, M., "Design of narrow band-pass filters based on the resonanttunneling phenomenon in multi-core photonic crystal fibers," Optics Express, vol. 13, pp. 10327–10335, 2005.

[39] Iizawa, K., Varshney, S. K., Tsuchida, Y., Saitoh, K., and Koshiba, M., "Bend-insensitive lasing characteristics of singlemode, large-mode-area Ytterbium-doped photonic crystal fiber," Optics Express, vol. 16, pp. 579–591, 2008.

[40] Rahman, B. M. A., Kejalakshmy, N., Uthman, M., Agrawal, A., Wongcharoen, T., Grattan, K. T. V., "Mode degeneration in Bent Photonic Crystal Fiber Study By Using The Finite Element Method," Applied Optics, vol. 48, G131, 2009.

[41] Saitoh, K., Florous, N., and Koshiba, M., "Ultra-flattened Chromatic Dispersion Controllability Using a Defected Core Photonic Crystal Fiber with Low Confinement Losses," Opt. Exp., vol. 13, no. 21, pp. 8365-8371, 2005.

[42] Matsui, T., Sakamoto, T., Tsujikawa, K., Tomita, S., and Tsubokawa, M., "Single-mode photonic crystal fiber design with ultralarge effective area and low bending loss for ultra-high speed WDM transmission," J. Lightw. Technol., vol. 29, no. 4, pp. 511–515, Feb. 2011.

[43] Tsuchida, Y., Saitoh, K., and Koshiba, M., "Design of single-moded holey fibers with large-mode-area and low bending losses: the significance of the ring-core region," Opt. Exp., vol. 15, no. 4, pp. 1794–1803, 2007.

[44] Tsuchida, Y., Saitoh, K., and Koshiba, M., "Design and characterization of single-mode holey fibers with low bending losses," Opt. Exp., vol. 13, pp. 4770–4779, June 2005.

[45] Napierała, M., Nasiłowski, T., Bereś-Pawlik, E., Mergo, P., Berghmans, F., and Thienpont, H., "Large-mode-area photonic crystal fiber with double lattice constant structure and low bending loss," Opt. Exp., vol. 19, no. 23, pp. 22628–22636, 2010.

[46] Hossain, M. N., Alam, M. S., Hasan, D. M. N., and Mohsin, K. M., "A Highly Nonlinear Spiral Photonic Crystal Fiber for Tailoring Two Zero Dispersion Wavelengths in the Visible Region," Photonics Letters of Poland, vol. 2, pp. 143-145, 2010.

[47] Koshiba, M., "Full-Vector Analysis of Photonic Crystal Fibers Using the Finite Element Method," IEICE Transactions on Electronics, vol. E85-C, no. 4, pp. 881-888, 2002.

[48] COMSOL Multiphysics, version 3.4, 2007.

[49] Berenger, J., "A perfectly matched layer for the absorption of electromagnetic waves," Journal of Computational Physics, vol. 114, no. 2, pp. 185–200, 1994.

[50] Viale, P., Février, S., Gérôme, F., and Vilard, H., "Confinement Loss Computations in Photonic Crystal Fibres using a Novel Perfectly Matched Layer Design," Excerpt from the Proceedings of the COMSOL Multiphysics User's Conference, Paris, 2005.

[51] Saitoh, K., Florous, N., and Koshiba, M., "Ultra-flattened Chromatic Dispersion Controllability Using a Defected Core Photonic Crystal Fiber with Low Confinement Losses," Optics Express, vol. 13, no. 21, pp. 8365-8371, 2005.

[52] Yue, Y., Kai, G., Wang, Z., Sun, T., Jin, L., Lu, Y., Zhang, C., Liu, J., Li, Y., Liu, Y., Yuan, S., and Dong, X., "Highly birefringent elliptic-hole photonic crystal fibre with squeezed hexagonal lattice," Optics Letters, vol. 32, pp. 469-471, 2007.

[53] Chen, D. and Shen, L., "Ultrahigh Birefringent Photonic Crystal Fiber with Ultralow Confinement Loss," IEEE Photonics Technology Letters, vol. 19, no. 4, pp. 185-187, 2007.

[54] Agrawal, A., Kejalakshmy, N., Chen, J., Rahman, B. M. A., and Grattan, K. T. V., "Golden spiral photonic crystal fiber: polarization and dispersion properties," Optics Letters, vol. 33, no. 22, pp. 2716-2718, Nov. 2008.

[55] Agrawal, A., Kejalakshmy, N., Rahman, B. M. A., and Grattan, K. T. V., "Polarization and Dispersion Properties of Elliptical Hole Golden Spiral Photonic Crystal Fiber," Applied Physics B, vol. 99, no. 4, pp. 717-726, 2010.

[56] Alam, M. S., Saitoh, K., and Koshiba, M., "High group birefringence in air-core photonic bandgap fibers," Optics Letters, vol. 30, no. 8, pp. 824-826, 2005.

[57] Fini, J., "Design of solid and microstructure fibers for suppression of higher-order modes," Optics Express, vol. 13, no. 9, pp. 3477–3490, 2005.

[58] Islam, M. A. and Alam, M. S., "Design of a Polarization Maintaining Equiangular Spiral Photonic Crystal Fiber for Residual Dispersion Compensation Over E+S+C+L+U

Wavelength Bands," IEEE Photonics Technology Letters, vol. 24, no. 11, pp. 930-932, June 2012.

[59] Razzak, S. M. A. and Namihira, Y., "Tailoring dispersion and confinement losses of photonic crystal fibers using hybrid cladding," Journal of Lightwave Technology, vol. 26, no. 13, pp. 1909–1914, July 2008.

[60] Xiao, L., Jin, W., and Demokan, M. S., "Fusion splicing small-core photonic crystal fibers and single-mode fibers by repeated arc discharges," Optics Letters, vol. 32, no. 2, pp. 115–117, 2007.

PUBLICATIONS RELATED TO THIS WORK

[1] Islam, M. A. and Alam, M. S., "Design of a Polarization Maintaining Equiangular Spiral Photonic Crystal Fiber for Residual Dispersion Compensation Over E+S+C+L+U Wavelength Bands," IEEE Photonics Technology Letters, vol. 24, no. 11, pp. 930-932, June 2012.

[2] Islam, M. A. and Alam, M. S., "Design optimization of equiangular spiral photonic crystal fiber with large negative flat dispersion and high birefringence," Journal of Lightwave Technology, vol. 30, no. 22, pp. 3545-3551, Nov. 2012.

[3] Islam, M. A. and Alam, M. S., "A Liquid Crystal Infiltrated Single Polarization Spiral Photonic Crystal Fiber with Large Negative Flat Dispersion," presented at the 7th International Conference on Electrical and Computer Engineering (ICECE), Dhaka, Bangladesh, Dec 20-22, 2012.

[4] Islam, M. A. and Alam, M. S., "Bend insensitive single mode photonic crystal fiber with ultralarge effective area for dual applications," accepted in Optical Engineering Letters on Mar. 2013, to be published.